MATHEMATICAL SIMULATION OF ELECTROCHEMICAL FLUIDIZED BED

A Thesis
Submitted to the College of Engineering
of Nahrain University in Partial Fulfillment
of the Requirements for the Degree of
Master of Science
in
Chemical Engineering

by
MOHANNAD JUAD KADHUM
(B.Sc. in Chemical Engineering 2004)

Thi Qada **1428**
November **2007**

Certification

I certify that this thesis entitled **"Mathematical Simulation of Electrochemical Fluidized Bed"** was prepared by **Mohannad Juad Kadhum** under my supervision at Nahrain University/ College of Engineering in partial fulfillment of the requirements for the degree of Master of Science in Chemical engineering.

Signature:
Name: **Prof. Dr. Qasim. J. M. Slaiman**
(Supervisor)
Date: 16 / 12/ 2007

Signature:
Name: **Prof. Dr. Qasim. J. M. Slaiman**
(Head of Department)
Date: 16 / 12 / 2007

Certificate

We certify, as an examining committee, that we have read this thesis entitled **"Mathematical Simulation of Electrochemical Fluidized Bed"**, examined the student **Mohannad Juad Kadhum** in its content and found it meets the standard of thesis for the degree of Master of Science in Chemical Engineering.

Signature:
Name:**Prof. Dr. Qasim J.M. Slaiman**
(Supervisor)
Date: 16/ 12 / 2007

Signature: M.Shc
Name: **Dr. Muslet S. Hussain**
(Member)
Date: 16 / 12 / 2007

Signature:
Name: **Dr. Basim O. Hasan**
(Member)
Date: 16 / 12 / 2007

Signature: Mahmoud Omar Abdullah
Name: **Prof. Dr. Mahmoud O.Abdullah**
(Chairman)
Date: 16 / 12 / 2007

Approval of the College of Engineering

Prof Dr. Raad Sami Fyath
Signature:
Name: **Prof. Dr. Muhsin J. Jweeg**
(Acting Dean)
Date: 16 / 12 / 2007

Abstract

In this work it is attempted to find a model describes potential, current, and concentration distributions in addition to hydrodynamic study along an electrochemical fluidized bed reactor. Electrochemical fluidized bed reactor consists of a bed of particles which fluidizes and expands by an upward moving electrolyte. An electrical potential difference is applied between the upper and lower parts of the bed which induces the electrochemical reaction to take place on the surfaces of the particles. Electrochemical fluidized bed reactor represents one of the most useful applications in electrochemical engineering and its main uses are: electrowinning, pollution inhibition, and purification.

Three cases have been considered in this work linear, Tafel, and concentration polarization models. Models have been developed starting from Ohm's law and using Laplace transformation to solve for the potential distribution across the bed. Tafel polarization has been tested and found that the resistivity equation suggested by Fleischmann et al (1971) is invalid since Fleischmann suggestion assumes constant metal phase resistivity along the bed while in fact this is not the case since the particles are discrete in the bottom of the bed and become closer up to the end of the reactor. So, an expression has been developed to describe the local metal phase resistivity which depends on both local position and bed expansion due to fluidization. A correction factor has been used and inserted to equation suggested by

Fleischmann et al and it covers a wide range of particle diameter. The error has been reduced greatly by this assumption for both solution and metal phase potential profiles. Concentration profiles have also been studied in this work in addition to velocity change and pressure drop change with percentage expansion of fluidized bed.

List of Contents

Contents **Pages**

Chapter One: Introduction

Chapter Two: Electrochemical Reactors and Literature Survey of Electrochemical Fluidized Bed Reactor

Chapter Three: Theory of Particulate Beds

Chapter Four: Calculations and Interpretations

Chapter Five: Discussions

Chapter Six: Recommendations for Future Work

NOTATIONS

Symbol	Definition	Unit
A	Cross Sectional area of bed	m^2
A_R	Area of reaction surface	m^2
a	1) Surface area of particles/unit volume of bed	m^2/m^3
	2) First Tafel coefficient	Volts
a_R	Activity of reduced species	-
a_O	Activity of oxidized species	-
$a_\circ$	Surface area of particles per unit volume of bed at static conditions	m^2/m^3
b	Second Tafel coefficient	Volts
C	Double layer capacity	$Farads/m^2$
C_{av}	Average bulk concentration	mol/m^3
C_{O_b}	Bulk concentration of oxidized species	mol/m^3
C_{O_s}	Surface concentration of oxidized species	mol/m^3
C_i	Concentration of species i	mol/m^3
C_{R_b}	Bulk concentration of reduced species	mol/m^3
C_{R_s}	Surface concentration of reduced species	mol/m^3
D	Diffusivity	m^2/s

D_j	Diffusivity of component j	m^2/s
d	Diameter of particle	m
F	Faraday constant 96487	coulomb/equiv.
f_r	Collision frequencies of particles per unit area	Hertz=1/s
g	Gravitational acceleration 9.81	m/s^2
I	Total current density	A/m^2
I_j	Current density of component j	A
I_{total}	Total current	A
i	Local current density	A/m^2
i_a	Anodic current density	A/m^2
i_c	Cathodic current density	A/m^2
i_L	Limiting current density	A/m^2
i_m	Metal phase current density	A/m^2
i_o	Exchange current density	A/m^2
i_s	Solution phase current density	A/m^2
J_j	Molar flux per unit area	$mol/s.m^2$
j_D	Mass transfer j-factor$=\frac{K_{av}}{U_{av}}Sc^{2/3}$	-
k_a	Anodic reaction rate constant	m/s
k_c	Cathodic reaction rate constant	m/s
K_{av}	Mass transfer coefficient	m/s
K_s	Solution conductivity	$\Omega^{-1}.m^{-1}$
K_m	Metal phase conductivity	$\Omega^{-1}.m^{-1}$
L	Height of bed	m
M_j	Molecular weight of species j	g/g.mole

n_j	Molar flux of component j	mol/s
R	Gas constant 8.314	J/g.mole.K
Re_p	Reynolds number= $U_{av}d_p/\nu$	-
r	Radius of particle	m
Sc	Schmidt number= ν/D	-
T	Temperature of fluidized bed	K
U_{av}	Superficial average velocity in empty section of bed	m/s
u_p	Velocity of particle	m/s
u_t	Terminal settling velocity	m/s
u_x	Local Velocity	m/s
V	a) Voltage of electrolysis b) Specific volume of diffusion layer	Volts m^3
V_a	Anodic potential	Volts
V_c	Cathodic potential	Volts
V_{ohm}	Voltage contribution due to solution resistance	Volts
V_{min}	Minimum voltage of electrolysis	Volts
x	Distance from bottom of bed	m
z	Number of electrons associated with electrochemical reaction	-

Greek Letters	**Definition**	**Unit**
α	Transfer coefficient	-
δ	Diffusion layer thickness	m

Γ	Expansion coefficient	-
ε	Porosity of bed= (volume of spaces/ volume of bed)	-
ε_j	Current efficiency	-
ϕ	1) Sphericity of particle	-
	2) Potential	Volts
ϕ_m	Metal potential	Volts
ϕ_s	Solution potential	Volts
η	Overpotential	Volts
η_a	Anodic overpotential	Volts
η_c	Cathodic potential	Volts
μ	Dynamic viscosity	Kg/m.s
ν	Kinematic viscosity	m^2/s
ν_j	Stoichiometric coefficient	-
ν_p	Interstitial velocity	m/s
ρ	Density of solution	Kg/m^3
ρ_m	Density of solid	Kg/m^3
χ_m	Resistivity of metal phase	Ω.m
χ_s	Resistivity of solution phase	Ω.m
Ψ	Local resistivity correction factor	-

Abbreviations

c.d.	Current density
EFBR	Electrochemical fluidized bed reactor
emf	Electromotive force

List of Tables

List of Figures

Chapter One

Introduction

1.1 Introduction

Since 1960, there were significant developments in electrolytic cells, partly by the application of chemical engineering principles to their design and partly by the development and use of new materials of construction. This has resulted in a trend away from the concept of an electrolytic cell as represented by a number of plate electrodes dipping into a rectangular tank and has led to the use of the so called three dimensional electrodes in the form of fixed and fluidized beds of electronically conducting particles in contact with a usually metallic plate, rod or gauze, termed the current feeder. As a result of these developments, packed and fluidized beds are now competitive with other types in terms of space time yield, the purity of product, and production costs [1].

An electrochemical fluidized bed reactor (EFBR) consists of a bed of electrically conducting particles fluidized by electrolyte flow, to which direct current is fed by one or more connecting rods or plates known as the current feeder, and which are often separated from one or more immersed counter electrodes by a diaphragm of porous or ionically conductive material that is desirably long lasting. Provided the bed expansion from the static condition is small, e.g. 5-25%, some electrical contact is maintained between the particles and the current feeder and between the particles themselves, so that the surfaces of the particles then act as a large extension of the feeder surface, thereby greatly increasing the current density based on the counter electrode surface area. Though the many trials and proposed applications of EFBRs include their use for fuel cell, organic and inorganic synthesis, industrial wastewater treatment and electrowinning(or electrodeposition) of metals, the qualified success of this technology has been mainly in the area of electrowinning, especially from dilute solutions, with the concomitant reduction of metallic components in the solutions involved [2]. It has the advantages that material transport and adsorption/desorption are spatially separated from electron transfer process (which is usually rapid), high space time yield, and giving very high specific surface area per unit volume of the bed for low real current densities. This advantage allows very dilute solutions to be electrolyzed [3].

1.2 Scope of Present Work

This work studies the potential, overpotential, and concentration profile in an EFBR in copper electrolyte system. New equations have been developed using Laplace transformation for the two cases of linear and concentration overpotentials. For the case of Tafel overpotential, a trial and error equation developed by Fleischmann (1971) has been simplified to a simpler one. The main problem was the great difference between experimental and theoretical solution potential profile. By developing an equation for the metal phase resistivity (or dispersed phase) varying with distance and percent expansion rather than a constant value along the bed suggested by Fleischmann. An important issue is that all the equations based on integration of an Ohm's law equation which contains metal phase resistivity as a parameter. Assuming that metal phase resistivity is constant along the bed will eventually lead to false potential profiles. So, using local values of resistivity will greatly reduce the difference and could be generalized to other electrochemical systems.

Chapter Two

Electrochemical Reactors and Literature Survey of Electrochemical Fluidized Bed Reactor

2.1 Introduction

The electrochemical reactor which is also called “electrolyser” or “electrolytic cell” or “electrochemical cell” which consists of two compartments (electrodes) connected to external direct current (d.c.) power supply and immersed in a conducting liquid called electrolyte. When an electromotive force (emf) of a sufficient magnitude is applied, electrons transfer occurs between each electrode and the liquid. Electrical conduction in the liquid phase is due to the motion of charged species called ions which results from the dissolving or melting of the chemical compound. This ionic movement or migration which takes place due to the potential gradient is in fact is a slow process. The main means of ionic transfer is nearly always due to mass transfer arising from concentration differences between various parts of the solution [4].

An electrode is a material in which electrons are the mobile species and therefore can be used to sense (or control) the potential of electrons. In electrochemistry, an electrode is considered to be an electronic conductor that carries out an electrochemical reaction or some similar interaction with an adjacent phase. Electronic conductivity generally decreases slightly with increasing temperature and is of the order 10^2 to 10^4 S/cm, where a siemens (S) is an inverse ohm (Ω^{-1}).The primary distinction between an electrochemical reaction and a chemical redox reaction is that, in an electrochemical reaction, reduction occurs at one electrode and oxidation occurs at the other, while in a chemical reaction, both reduction and oxidation occur in the same place [5].

Electrolysis is the conversion of electrical energy into chemical energy in order to convert substances by oxidation or reduction, so that products are formed as the element or an appropriate compound. Also included is the generation of charged intermediates that link to other species, as in electrosynthesis. The design of the cells where these reactions take place, together with associated operations, is electrochemical engineering [6].

One of the most essential characteristics of electrochemical systems is their ability to conduct electric currents. No matter whether they are ionic or electronic conductors, neutral components are always used in their construction, and the electrical conductivity is possible due to the decomposition of some of them in mobile charged species (i.e., ions, electrons, etc.) [7].

The general form of the electrochemical reaction equations can generally be written as [8]

$$\sum_{ox} \nu_j X_j + ze^- \Leftrightarrow \sum_{red} \nu_j X_{j'} \qquad 2.1$$

where X_j are the species involved in the reaction and ν_j are their stoichiometric coefficients. The summation index “ox” and “red” implies that the sum is taken over the oxidized and reduced form of the principal reaction components respectively and z is the number of electron associated with the overall electrochemical reaction. Sometimes a general conventional formulation can be used for relatively simple redox reactions [8]

$$O_x + ze \rightleftharpoons R_{ed} \qquad 2.2$$

where O_x and R_{ed} are the oxidized and reduced form of the principal reaction components respectively.

2.2 Factors Affecting Electrode Reaction Rate and Current

Consider an overall electrode reaction, $O_x + ze \rightleftharpoons R_{ed}$, composed of a series of steps that cause the conversion of the dissolved oxidized species, O_x, to a reduced form, R_{ed}. In general, the current (or electrode reaction rate) is governed by the rates of processes such as [9]:

1. Mass transfer (e.g., of O_x from the bulk solution to the electrode surface).
2. Electron transfer at the electrode surface.
3. Chemical reactions preceding or following the electron transfer. These might be homogeneous processes (e.g., protonation or dimerization) or heterogeneous ones (e.g., catalytic decomposition) on the electrode surface.
4. Other surface reactions, such as adsorption, desorption, or crystallization (electrodeposition) [9].

2.3 Types of Electrochemical Reactors

Several types of electrochemical reactors have been used in chemical industries starting from the simplest one which is the two plate reactors and rectangular tank reactor, then for more difficult ones, which includes filter press type, and goes further with complexity to the packed and fluidized bed reactors. The most known types of electrochemical reactors which are commonly used in chemical industry are:

1) Plate and frame cell: The most frequently employed in industrial organic electrochemical synthesis is the plate and frame cell or filter press design. In this cell, anolyte and catholyte streams flow in parallel

and are separated from each other by a diaphragm. Electrodes are normally linked in bipolar manner as shown in Fig. 2.1.

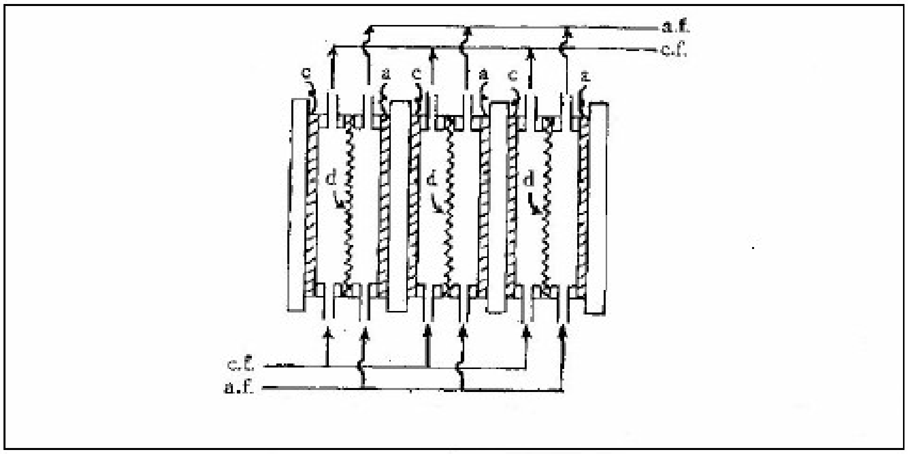

Fig. 2.1 Schematic drawing of filter press reactor. a, anode;c, cathode; d, diaphragm; a.f, anolyte flow; c.f, catholyte flow [1].

2) Seachlor Cell: is shown in Fig. 2.2 and was designed by De Nora, for the production of hypochlorite from seawater. It is undivided cell with bipolar electrodes, and its most important feature is the flow of electrolyte through successive anodic and cathodic regions. In this way, the design avoids the deposition of hydroxides on the cathode when the pH becomes too high [1].
3) Chemelec Cell: was developed by the Electricity Research Council at Capenhurst for the removal of metal from dilute solutions. Its construction is similar to the plate and frame cell shown in Fig. 2.1. The metal is deposited on a gauze cathode in contact with a bed of non conducting glass beads, which are fluidized by the flow of electrolyte [1].

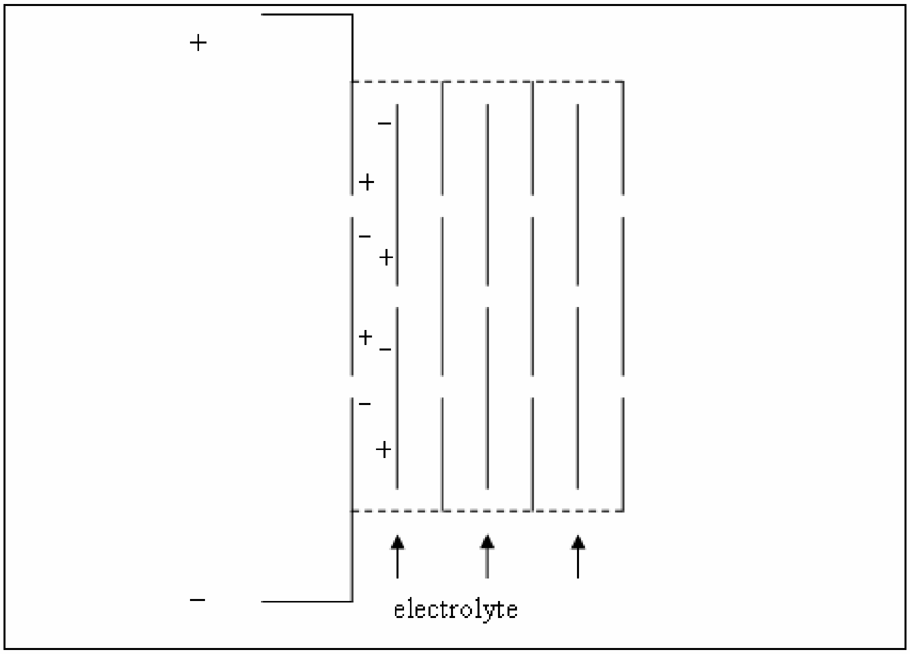

Fig. 2.2 Schematic diagram of a Seachlor cell [1].

4) Fluidized bed cell: Figure 2.3 shows a typical rectangular fluidized bed. The fluidized beds have been dealt with extensively through the body of this thesis.
5) Fixed bed cell: Figure 2.4 shows an example developed by the Nalco Chemical Company for the production of alkyl lead compounds. The modeling is easier than fluidized bed since the metal particles are in close contact with each other and hence charge transfer by electron flow as through a continuous conductor can be assumed [4].

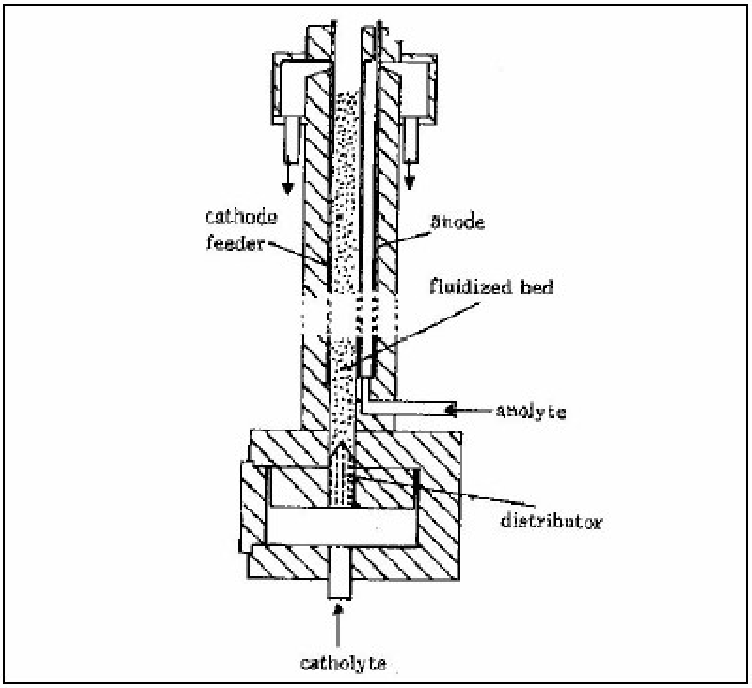

Fig. 2.3 Fluidized bed cell with rectangular geometry [1].

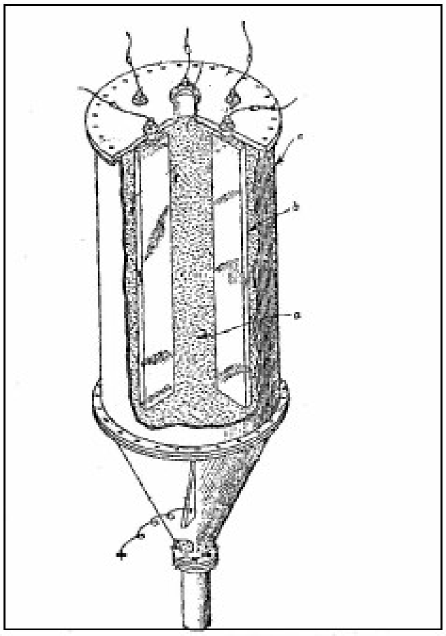

Fig. 2.4 Fixed bed cell with cylindrical shell [1].

2.4 Modes of Mass Transfer

The movement of material from one location in solution to another arises from differences in electrical or chemical potential at the two locations, or from movement of volume element of solution. The modes of mass transfer are:

1) Migration which is the movement of a charged body under the influence of an electric field (a gradient of electrical potential).
2) Diffusion which is the movement of a species under the influence of a gradient of chemical potential (concentration gradient).
3) Convection which is the stirring or hydrodynamic transport [5, 9, 10] as shown in Fig. 2.5.

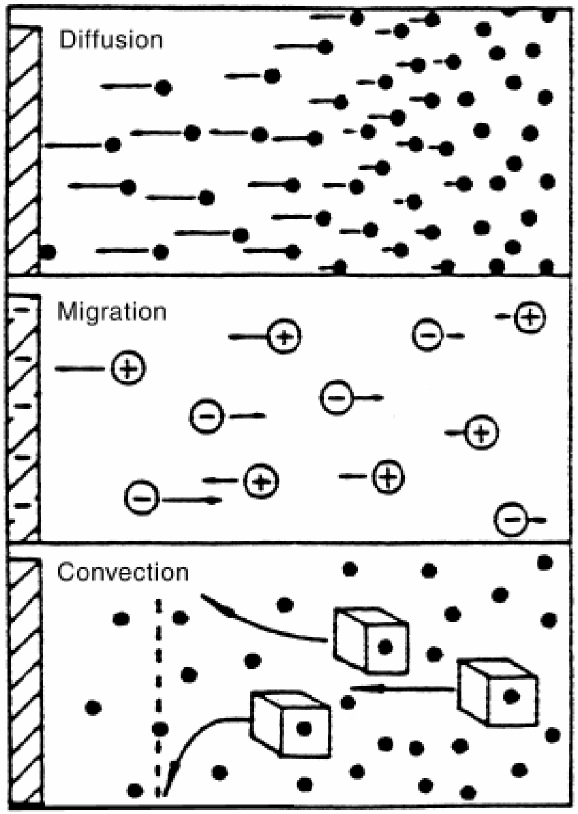

Fig. 2.5 The three modes of mass transfer [10].

Mass transfer to an electrode is governed by the Nernst-Planck equation, written for one dimensional mass transfer along the x-axis as

$$J_j(x) = -D_j \frac{\partial C_j(x)}{\partial x} - \frac{z_j F}{RT} D_j C_j \frac{\partial \phi(x)}{\partial x} + C_j u(x) \qquad 2.3$$

where $J_j(x)$ is the flux of species j (mol/sec.m^2) at distance x from the surface, D_j is the diffusion coefficient (m^2/s), $\partial C_j(x) / \partial x$ is the concentration gradient at distance x, $\partial \phi(x) / \partial x$ is the potential gradient, z_j is the number of electrons associated with the production of a molecule j, F is the Faraday number, C_j is the concentration of species i (mol/m^3), and $u(x)$ is the velocity (m/s) with which a volume element in solution moves along the axis [9].

The rate of electrochemical reaction is measured by the number of moles produced n_j at an electrode by a current I_j for t seconds [4].

$$n_j = \frac{I_j t}{z_j F} \qquad 2.4$$

for a number of reactions at an electrode we can write [4]

$$\sum n_j = \frac{t}{F} \sum \frac{I_j}{n_j} \qquad 2.5$$

where $\sum n_j$ is the total number of moles produced. The total current I is the sum of all currents [4].

$$I = \sum I_j \qquad 2.6$$

The current efficiency ε_j of a given species j is given by [4]

$$\varepsilon_j = \frac{I_j}{I} \qquad 2.7$$

The sum of the respective current efficiencies for all of the reactions in the systems is equal to unity ($\sum \varepsilon_j = 1$) [4].

2.5 Voltage Required for Electrolysis

The voltage required for electrolysis is the difference between the two terminals potential of the power supply, which is [6]

$$V = \phi_+ - \phi_- \qquad 2.8$$

where ϕ_+ and ϕ_- are the electrical potentials of the positive and negative terminals of the power supply. When there is no current applied, the voltage is called the minimum voltage ($V_{\min}$) which is [6]

$$V_{\min} = \frac{\Delta G}{zF} \qquad 2.9$$

where ΔG is the Gibbs free energy of the electrochemical reaction in J/mol. Another expression for $V_{\min}$ is found by Nernst equation[6]

$$V_{\min} = V^{\circ}_{\min} - \frac{RT}{zF} \ln \frac{\Pi a_R^{\,v_r}}{\Pi a_O^{\,v_o}} \qquad 2.10$$

$V^{\circ}_{\min}$ is the standard minimum electrolyzing voltage corresponding to unit activities of the oxidized and reduced species a_O and a_R. The electrolyzing voltage is written as [5]

$$V = (\phi_a - \phi_{s1}) + (\phi_{s1} - \phi_{s2}) + (\phi_{s2} - \phi_c) \qquad 2.11$$

where ϕ_{s1} and ϕ_{s2} are the solution potentials adjacent to the anode and cathode respectively, ϕ_a and ϕ_c are the anode and cathode potentials and equal to the positive and negative power supply terminals respectively. Fig. 2.6 shows the cases when there is a current flowing in the system, and the case of zero current [4].

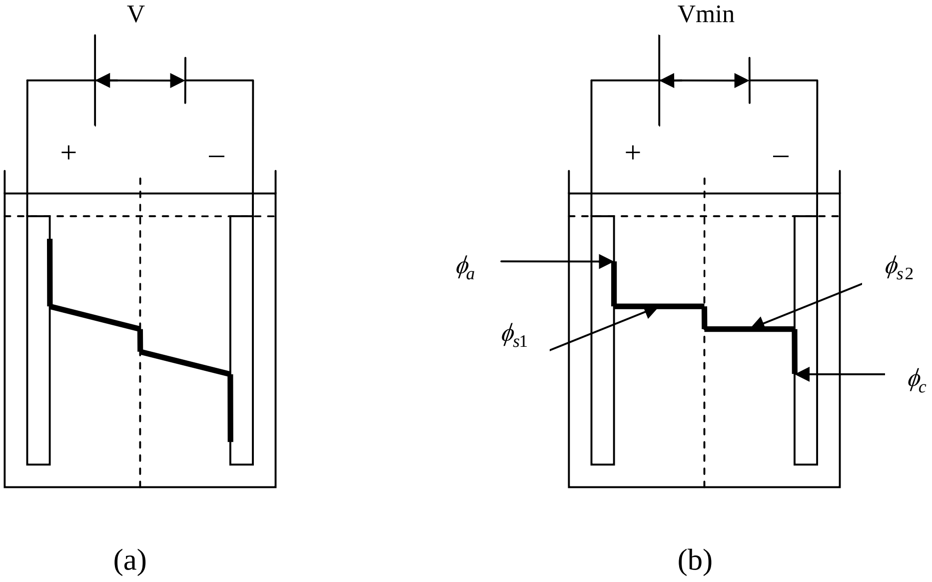

Fig. 2.6 The voltage components in a two compartment reactor. (a) Finite current (b) Zero current [4]

Equation 2.11 can be written in an alternative form by replacing the first and last term by the voltage of anode and cathode compartments, as follows [4]

$$V = V_a + (\phi_{s1} - \phi_{s2}) + V_c \qquad 2.12$$

or $$V = V_a - (-V_c) + (\phi_{s1} - \phi_{s2}) \qquad 2.13$$

The anodic and cathodic potential can be written in accordance with equation 2.10 as [6]

$$V_a = V_a^\circ - \frac{RT}{zF}\ln\frac{a_M}{a_M^{z+}} \qquad 2.14$$

and $$(-V_c) = (-V_c^\circ) - \frac{RT}{zF}\ln\frac{a_N}{a_N^{z+}} \qquad 2.15$$

where V_a° and V_c° are the standard anode and cathode potentials respectively, and M and N are the oxidized and reduced species respectively.

For processes which occur in a single compartment reactor, $(\phi_{s1} - \phi_{s2})$ vanishes and equation 2.13 becomes at equilibrium [4]

$$V = V_a - (-V_c) = V_{\min} \qquad 2.16$$

If both the electrode processes were perfectly reversible in the thermodynamic sense, it would be possible to pass a large current through the reactor without the electrode potentials deviating noticeably from their equilibrium values, an electrode which is capable of participating in a perfectly reversible process is referred to as ”non polarizing electrode” under such operation. In practical processes, an electrode shows deviation from any equilibrium potential and is said to be “polarized” or to exhibit polarization. The magnitude of this deviation in potential is known as the overpotential (η) or less frequently as the overvoltage. So, equation 2.16 can be written as [4]

$$V = V_a^* - (-V_c^*) + V_{ohm} \qquad 2.17$$

where V_{ohm} represents the voltage contribution due to the solution resistance. Subtracting equation 2.16 from 2.17and rearranging to get [5]

$$V = V_{\min} + (V_a^* - V_a) - (-V_c^* - (-V_c)) + V_{ohm} \qquad 2.18$$

$$V = V_{\min} + \eta_a - \eta_c + V_{ohm} \qquad 2.19$$

where η_a and η_c are the anodic and cathodic overpotentials defined by [5]

$$\eta_a = V_a^* - V_a \qquad 2.20$$

and $$\eta_c = -(V_c^*) - (-V_c) \qquad 2.21$$

Since the overpotential has a negative value but causes an increase in the operating voltage, we can write equation 2.19 in an alternative form [5]

$$V = V_{\min} + \eta_a + |\eta_c| + V_{ohm} \qquad 2.22$$

Two types of overpotential are arises in most of the systems. The first one is the “concentration overpotential” which is caused by change in the concentration of species participating in an electrode reaction. The second one is the “activation overpotential” which arises due to phenomena associated with an electrode reaction. The essential feature of any electrode reaction is electron transfer across the electrode/solution interface but this process is only one in a sequence of reaction steps. The typical sequence includes adsorption and desorption of reactants, products and intermediates together with surface diffusion and surface chemical reactions. The rate determining step will be the slowest step between them. The rate determining step represents the state of maximum energy for a system and the difference between these states and the original state is known as the activation energy [4].

2.6 Current, Exchange Current, Limiting Current and Tafel Equation

The general electrode reaction is $O + ze \rightleftharpoons R$. The current which flows when the electrode is polarized cathodically represent the difference between the rates of forward (cathodic) and reverse (anodic) reactions [11].

The current density (i) , which will be considered a positive quantity is [4]

$$i = i_c - i_a \qquad 2.23$$

where i_c and i_a is the partial current density for the cathodic and anodic reaction. By analogy with chemical kinetics, the rate of the forward reaction can be written as [4]

$$\frac{i_c}{zF} = k_c C_{OS} \qquad 2.24$$

where k_c is the electrochemical rate constant and C_{OS} is the concentration of O at the point close to the electrode surface, for reverse reaction we can write [4]

$$\frac{i_a}{zF} = k_a C_{RS} \qquad 2.25$$

where k_a and C_{RS} have corresponding meaning to those above. By substituting equations 2.24 and 2.25 into 2.23 to get

$$i = zFk_c C_{OS} - zFk_a C_{RS} \qquad 2.26$$

Using an Arrhenius type of rate constant activation energy type [11]

$$k_c = k_c^\circ \exp\left[\frac{-\alpha zF(-V_c^*)}{RT}\right] \quad 2.27$$

and $$k_a = k_a^\circ \exp\left[\frac{(1-\alpha)zF(-V_c^*)}{RT}\right] \quad 2.28$$

where k_c° and k_a° are standard rate constants referenced to some particular electrode potential, and α is the transfer coefficient. Substituting 2.27 and 2.28 into equation 2.26 to eliminate the rate constants k_c and k_a. We get [6]

$$i = zFk_c^\circ \exp\left[\frac{-\alpha zF(-V_c^*)}{RT}\right]C_{OS} - zFk_a^\circ \exp\left[\frac{(1-\alpha)zF(-V_c^*)}{RT}\right]C_{RS} \quad 2.29$$

At equilibrium, $-V_c^* = -V_c$, the bulk concentration of O and R are denoted by C_{O_b} and C_{R_b} respectively, and $i = 0$, so that [6]

$$i_\circ = zFk_c^\circ \exp\left[\frac{-\alpha zF(-V_c)}{RT}\right]C_{Ob} = zFk_a^\circ \exp\left[\frac{(1-\alpha)zF(-V_c)}{RT}\right]C_{Rb} \quad 2.30$$

where $i_\circ$ is the exchange current density and represents the rates of forward and reverse reactions at equilibrium. Substituting equations 2.30 into 2.29 to get [6]

$$i = i_\circ\left\{\frac{C_{OS}}{C_{Ob}}\exp\left[\frac{-\alpha zF\eta}{RT}\right] - \frac{C_{RS}}{C_{Rb}}\exp\left[\frac{(1-\alpha)zF\eta}{RT}\right]\right\} \quad 2.31$$

Cathodic polarization causes an increase in the forward reaction rate, and simultaneously, a decrease in the reverse reaction rate, so that initially the current arises steeply. The increase in the forward reaction rate is accompanied by a decrease in the concentration of O at the electrode surface. At low to moderate overpotentials, the rate of reduction of O is compensated by the low rate of mass transfer of O from the solution bulk, but at high overpotential, the surface concentration of O is limited by the rate of mass transfer. This results in a constant current density known as the “limiting current density" [4]. Fig. 2.7 shows the relation between overpotential and current.

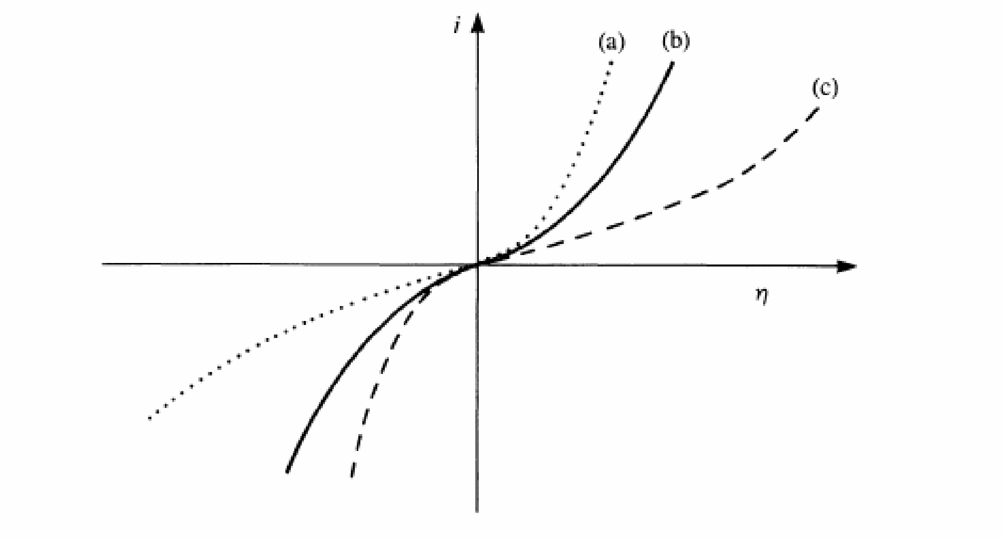

Fig. 2.7 The effect of the value of α on the current density, i (a) α = 0.25: oxidation favored (b) α = 0.50: symmetric (c) α = 0.75: reduction favored [6].

At low overpotentials, surface concentration of O and R do not much differ from their values in the bulk, so, equation 2.32 can be approximated to [5]:

$$i = i_\circ \left\{ \exp\left[\frac{-\alpha zF\eta}{RT}\right] - \exp\left[\frac{(1-\alpha)zF\eta}{RT}\right]\right\} \qquad 2.32$$

For appreciable cathodic polarization, the second exponential term is almost zero, so, equation 2.32 can be written as

$$i = i_\circ \left\{ \exp\left[\frac{-\alpha zF\eta}{RT}\right]\right\} \qquad 2.33$$

or $$\eta = \frac{RT}{\alpha zF}\ln i_\circ - \frac{RT}{\alpha zF}\ln i \qquad 2.34$$

It has been found experimentally that for many reactions, the cathodic overpotential can be expressed by an empirical equation [10]

$$\eta = a + b\log i \qquad 2.35$$

where $a = (RT\ /\alpha zF)\ln i_{\circ}$ and $b = -2.303RT\ /\alpha zF$

Nernst and Merriam suggested that mass transfer occurs solely by molecular diffusion through a thin layer of solution adjacent to an electrode. This layer has a linear concentration gradient across it and the outer edge which is assumed to be maintained at constant bulk concentration by migration and convection as shown in the next figure [9].

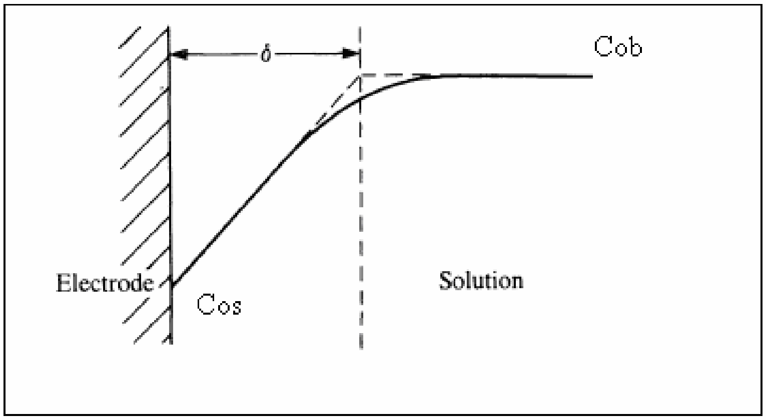

Fig. 2.8 Diffusion layer thickness [9]

The molar flux of O, N_o, across this diffusion layer can be expressed by Fick's Law as [4]

$$N_o = \frac{D}{\delta}(C_{Ob} - C_{Os}) \qquad 2.36$$

Flux can be expressed in terms of current density by Faraday's Law so that

$$\frac{i}{zF} = \frac{D}{\delta}(C_{Ob} - C_{Os}) \qquad 2.37$$

Noting that the smaller δ, the larger the concentration gradient at the electrode surface, leading to higher currents. The factor D/δ can be replaced by the mass transfer coefficient K_c. So, equation 2.37 can be written as [5]

$$\frac{i}{zF} = K_c(C_{Ob} - C_{Os}) \qquad 2.38$$

As the current density increases, the surface concentration of O decreases until it becomes so small that a substantially constant current density is reached. This constant current or limiting current density (i_L) can be expressed in the form of equation 2.38 with $C_{Os} = 0$ so that [5]

$$\frac{i_L}{zF} = K_c C_{Ob} \qquad 2.39$$

2.7 Pattern of Flow in Fluidized Bed

Fluidization is the operation by which fine solids are transformed into a fluidlike state through contact with a gas or liquid. By passing a fluid upward through a bed of fine particles as shown in Fig. 2.9, patterns of flow will appear in the bed. At a low flow rate, fluid merely percolates through the void spaces between stationary particles. This is a fixed bed. With an increase in flow rate, particles move apart and a few are seen to vibrate and move about in restricted regions. This is the expanded bed. At a still higher velocity, a point is reached when the particles are all just suspended in the upward flowing gas or liquid. At this point the frictional force between a particle and fluid counterbalances the weight of the particle. This is referred as an incipiently fluidized bed or a bed at minimum fluidization. In liquid solid systems, an increase in flow rate above minimum fluidization usually results in a smooth, progressive expansion of the bed. Gross flow instabilities are damped and remain small, and large scale bubbling or heterogeneity is not observed under normal conditions. A bed such as is called a particulate fluidized bed, a homogeneous fluidized bed, a smooth fluidized bed, or simply a liquid fluidized bed. Gas solid systems are beyond the scope of this thesis and generally, they behave in a quite different manner. With an increase in flow rate beyond minimum fluidization, large instabilities with bubbling and channeling of gas are observed [11].

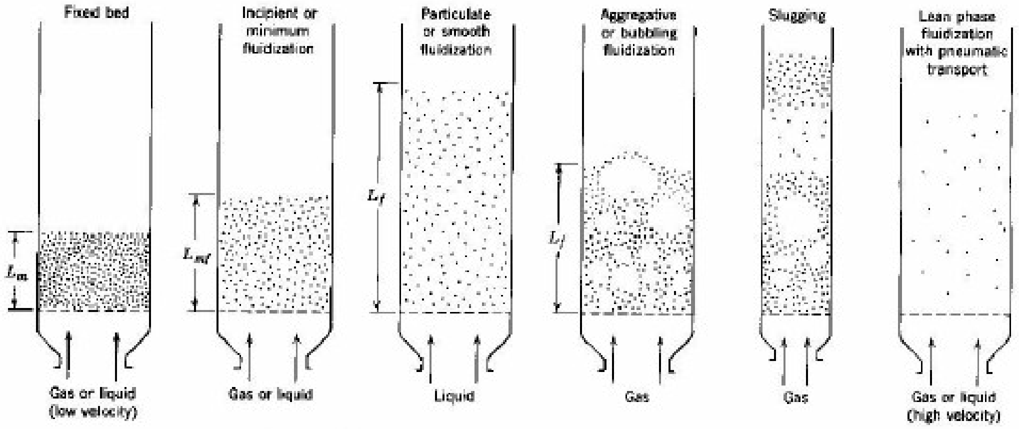

Fig. 2.9 Various kinds of contacting of a batch of solid by a fluid [11].

2.8 Literature Survey on Electrochemical Fluidized Bed

Many have written on bipolarity of electrochemical fluidized bed, **Goodridge in 1977** **[12]** studied monopolar and bipolar electrochemical fluidized bed. In monopolar bed all the particles behave either in a cathodic or anodic manner, while in bipolar bed each individual particle exhibits a cathodic and anodic side. Goodridge suggested that in monopolar fluidized beds, the electronic current I_m leaves or enters the bed via the current feeder; whilst the ionic current I_s does the same at the opposing boundary. The two basic equations for flow of current in the particulate bed and the electrolyte phase are:

$$I_m = -K_m A \frac{d\phi_m}{dx} \qquad 2.40$$

and $$I_s = -K_s A \frac{d\phi_s}{dx} \qquad 2.41$$

where ϕ_m and ϕ_s are the potentials in the metallic (dispersed phase) and in the solution phase respectively. x is the direction of current flow, A is the cross sectional area of the plane. K_s is the effective specific conductivity of the electrolyte modified by the voidage of the particulate phase, and K_m is dependent on hydrodynamic conditions and not simply the conductivity of solid modified by the porosity, two cases have been considered by assuming two relative values of K_s and K_m, first when assuming $K_m \gg K_s$ then for a potential dependent reaction, most of the activity occurs in the region furthest away from the current feeder in direction of current flow, whilst for case $K_m \approx K_s$, an inactive region is found in the center of that coordinate as shown in Fig. 2.10a and b.

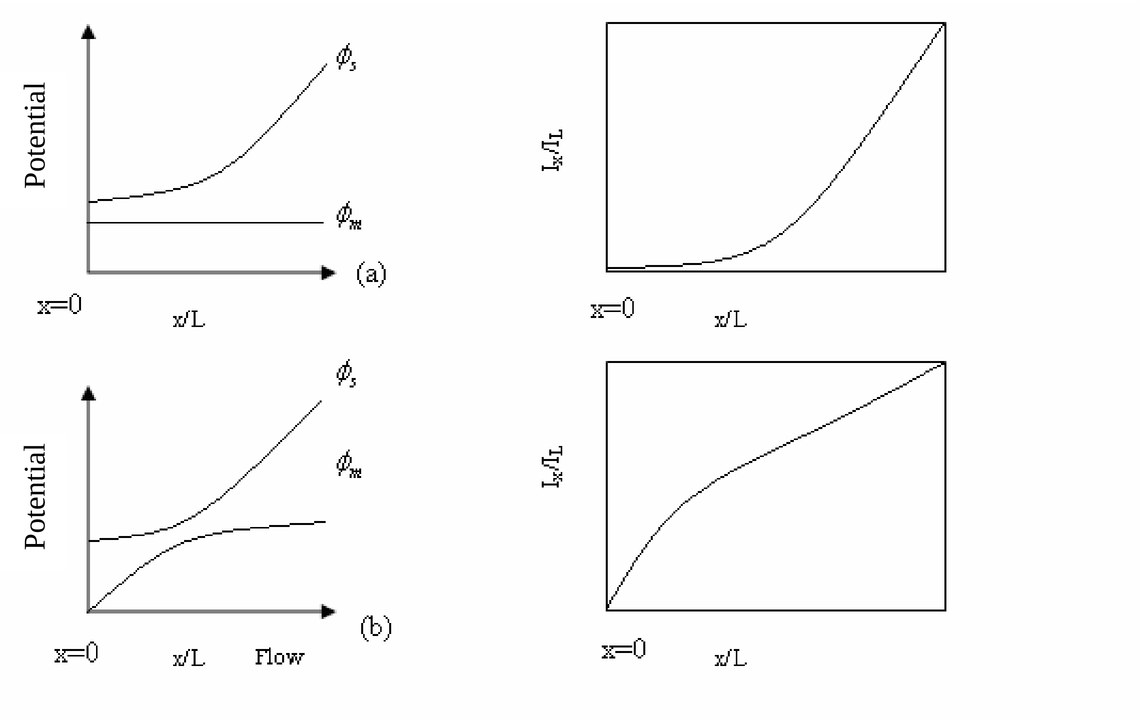

Fig.2.10 Potential and current distribution from monopolar bed prospective.

In bipolar bed, Goodridge suggested that the particle has anodic and cathodic sides, and because of particle rotation, anodic areas become cathodic and vice versa which leads to a self cleaning action which is analogous to an automatic current reversal.

Lee, Shemilt, and Chun in 1989 [13] studied the bipolarity in fluidized bed electrode; a series of experiments to determine the anodic reaction products on fluidized bed electrode reactor. The anodic reaction products were qualitatively measured in the reactor for both silver particle in acidic chloride solution system and copper particle in basic chloride solution system, and were quantitatively measured using the lead particle basic carbonate solution system. From the results, it may be concluded that charge transfer occurs by the bipolar mechanism in a nominally monopolar fluidized bed electrode. In the nominally cathodic fluidized bed electrode under the kinetically controlling step, the experimental current efficiencies have been found to be lower than the theoretical ones. This phenomenon can be explained by the presence of bipolarity in the bed. Anodic overpotentials due to the bipolarity causes metal dissolution to take place partly in the metal electrodeposition system, and therefore give current efficiencies lower than the theoretical ones. It has been found that the bipolar intensity increases for a decrease in superficial current density and slightly increased for an increase in bed voidage.

Goodridge, King, and Wright in 1977 [14] studied bipolar beds. They investigated three reactions, the production of hypobromite, the electrolysis of sea water, and the synthesis of dimethyl sebacate. It was shown that electrochemical fluidized bed can be used for a variety of different reaction systems, both inorganic and organic in nature. Advantages of the design are seen to be the simplicity of construction, the possibility of scale up, and the self cleaning action of the bed particles.

Fleischmann and Kersall in 1984 [15]studied copper deposition in fluidized bed electrode, they used solid copper powder sieved into the sizes ranges of 355-420, 420-500, 500-600, 600-710, 710-850, and 850-1000 μm. The supporting electrolyte was 0.5 M Na_2SO_4, and 10^{-3} M H_2SO_4. It was found that the data obtained in the investigation could be fitted by the equation

$$I = 2126 d^{-1.11} L^{-0.09} \eta^{1.17} \varepsilon^{-0.08} M^{0.40} u^{0.20} \qquad 2.42$$

where d is the particle diameter in m, L is the bed length in m, η is the overpotential in Volts, ε is the porosity, M is the concentration of copper in feed in mol/liter, and u is the superficial velocity in m/s. There is uncertainty in the exponent coefficients of L lay in the range -0.122 to -0.054 and ε in the range -0.1 to -0.056. It is significant that these two parameters were those containing the largest errors, as the bed lengths were merely read from a graduated scale.

Coeuret in 1980 **[16]** worked on continuous recovery of metals. Reviewing the application of the fluidized bed electrode to the recovery of metals and principally copper. In case of copper, Coeuret stated the problems of agglomeration and redissolution have been noted for solutions containing more than 1g/l of Cu^{+2}. Particle agglomeration is the problem which limits the operating duration time of electrochemical fluidized bed for metal recovery. In copper systems, the experiments showed anodic or pseudo anodic parts which do not exist when the bed is fixed, leads one to consider the significance that should be given to the concept of electrochemical fluidized bed. It could be that the bipolarity of the particles is the principal drawback, essentially due to the homogeneous character of the liquid solid fluidization.

Germain and Goodridge in 1976 **[17]** have studied the copper deposition using a mathematical analysis technique to obtain a potential distribution in the dispersed phase. Charge transfer occurring in fluidized bed can be expressed in terms of two charge transfer coefficients K_m for particulate phase and K_s for the electrolyte. The flowing current equations are the same as in equation 2.40 and 2.41 and the current and flow are having the same direction. The directions are the same as in Fig. 2.10. The total current (I_{total}) is written as:

$$I_{total} = I_M + I_S \tag{2.43}$$

or
$$I_{total} = -K_s A \left.\frac{d\phi_s}{dx}\right|_L = -K_s A \left.\frac{d\phi_s}{dx}\right|_x - K_m A \left.\frac{d\phi_m}{dx}\right|_x \tag{2.44}$$

and by rearranging

$$\left.\frac{d\phi_m}{dx}\right|_x = \frac{K_s}{K_m}\left(\left.\frac{d\phi_s}{dx}\right|_L - \left.\frac{d\phi_s}{dx}\right|_x\right) \tag{2.45}$$

and by integration to get

$$\phi_m\big|_x = \frac{K_s}{K_m}\left(\left.\frac{d\phi_s}{dx}\right|_L x - \int_0^x \left.\frac{d\phi_s}{dx}\right|_x dx\right) \tag{2.46}$$

And by the least square fitting and comparing with experimental data, they found that K_m decreases with increasing bed expansion as expected since it is a function of the frequency of particle contact.

Fleischmann and Kersall in 1984 [18] made a study of mercury deposition in a lead fluidized bed electrode as continuity to their work on copper deposition. The experimental results established that a lead fluidized bed electrode can be used for the removal of Hg(II) species from aqueous chloride solutions, as typified by chlor-alkali plant effluent. With careful choice of operating conditions, typical current efficiencies of 99% can be achieved, leaving too small amount of Hg(II) in solution.

Fleischmann, Oldfield, and Tennakoon in 1971 [19] studied electrodeposition of copper in a fluidized bed of copper coated spheres. They developed an expression for χ_m which is the effective resistivity of the discontinuous metal phase based on the assumption of charge sharing between the particles following elastic collisions in the fluidized bed. The theoretical expression which has been derived for χ_m is

$$\chi_m = \frac{0.28(1+\Gamma)^{\frac{2}{3}}((1+\Gamma)^{\frac{1}{3}}-1)E^{\frac{1}{3}}\chi_s}{(\rho_m-\rho_s)^{\frac{1}{3}}v_p^{\frac{2}{3}}} \qquad 2.47$$

where Γ is the expansion coefficient, E is the modulus of elasticity, χ_s is the effective specific resistivity of solution phase, ρ_m is the density of solid , ρ_s is the density of solution, and v_p is the mean particle velocity. The basic assumptions of this model are:

1) The collisions between particles are elastic.
2) The particle motion can be described by the simple kinetic theory of gases.
3) Charge transfer occurs by complete or partial charge sharing during collisions.

Kreysa in 1980[20] studied the particle phase conductivity of an electrochemical fluidized bed. Kreysa developed an expression for the particle phase conductivity and resistivity as

$$\chi_m = \frac{1}{K_m} = 0.159(1+\Gamma)^{1/3}((1+\Gamma)^{1/3}-1)(1-\varepsilon)/u_pC \qquad 2.48$$

where K_m is the conductivity of particle phase, χ_m is the resistivity, Γ is the relative bed expansion, ε is the voidage, u_p is particle velocity, and C is the double layer capacity. It was found that at high bed expansions a good agreement between experimental work and theory. But at low bed expansions, the experimental values are lower than theory.

LeRoy in 1987 [21, 22] studied the electrowinning in electrochemical fluidized bed, LeRoy studied the general modes of operation and the operation at constant current density. LeRoy developed a model which allows calculation of a fluidized bed under semi-continuous operating condition. The results showed the distribution of particle diameters in the cathode evolving from its initial form towards a steady state condition over a period of 10 to 40 electrowinning cycles. The steady state is attained as the last of the original electrode particles are removed from the electrode. By operating at constant current density, LeRoy found that decreasing electrowinning fractions will decrease the steady state electrode weight in the constant current density mode. Thus, a wide range of possible operating conditions could be envisioned under which a fluidized bed could be operated at constant current density.

Kreysa, Juttner, and Bisang in 1993 [23] studied packed and fluidized bed electrodes under limiting current conditions. These two types are also known as three dimensional electrodes. They can be realized by different arrangements with respect to the direction of current flow, electrolyte flow, and electrode positions. The following possibilities exist

A: Parallel current and electrolyte flow. (There is no principal difference between rectangular and cylindrical arrangements):

- i) Counter electrode positioned at the current feeder side of the bed electrode.
- ii) Counter electrode positioned opposite the feeder side of the bed electrode.

B: Current and electrolyte flowing at right angles.

- i) Rectangular arrangement with a counter electrode positioned at the feeder side of the bed electrode.
- ii) Rectangular arrangement with a counter electrode positioned opposite the feeder side of the bed electrode.
- iii) Cylindrical concentric arrangement with inner position of both the counter electrode and the feeder with a separator between them.

iv) Cylindrical concentric arrangement with outer position of the counter electrode and the feeder positioned centrally.

v) Cylindrical concentric arrangement with outer position of both the counter electrode and the feeder with a separator between them.

vi) Cylindrical concentric arrangement with central position of the counter electrode and outer position of the feeder.

From the experiments made by them, a number of conclusions have been reached:

1) The cylindrical arrangement of the bed presents a more complex situation than rectangular arrangement and the calculation of bed length requires a more detailed analysis of the effective resistivities of both phases together with geometric parameters.
2) For cylindrical packed bed electrodes with current and electrolyte flows at right angles, the largest bed depth is obtained with an external counter electrode.

Dweik, Liu, and Savinell in 1996 [24] studied the hydrodynamic modeling of the liquid solid behavior in the electrochemical fluidized bed. The experiments demonstrated that the fluid and particle dynamics of the liquid solid particle bed are a function of several parameters such as, particle size, particle density, solution flow rate, and cell tilt angle. Observations showed that as the fluid flow rate increases, the bed expands and begins to divide perpendicular to the flow direction into two distinct dynamic regions. The first region is the rising layer which is characterized by a narrow zone of particles moving upward with the fluid flow. The volume fraction in this zone is dilute. As the particles reach the top of the bed, the action of the gravity causes them to spill to the downward moving packed bed region of the cell thus forming the second region, the descending layer. This region is slightly expanded packed bed and it occupies the majority of the bed. When the particles reach the bottom of the cell, they reenter the rising layer. The pressure drop has been used to define the relative interstitial velocity in the descending layer. The rising layer is assumed to behave as an entrained bed, while the descending bed is assumed to be an expanded packed bed.

Hutin and Coeuret in 1977 [25] made experimental study on copper deposition in electrochemical fluidized bed. Hutin, and Coeuret used three electrolytes with different copper concentration with cylindrical copper particles (diameter 1mm, length 1.2mm). It is found that by using relatively high bed heights and high expansions, the bed is almost anodic and 80% of the bed is completely anodic. This very example is considered in detail in the next chapter. They found that copper deposition improved by increasing the current density and/ or decreasing bed porosity, and bed thickness in the direction of current flow. Low current efficiencies seem to be due to the existence of a definite dissolution zone within the bed.

Kreysa in 1978 [26] studied the kinetic behavior of electrochemical packed and fluidized beds. Kreysa stated that the electrochemical rate equation for reactions with full or partial diffusion is

$$i = f\,(\eta, c, u, T) \qquad 2.49$$

where i is the current, η is the overvoltage, u is the flow velocity, and T is the temperature. The current is related to rate by Faraday's Law. Equation 2.49 can be observed at a plane electrode in a laboratory cell. It was stated that electrochemical behavior of packed and fluidized beds is much more complicated by some more parameters

$$i = f\,(\eta, c, u, T, K_s, K_m, d_p, \varepsilon, L) \qquad 2.50$$

where K_s is the electrolyte conductivity, K_m is the particle conductivity, d_p is the particle diameter, ε is the voidage, and L is the bed depth. It was noted that not all of the parameters in equation 2.50 are independent from each other. The particle conductivity K_s is constant for a certain metal and changing only with voidage. Voidage also could be related to empty tube flow velocity. Because of small local current densities within electrochemical packed and fluidized beds, an isothermal behavior results, therefore the influence of temperature can be neglected. Also the particle diameter is constant, as only particles with constant diameter were available. Also, concentration could be assumed constant in entrance.

$$i = f\ (\eta, u, K_s, L)_{c,T,d_p} \qquad 2.51$$

It was concluded that both packed and fluidized bed electrodes can be described by the same theoretical concept.

Jiricny and Stanek in 1994 [27] studied the production of D-arabinose in a pilot plant fluidized bed electrochemical reactor. A new method was developed for the production of D-arabinose by direct electrochemical oxidation in an electrochemical tank type pilot plant reactor with the fluidized bed anode with an annual capacity of 1 metric ton of D-arabinose. This method has the following advantages:

i) The starting material is the reaction mixture from the fermentation oxidation of D-gluconate without addition of auxiliary electrolytes.

ii) The apparatus is constructed from non toxic materials satisfying criteria for a pharmaceutical production.

iii) Subsequent separation of the product from the reaction mixture is simple and unreacted gluconate is recycled.

iv) The amount of salts generated in the process is by several orders of magnitude less in comparison with other processes, such as the hypochlorite method.

v) The associated investment costs are low compared to plate-plate electrolysers, while the operation and maintenance is simple.

Walker and Wragg in 1980 [28] studied the mass transfer in fluidized bed electrochemical reactors. Two distinct cases have been studied:

a) Determination of mass transfer rates at a plane wall electrode in the presence of a fluidized bed of inert particles (glass beads). In this work, bed height, particle size, and fluidization conditions have been varied and a correlating equation:

$$j_D \varepsilon = 0.138 \left[\frac{\mathrm{Re}_{dp}}{(1-\varepsilon)} \right]^{-0.39} \left[\frac{d_p}{d_e} \right]^{-0.39} \qquad 2.52$$

is suggested over the range

$$0.936 < \frac{\mathrm{Re}_{dp}}{(1-\varepsilon)} < 67$$

b) Determination of mass transfer rates between electrolyte and particles within an active bed of conducting copper particles. Analysis of the data yields a correlating equation:

$$j_D = \frac{K_{av}}{U_{av}} Sc^{2/3} = 1.55 \left[\frac{\mathrm{Re}_{dp}}{(1-\varepsilon)} \right]^{-0.49} \qquad 2.53$$

in the range

$$2.6 < \frac{\mathrm{Re}_{dp}}{(1-\varepsilon)} < 30$$

where j_D is the mass transfer j-factor, ε is the bed voidage, K_{av} is the mass transfer coefficient, u is the fluid velocity, $Sc = \nu / D$, ν is the kinematic viscosity, D is the diffusion coefficient, $\mathrm{Re} = \frac{d_p u}{\nu}$, d_p is the particle diameter, and d_e is the channel equivalent diameter.

Shvab, Stefanjak, Kazdobin, and Wragg in 2000 [29,30] studied mass transfer in fluidized bed of inert particles. First they studied the role of collision currents in mass transfer to electrode with the bed containing PVC or Nylon spheres with electrolyte containing Cu^{+2} ions. A model describing the influence of particle-wall collisions on the mass transfer rate is proposed. The model assumes that the Cu^{+2} ions, penetrating the diffusion layer during collision and are completely consumed in electrochemical reaction, so, the collision currents can be calculated from the equation:

$$i_c = zFc_{\circ}f_r \sum \Delta V \tag{2.54}$$

where z is the number of electrons associated with the reaction, F is the Faraday's number, c_o is the bulk concentration of the electroactive species, f_r is collision frequency of particles per unit area, and ΔV is the value of the specific microvolume introduced into the diffusion layer by a single particle. The values of the collision currents i_c , to mass transfer to electrodes in fluidized beds of inert particles can be calculated from the proposed model and compared to those obtained from experimental data which is the experimental method of measuring i_c. This is explained in detail in the original paper. The values of i_c obtained by the two independent methods are in good agreement. So, the mass transfer contribution due to electrolyte flow increases with increase in particle diameter, while that due to particle collision decreases.

The second study is the effect of particle size and density on mass transfer. It was found that the use of particles of materials of different density in fluidized bed of inert particles allows variation of the contributory influences on mass transfer. In fluidized bed of inert particles, if the materials are of low density, then the influence of collisions prevails. If the bed is of high density, then the influence of interstitial velocity dominates. The ratio of the influences changes with reduction in the size of particles of the same density, since with reduction of particle size the influence of collision currents increases. These phenomena explain the smoothing of mass transfer maxima in beds of particles of both small and high density.

Roessler, Crettenand, Dossenbach, and Rys in 2003 [31] studied the reduction of indigo in fixed and fluidized beds of graphite granules. Graphite granules were used as electrode material in a fixed and fluidized bed reactor to address the question of the industrial feasibility of this new direct electrochemical reduction method for vat dyes. Optimized conditions in the system were required, and a scale-up in indigo concentration to 10 g/liter was achieved. Increasing pH and temperature can enhance the reduction rate, and a maximum conversion has been found by optimizing current density and flow velocity in the reactor. Special pretreatment of the graphite (i.e., soaking with hydrogen peroxide or preanodization) enhances the reduction rate by inducing the formation of quinine-like functional groups. Immobilizing noble metal particles on the graphite surface cause electrocatalytic hydrogenation in addition to the electron transfer process resulting in fair and good electrogenolysis efficiencies. These results are a basis for the further development of a cheap, continuously and ecologically working cell for the direct electrochemical reduction of dispersed indigo and other vat dyes. Especially, the introduction of surface functionalities by chemical reaction routes is at present an exciting research area. Hopefully, the immobilization of redox-active substances (i.e., metal complexes) will lead to even higher reduction rates. However, the next step will be pilot-plant trials after a scale-up procedure. Increasing the reactor size and indigo concentration to more than 100 g/liter may cause a blocking of the fixed bed. Therefore, optimization of the cell design will be a requirement for the successful realization of this method.

Scott in 1988 [32] studied circulating packed and fluidized bed electrochemical reactors. Scott studied the recovery of copper and proved that the recovery is more efficient when electrolyte solutions are of low pH. When only moderately acidic electrolytes are treated, the energy consumption incurs a double penalty in terms of lower current efficiency and a higher cell voltage resulting from the low electrolyte conductivity. The treatment of dilute metal bearing liquors may therefore benefit from the addition of a low grade acid. In general, the selection of device used in this application will be based on other factors as:

i) Mode of operation: to induce bed circulation relatively high liquid velocities are required to initiate particle transport. Only a relatively small fraction of the total flow passes through the packed bed region.

ii) Gas evolution: the occurrence of hydrogen evolution in metal deposition reactions is common and has to be identified as a contributing factor in the current efficiency of circulating electrodes. If the rate of gas evolution is relatively small, then due to the downward motion of the bed, slugging may occur.

iii) Scale up: this factor is of a prime importance if adoption of circulating bed technology is to be realized. In flow by electrodes, an increase in scale can only be effectively achieved in the two dimensions associated with the diaphragm or feeder cross sectional areas. Experience with a similar configuration of moving bed has shown that on scale up perpendicular to electrolyte flow, regions of the bed become stationary and susceptible to agglomeration during deposition.

Huh, Savaskan, and Evans in 1992 [33] studied regeneration of zinc particles and electrolyte by fluidized bed electrodeposition. It was suggested that this method appears to be an efficient way of regenerating zinc particles and electrolyte using different particles of copper, graphite, and lead. Reacheing the following results after a series of experiments:

i) The zinc particles can be regenerated without any operating problems by means of fluidized bed electrodeposition.

ii) Lead and graphite are more suitable materials than copper in terms of current efficiency. When cell voltage is considered, lead appears superior to graphite.

Zhou, Wu, Ma, Cong, Ye, and Wang in 2004 [34] studied electrochemical fluidized bed reactor for organic pollutant abatement. By investigating many parameters affecting the pollutant removal, it was found that higher liquid flowrate could improve mass transfer, which makes mass transfer no longer the reaction limiting step.

Rozik, Orinakova, Markusova, and Trnkova in 2006 [35] studied Ni-Co binary alloy deposition on iron powder particles in an electrochemical fluidized bed using voltammetric measurements. Electrodeposition of individual metals (Ni, Co) and binary alloy (Ni-Co) was studied. It was found that the deposition potentials were -1.000 V, -1.000 V, -1.120 V for Co, Ni-Co, and Ni, respectively. Using Tafel plot for the calculation of the charge transfer coefficient(conductivity of metal phase) in close proximity to the deposition potential of metals. It is found that with the increase of the number of powder particles in the bed, the charge transfer coefficient (metal phase conductivity) decreases, i.e. electrodeposition of the binary Ni-Co layer slows down. The values of charge transfer coefficient for the Ni-Co co-deposition were found to be lower than that for individual metals. It was found that the rate of binary alloy deposition increases with increasing cobalt ions concentration but it decreases with increasing nickel ion concentration. It was concluded that the co-deposition of Ni-Co was enhanced by less noble metal (Co) and inhibited by more noble metal (Ni).

Zhou and Lei in 2006 [36] studied the electrochemical regeneration of activated carbon loaded with *p*-nitrophenol in electrochemical fluidized bed. The regeneration parameters such as current density, flow rate, NaCl concentration, pH of the solution and regeneration time were systematically investigated to optimize performance and improve the cost-effectiveness of the process. Higher current density can achieve better regeneration efficiency but energy cost would also be elevated. It was also confirmed that the adsorption of organics was occurred in the micro pore of activated carbon, and during activated carbon regeneration the micro pore recovered gradually with the decomposition of organics by attack of active species such as hydroxyl radicals that generated by electrochemical oxidation.

Chapter Three

Theory of Particulate Beds

3.1 Introduction

Electrochemical fluidized bed is a type of electrochemical particulate bed reactors which utilizes a considerably large surface area available for the reaction and an electrical potential difference which induces the reaction. It provides a very large electrode area in proportion to their size (e.g. $10^6 m^2/m^3$ volume) and this is several times greater in magnitude than that for non porous structure (typically not greater than $10^2 m^2/m^3$ for a parallel plate system). These devices are exceptionally useful when dealing with low reactant concentration or slow reactions since they realize reasonable overall reaction rates. Particulate bed includes packed and fluidized beds and anything with the general category of porous electrodes such as sintered or a pasted electrode (a lead acid battery electrode) and those which are composed of discrete particles with little or no mechanical adhesion [4].

A conducting particle fluidized bed electrode has some advantages over a conventional electrode as high space time yields, low inventory of materials, and low operating costs. It also has uses in metal recovery from dilute solutions, and in the electrolysis of reactants with high activation energies. Several mechanisms for the charge transfer or flow of current through a conducting particle fluidized bed electrode have been proposed. One of the first postulated mechanisms was the so called ”collisional mechanisms” which described the passage of current in terms of the transfer of discrete packages of charge from feeder to particle and particle to particle by a charge sharing process following collision. Simple calculations based on the capacitance of a single particle indicated that for this mechanism to account for observed currents, collision frequencies with the order of 10^5-10^6 $s^{-1}cm^{-2}$ would be necessary. Such a frequency seems unrealistically high, concluding that charge transfer based upon single particle collisions was unable to account for the observed behavior of fluidized beds. The second mechanism is based on the collision of aggregates of particles, based on measurements of bed effective resistivities as a function of the frequency of an imposed alternating current. In this mechanism, chains of particle are assumed to be in contact with the current feeder, and the current is passed through these continuous chains. However, these two monopolar mechanisms may not be appropriate for explaining the phenomenon of a non-cathodically protected zone (or anodic zones) appearing in the bed when the overpotential distributions are measured in a nominally cathodic fluidized bed. At low current density and high bed voidages, the current efficiencies are negative. Fluidized systems are, however, dynamic and when conditions in the bed are examined as a function of time it is observed that the local overpotentials in a nominally monopolar bed are characterized by rapid fluctuations, both anodic and cathodic, and that the peak values attained on either side of the rest potential are comparable [13]. This leads to the recently proposed the "bipolar mechanisms" which will be explained in this thesis.

A particulate bed electrode may consist of one of the three configurations shown in Fig. 3-1.

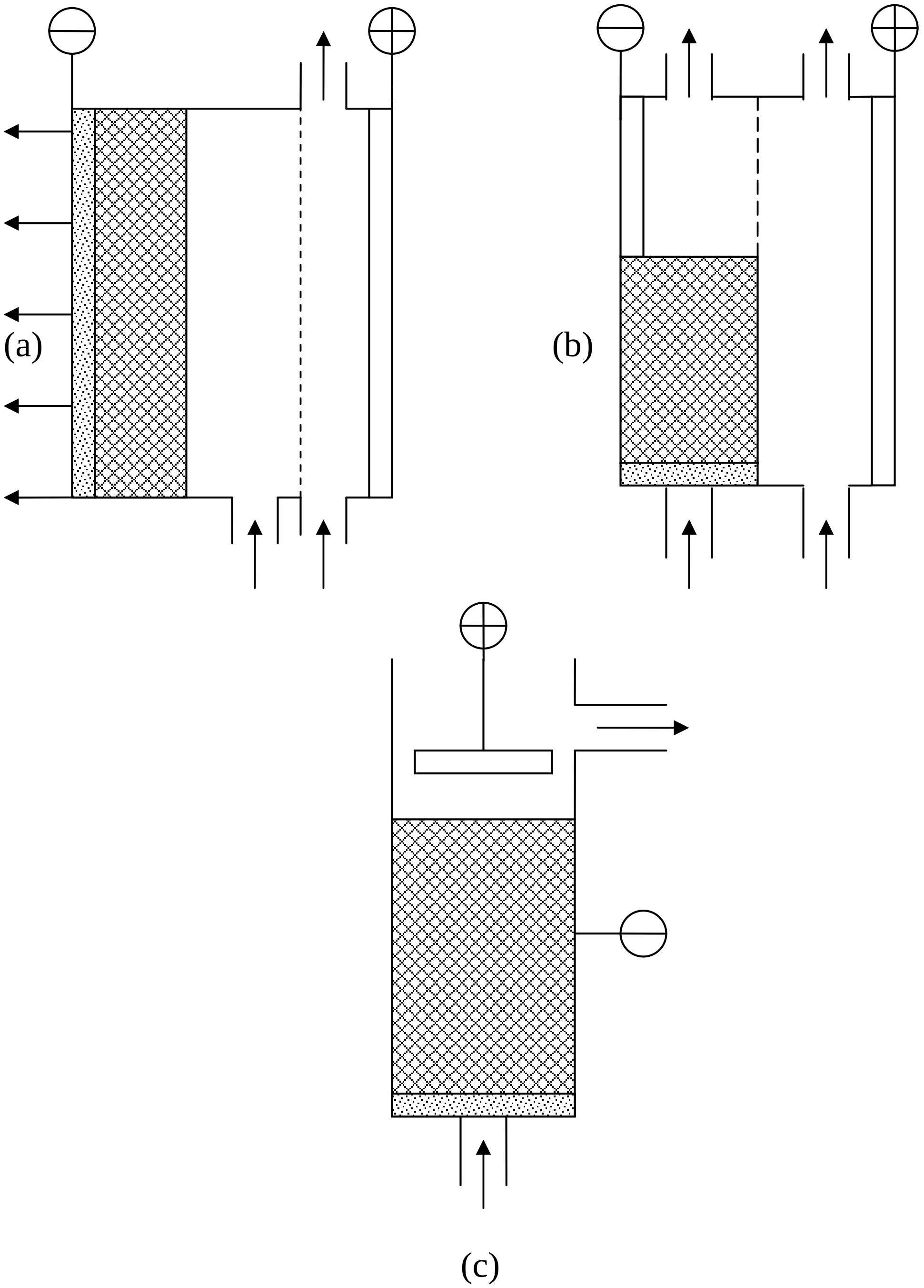

Fig. 3-1 Particulate electrode configurations (a) “flow through“ two compartment reactor(packed bed) (b) “flow by” two compartment reactor(packed bed) (c) ”Flow through” single compartment reactor(fluidized bed) [4].

In Fig. 3-1 (a) two compartment reactor with flow through model is considered. The electrode is a slab of porous material with a perforated solid backing plate at one end which functions as the current "feeder" or "collector". Flow of current goes through the metal and solution phases concurrently with the solution. In Fig. 3-1 (b) the flow of solution and electricity are orthogonal and we could distinguish between situations (a) and (b) as "flow through" or "flow by" systems respectively. In Fig. 3-1 (c) a "flow through" single compartment reactor model is considered. Two modes of reactions are considered here; fast and slow reaction. The complexity of operation of a particulate electrode is easily envisaged from the one dimensional sketch in Fig. 3-2. The total electric charge passing through the electrode normal to the flow is constant from continuity considerations [4].

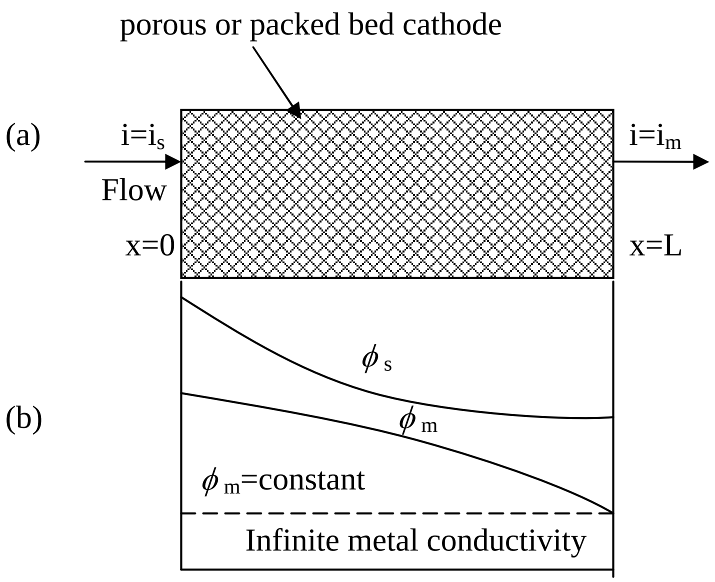

Fig. 3-2 One dimensional particulate bed cathode a) current and solution paths b) solution and metal potential distribution along the electrode [4].

3.2 Bipolarity in Electrochemical Fluidized Bed

In the bipolar mechanism, it is proposed that particle aggregates formed in a nominally monopolar electrochemical fluidized bed are made partly bipolar when they are isolated from the current feeder. Aggregates in contact with the feeder take on the same polarity as the feeder. Anodic and cathodic polarities on each side of an aggregate isolated from the feeder give rise to appropriate anodic and cathodic reactions in the coulombic sense [13]. The behavior of single particle is shown in the next figure (Fig. 3.3) where $(-V_c^*)$ is the potential difference and r is the radius.

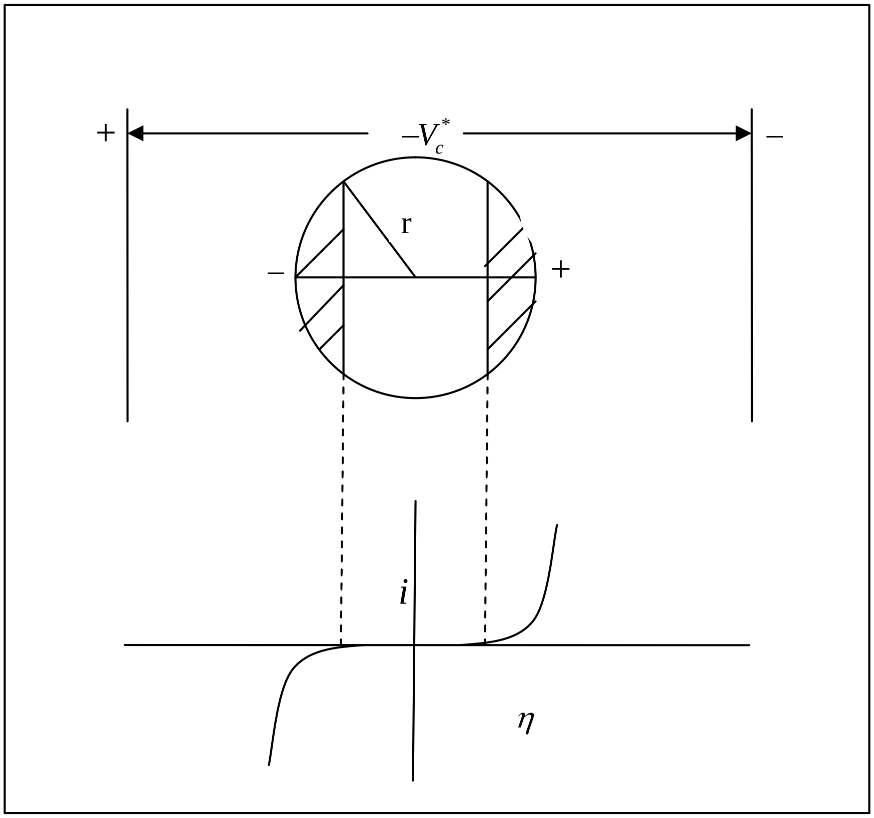

Fig. 3.3 Polarization of particles [14].

Typical fluidized bed behaves in one of two ways. When the bed height is relatively low, the bed behaves as a monopolar cathodic bed with no anodic pockets appearing. When the bed height increases, the bipolarity reveals and increases rapidly and about 80% of the bed is completely anodic. Fig 3.4 represents the work of Hutin, and Coeuret [25]. In their work the influence of bed height L on the overpotential η at constant current density and bed porosity was considered. One can see that a thin fluidized bed electrode behaves cathodically at every point including the current feeder but that the local electrochemical activity increases rapidly with the distance above the feeder. For higher bed heights, positive values of the overpotential which characterize anodic behavior appear in the distributions [25].

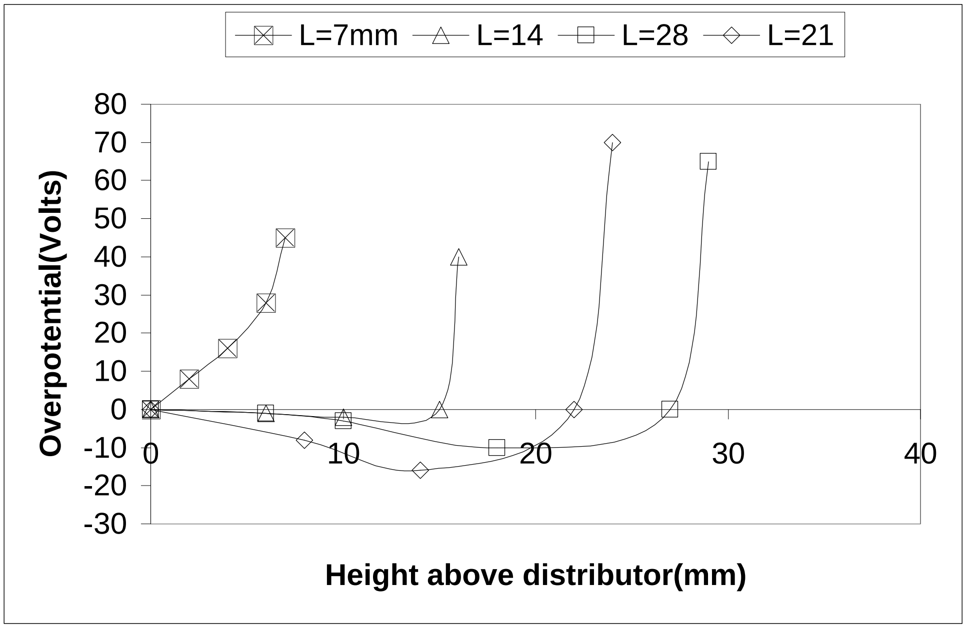

Fig.3.4 Effect of height on fluidized bed electrode overpotential distributions [25].

3.3 Metal Phase Resistivity

A number of papers have been published concerning metal phase resistivities, the papers were mentioned in Chapter Two. However, they will be dealt with again:

A) Model based on charge sharing during collision: The metal phase resistivity which is the reciprocal of conductivity has been derived based on the following assumptions [37]:

- i) Charge transfer in an electrochemical fluidized bed occurs by complete or partial charge sharing during collision.
- ii) Collisions between particles are elastic.
- iii) The motion of a single particle can be satisfactorily mapped by assuming that the remaining particles from a stationary matrix (as in the simple kinetic theory of gases).

Fleischmann and Oldfield [37] reached the following expression for resistivity of metal phase χ_m which is

$$\chi_m = \frac{0.28(1+\Gamma)^{\frac{2}{3}}((1+\Gamma)^{\frac{1}{3}}-1)E^{\frac{1}{3}}\chi_s}{(\rho_m-\rho)^{\frac{1}{3}}v_p^{\frac{2}{3}}} \qquad 2.47$$

where Γ is the expansion coefficient of fluidized bed, E is the modulus of elasticity, χ_s is the effective specific resistivity of solution phase, ρ is the density of electrolyte, ρ_m is the density of metal, and v_p is the interstitial velocity. The interstitial velocity equals U_{av} / ε

B) Model based on resistance of the solution between two particles, Kreysa [20] developed the expression

$$\chi_m = \frac{1}{K_m} = 0.159(1+\Gamma)^{1/3}((1+\Gamma)^{1/3} - 1)(1-\varepsilon)/u_p C \qquad 2.48$$

where K_m is the conductivity, χ_m is the resistivity, Γ is the relative bed expansion, ε is the voidage, u_p is particle velocity, and C is the double layer capacity.

The work of Fleischmann, and Oldfield [19] found that the numerical factor in equation 2.47 must be divided by 6.7. So, equation 2.47 becomes

$$\chi_m = \frac{0.04179(1+\Gamma)^{\frac{2}{3}}((1+\Gamma)^{\frac{1}{3}} - 1)E^{\frac{1}{3}}\chi_s}{(\rho_m - \rho\ )^{\frac{1}{3}}\nu_p^{\frac{2}{3}}} \qquad 3.1$$

The reason for this discrepancy that the fluidization being not uniform across the bed and there is a small stagnation zone close to the feeder. Equation 3.1 has been tested and a good agreement was obtained. In order to be used in this work, the reciprocal of resistivity which is the conductivity is adopted as shown in equation 3.2

$$K_m = \frac{23.928K_s(\rho_m - \rho)^{1/3}\nu_p^{2/3}}{(1+\Gamma)^{1/3}[(1+\Gamma)^{1/3} - 1]E^{1/3}} \qquad 3.2$$

The solution resistivity χ_s is a function of porosity and can be found from the following expression [38]

$$\chi_s = \chi_s^{\circ}/\varepsilon \qquad 3.3$$

where χ_s° is the resistivity of particles free solution, and ε is the porosity of bed.

3.4 Hydrodynamics of Fluidized Bed

Fluidization is the process by which a bed of solids is changed to a fluid-like state by the passage of a gas or liquid through the bed. If the fluid velocity is initially very low, the bed behaves as a packed bed. If the fluid velocity continues to rise, then fluidization occurs [39].

The fractional expansion Γ in equation 3.2 can be easily related to the voidage of the electrode under static conditions $\varepsilon_\circ$ and height at static and fluidized conditions [40].

$$\Gamma = \frac{\varepsilon - \varepsilon_\circ}{1 - \varepsilon} \qquad 3.4a$$

$$\Gamma = \frac{L - L_\circ}{L_\circ} \qquad 3.4b$$

where $L_\circ$ and L are the bed heights under static and fluidized conditions respectively. The average velocity can be found by [4].

$$\varepsilon = \left(\frac{U_{av}}{u_t}\right)^{0.225\left(\frac{u_t d}{\upsilon}\right)^{0.1}} \qquad 3.5$$

where u_t is the terminal settling velocity and is calculated from the following relationships, U_{av} is the average solution velocity in the empty section of the bed, and ν is the kinematic viscosity. The terminal settling velocity is calculated from the following relations [11]:

$$u_t = \frac{g(\rho_s - \rho) d^2}{18\mu} \qquad \text{for} \quad Re_p < 0.4 \qquad 3.6a$$

$$u_t = \left[\frac{4}{225}\frac{(\rho_m - \rho)^2 g^2}{\rho\mu}\right]^{1/3} d \qquad \text{for} \quad 0.4 < Re_p < 500 \qquad 3.6b$$

$$u_t = \left[\frac{3.1 g\,(\rho_m - \rho) d}{\rho} \right]^{1/2} \qquad \text{for} \quad 500 < Re_p < 200{,}000 \qquad 3.6c$$

where g is the gravitational acceleration, ρ is the density of solution, ρ_m is the particle density, μ is the viscosity, and $\mathrm{Re_p} = {u_t d\,\rho}/{\mu}$.

For nonspherical particles the diameter may be replaced by equivalent diameter which is defined as [11]

$$d_{eq.} = (\text{diameter of sphere having the volume of particle}) \qquad 3.7$$

For nonspherical particles, a variety of measures of nonsphericity can be used; we define sphericity as [39]

$$\phi = (\text{surface of sphere/surface of particle})_{\text{both of same volume}} \qquad 3.8$$

With this definition, $\phi = 1$ for sphere, and $0 < \phi < 1$ for all other particle shapes. Table 4.1 lists calculated sphericities of different solids. Each equation contains the term (d) is replaced by ($\phi\, d$) [45].

Table 3.1 Data on sphericity ϕ [11].

Material	ϕ
Sand	0.600-0.861
Iron catalyst	0.578
Bituminous coal	0.625
Celite cylinders	0861
broken solids	0.63
Silica	0.554-0.628
pulverized coal	0.696

The pressure drop through fixed beds of uniformly sized solids has been correlated by Ergun using the equation [45].

$$\frac{\Delta p}{L} = 150\frac{(1-\varepsilon)^2}{\varepsilon^3}\frac{\mu U_{av}}{d_p^2} + 1.75\frac{(1-\varepsilon)}{\varepsilon^3}\frac{\rho U_{av}^2}{d_p} \qquad 3.9$$

Fluidization occurs when

(drag force by upward moving fluid)= (weight of particles)

or

(pressure drop across bed)(cross sectional area of tube)=

(volume of bed)(fraction of solids)(specific weight of solids)

or

$$\Delta p.A = A.L(1-\varepsilon)(\rho_m - \rho)g$$

by rearranging , we find that for fluidized condition [11].

$$\frac{\Delta p}{L} = (1-\varepsilon)(\rho_m - \rho)g \qquad 3.10$$

The pressure drop (ΔP) is drawn versus Reynolds number $\mathrm{Re} = {U_{av} d}/{\nu}$ as shown [41].

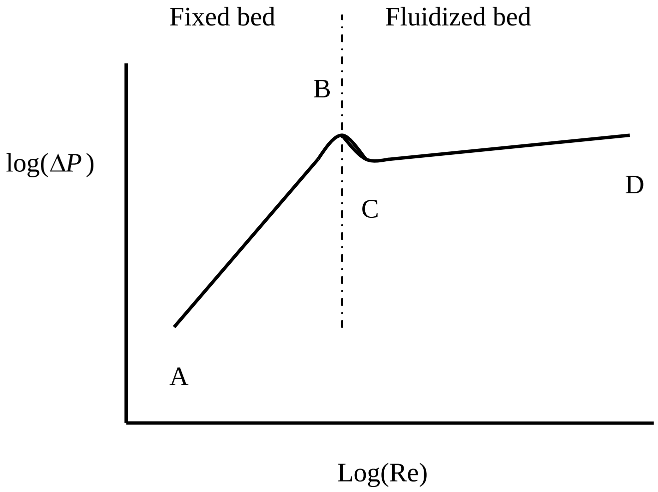

Fig. 3.5 Pressure drop change with Reynolds number [41].

The minimum fluidizing velocity(U_{mf}) can be found by combining equation 3.9 and 3.10 so that [11]

$$\frac{1.75}{\phi\varepsilon_{mf}^{3}}\left(\frac{dU_{mf}\,\rho}{\mu}\right)^{2}+\frac{150(1-\varepsilon_{mf})}{\phi^{2}\varepsilon_{mf}^{3}}\left(\frac{dU_{mf}\,\rho}{\mu}\right)=\frac{d^{3}\rho(\rho_{m}-\rho)g}{\mu^{2}} \qquad 3.11$$

where ε_{mf} is the porosity at minimum fluidization, and is found experimentally. The surface area per unit volume in an expanding bed is found by [4]:

$$a=\frac{a_{\circ}(1-\varepsilon)}{(1-\varepsilon_{\circ})} \qquad 3.12$$

The surface area per unit volume for a spherical particle can be found from definition as [39]

$$a_{\circ}=\frac{4\pi r^{2}}{\frac{4}{3}\pi r^{3}}(1-\varepsilon_{\circ})=\frac{3}{r}(1-\varepsilon_{\circ})=\frac{6}{d}(1-\varepsilon_{\circ}) \qquad 3.13$$

3.5 Mass Transfer in Fluidized Bed

In order to use this model for designing an electrochemical fluidized bed reactor, a suitable mass transfer correlation is required [40]. The equation for mass transfer is

$$\frac{K_{av}d}{D}=1.52\frac{(1-\varepsilon)^{1/2}}{\varepsilon}\mathrm{Re}_{d}^{1/2}Sc^{1/3} \qquad 3.14$$

where $Re_{\mathrm{d}}=\frac{U_{av}d}{\nu}$ and $Sc=\frac{\nu}{D}$

3.6 Mathematical Modeling of Polarization Equations and Potential Distribution

Two models have been developed in two different ways, the first one is the Fleishmann and Oldfield model [38] which uses direct integration of second order equations , and the second one is using the Laplace transformation to solve the differential equations of overpotential distribution.

3.6.1 Fleischmann and Oldfield Model

Starting with Ohm's law, we can apply it to the mobile solid section of the electrode. The current flow through the electrode can be expressed in the following way as [38]

$$i = \chi_m^{-1} \frac{d\phi_m}{dx} \qquad 3.15$$

where i is the local current density, χ_m is the effective resistivity of the discontinuous metallic phase, ϕ_m is the metal potential, and x is the distance. By applying Ohm's law for the flow of solution within the continuous phase. [4]

$$i = -\chi_s^{-1} \frac{d\phi_s}{dx} \qquad 3.16$$

where χ_s is the effective resistivity of the solution phase, and ϕ_S is the solution potential. If we consider the current flow in a section of the electrode dx , then the polarization equation can be written as [38]

$$di = f(\eta, C) a dx \qquad 3.17$$

Where η is the local activation polarization, $\phi_m - \phi_s$, C is the concentration of the reactive species and a is the surface area per unit volume. Combining equations 3.15, 3.16, and 3.17 to get the two primary equations [38]:

$$\chi_m^{-1}\frac{d^2\phi_m}{dx^2}-af(\eta,C)=0 \qquad 3.18$$

$$\chi_s^{-1}\frac{d^2\phi_s}{dx^2}+af(\eta,C)=0 \qquad 3.19$$

The two cases of polarization have been considered, activation, and concentration polarization.

Starting with Butler-Volmer equation 2.32 as a starting point, two cases have been considered, but with the overpotential has a negative sign [5,38]

$$i=i_\circ\left\{\exp\left[\frac{\alpha zF\eta}{RT}\right]-\exp\left[\frac{(\alpha-1)zF\eta}{RT}\right]\right\} \qquad 2.32$$

The first case is when $\eta \ll \frac{RT}{\alpha zF}$ or close to equilibrium, the second case is when $\eta \gg \frac{RT}{\alpha zF}$ or far from equilibrium, and the third case is mass transfer controlled.

3.6.1.1 Irreversible Process Close to Equilibrium

For the case when $\eta \ll \frac{RT}{\alpha zF}$, equation 3.19 can be reduced by taking the first two terms of the power series of the exponent terms. So,

$$i=f(\eta,C)=i_\circ\left\{1+\frac{\alpha zF\eta}{RT}-\left[1+\frac{(\alpha-1)zF\eta}{RT}\right]\right\}=\frac{i_\circ zF\eta}{RT} \qquad 3.20$$

by substituting equation 3.20 into 3.18 and 3.19 to get [38]

$$\chi_m^{-1}\frac{d^2\phi_m}{dx^2}-a\frac{i_\circ zF\eta}{RT}=0 \qquad 3.21$$

and $$\chi_s^{-1}\frac{d^2\phi_s}{dx^2}+a\frac{i_\circ zF\eta}{RT}=0 \qquad 3.22$$

Multiplying 3.21 by χ_m and 3.22 by χ_s, and subtracting the second equation from the first one to get

$$\frac{d^2\phi_m}{dx^2}-\frac{d^2\phi_s}{dx^2}-\frac{ai_\circ(\chi_m+\chi_s)zF\eta}{RT}=0 \qquad 3.23$$

The overpotential is defined as [19]

$$\eta=\phi_m-\phi_s \qquad 3.24$$

differentiating equation 3.24 twice to get

$$\frac{d^2\eta}{dx^2}=\frac{d\phi_m^2}{dx^2}-\frac{d\phi_s^2}{dx^2} \qquad 3.25$$

substituting equation 3.25 into 3.23 yields [38]

$$\frac{d^2\eta}{dx^2}-\frac{ai_\circ(\chi_m+\chi_s)zF\eta}{RT}=0 \qquad 3.26$$

Equation 3.26 can be integrated to get *[38]

$$\frac{d\eta}{dx}=\pm\left\{\frac{ai_\circ(\chi_m+\chi_s)zF\eta^2}{RT}-Y_1\right\}^{\frac{1}{2}} \qquad 3.27$$

$$\eta=\pm\left\{\frac{RTY_1}{ai_\circ(\chi_m+\chi_s)zF}\right\}\cosh\left\{\left(\frac{ai_\circ(\chi_m+\chi_s)zF}{RT}\right)^{\frac{1}{2}}x+Y_2\right\} \qquad 3.28$$

where Y_1 and Y_2 are the integration constants.

The boundary conditions for solving this equation are [38]:

$$\phi_m=\phi_m^\circ=\eta;\quad \phi_s=0 \text{ at } x=0 \qquad 3.29$$

$$\frac{d\phi_m}{dx}=0\ ;\quad \frac{d\phi_s}{dx}=\frac{d\eta}{dx} \text{ at } x=L \qquad 3.30$$

---

[*] The details of integration are in Appendix A-1

$$\frac{d\phi_s}{dx} = 0 \;\; ; \;\; \frac{d\phi_m}{dx} = \frac{d\eta}{dx} \text{ at } \; x=0 \qquad 3.31$$

The boundary conditions can be used to find the polarization equation as follows [38]

$$\frac{\left\{1 - I^2(\chi_m - \chi_s)/\gamma\phi_m^{\circ 2}\right\}^{\frac{1}{2}} + I\chi_s/\gamma^{\frac{1}{2}}\phi_m^{\circ}(\chi_m + \chi_s)^{\frac{1}{2}}}{1 - I\chi_m/\gamma^{\frac{1}{2}}\phi_m^{\circ}(\chi_m + \chi_s)^{\frac{1}{2}}} = \exp\left\{\gamma^{\frac{1}{2}}(\chi_m + \chi_s)^{\frac{1}{2}}L\right\}$$

……. 3.32

where

$$\gamma = {}^{ai_\circ zF}\!/\!_{RT} \qquad 3.33$$

The solution and metal phases potential profiles are found from Ohm's Law as follow [4]:

$$i_s = -\chi_s^{-1}\frac{d\phi_s}{dx} \qquad 3.34$$

$$i_m = -\chi_m^{-1}\frac{d\phi_m}{dx} \qquad 3.35$$

The total current density (*I*) is defined as [16]

$$I = i_m + i_s \qquad 3.36$$

Equation 3.34 and 3.35 substituted into 3.36, rearranged and integrated to get [38]

$$\eta(x) = \phi_m - \phi_s = \phi_m^{\circ} - I\chi_m x - (1 + \frac{\chi_m}{\chi_s})\phi_s \qquad 3.37$$

substituting equation 3.37 and the boundary conditions into equation 3.28 to get the solution potential profile as [38]

$$\frac{(1-\theta)+\left\{\theta^2-2\theta+I^2\chi_m^2/\gamma\phi_m^{\circ 2}(\chi_m+\chi_s)\right\}^{\frac{1}{2}}}{1-I\,\chi_m/\gamma^{\frac{1}{2}}\phi_m^{\circ}(\chi_m+\chi_s)^{\frac{1}{2}}}=\exp\left\{\gamma^{\frac{1}{2}}(\chi_m+\chi_s)^{\frac{1}{2}}x\right\} \qquad 3.38$$

where $$\theta=\left\{I\,\chi_m x+\left(\frac{\chi_m}{\chi_s}+1\right)\phi_s\right\}\Big/\phi_m^{\circ} \qquad 3.39$$

3.6.1.2 Irreversible Process Far from Equilibrium

For the case when $\eta \gg \frac{RT}{\alpha zF}$, equation 2.32 can be reduced by neglecting the second exponent term. So, [5]

$$i=f\,(\eta,C)=i_{\circ}\exp\left[\frac{\alpha zF\eta}{RT}\right] \qquad 3.40$$

Substituting equation 3.40 into 3.18 and 3.19 and subtracting in the same way before to get the following equation:

$$\frac{d^2\eta}{dx^2}-ai_{\circ}(\chi_m+\chi_s)\exp\left(\alpha zF\eta\big/RT\right)=0 \qquad 3.41$$

Equation 3.41 can be integrated to get †[38]:

$$\frac{d\eta}{dx}=\pm\left\{\frac{2i_{\circ}aRT}{\alpha zF}(\chi_m+\chi_s)\exp\left(\alpha zF\eta\big/RT\right)+Y_3\right\}^{\frac{1}{2}} \qquad 3.42$$

$$\eta=\pm\frac{RT}{\alpha zF}\left[\ln\left\{\cos\left(\frac{\alpha zFY_3^{\frac{1}{2}}x}{2RT}+Y_4\right)\right\}-\ln\left\{\frac{Y_3^{\frac{1}{2}}\alpha zF}{2i_{\circ}aRT\,(\chi_m+\chi_s)}\right\}\right] \qquad 3.43$$

where Y_3 and Y_4 are the integration constants, finding the constants will give the following polarization equation

---

† The details of integration are in Appendix A-2

$$\cos^{-1}\left\{1-\frac{I^{2}\chi_m^{2}}{\beta(\chi_m+\chi_s)}\exp-f\,\phi_m^{\circ}\right\}^{\frac{1}{2}}+\cos^{-1}\left\{\frac{1-\dfrac{I^{2}\chi_m^{2}}{\beta(\chi_m+\chi_s)}\exp-f\,\phi_m^{\circ}}{1-\dfrac{I^{2}(\chi_m^{2}-\chi_s^{2})}{\beta(\chi_m+\chi_s)}\exp-f\,\phi_m^{\circ}}\right\}^{\frac{1}{2}}$$

$$=\frac{1}{2}Lf\,\beta^{\frac{1}{2}}(\chi_m+\chi_s)^{\frac{1}{2}}\left\{1-\frac{I^{2}\chi_m^{2}}{\beta(\chi_m+\chi_s)}\exp-f\,\phi_m^{\circ}\right\}^{\frac{1}{2}}\exp\frac{1}{2}f\,\phi_m^{\circ} \qquad 3.44$$

The solution potential profile equation is [38]

$$\cos^{-1}\left\{1-\frac{I^{2}\chi_m^{2}}{\beta(\chi_m+\chi_s)}\exp-f\,\phi_m^{\circ}\right\}^{\frac{1}{2}}+\cos^{-1}\left\{\frac{1-\dfrac{I^{2}\chi_m^{2}}{\beta(\chi_m+\chi_s)}\exp-f\,\phi_m^{\circ}}{\exp\left[-f\left(I\,\chi_m x+\left(\dfrac{\chi_m}{\chi_s}+1\right)\phi_s\right)\right]}\right\}^{\frac{1}{2}}$$

$$=\frac{1}{2}xf\,\beta^{\frac{1}{2}}(\chi_m+\chi_s)^{\frac{1}{2}}\left\{1-\frac{I^{2}\chi_m^{2}}{\beta(\chi_m+\chi_s)}\exp-f\,\phi_m^{\circ}\right\}^{\frac{1}{2}}\exp\frac{1}{2}f\,\phi_m^{\circ} \qquad 3.45$$

where $\beta=\dfrac{2i_{\circ}aRT}{\alpha zF}$ 3.46

$f=\dfrac{\alpha zF}{RT}$ 3.47

3.6.1.3 Concentration Polarization

The polarization equation relevant to mass transfer process (diffusion controlled) is defined in the following equation [4]

$i=f(\eta,C)=zFDC(x)/\delta$ 3.48

Where *C(x)* is the concentration of the reacting species as a function of electrode length, *D* is the diffusion coefficient of the reacting species, and δ is the diffusion layer thickness.

A material balance over an elemental length operating at limiting current is done[‡]. According to the law of conservation of mass:

mass in − mass out + generation − consumption = accumulation

mass in = $U_{av}AC$

mass out = $U_{av}A(C+dC)$

generation = 0

consumption = $K_{av}A_RC$

A_R is the surface area of reaction, A is the cross sectional area of bed.

$A_R = aA\varepsilon dx$

$\therefore$ consumption = $K_{av}aA\varepsilon dx\ C$

At steady state: accumulation = 0

$\therefore \quad U_{av}AC - U_{av}A(C+dC) + 0 - K_{av}aA\varepsilon dx\ C = 0$

Rearranging to get equation 3.49 [4, 39].

$$\frac{dC}{dx} = -\frac{a\varepsilon K_{av}C}{U_{av}} \qquad 3.49$$

Integrating equation 3.49 yields [39]

$$C(x) = C_{\circ}\exp\left(\frac{-x}{\lambda}\right) \qquad 3.50$$

where

$$\lambda = \frac{U_{av}}{K_{av}a\varepsilon} \qquad 3.51$$

where a is the electrode area per unit volume of electrode, U is the average velocity, and K_{av} is the average mass transfer coefficient assumed independent of

---

[‡] This derivation is done by the writer of this thesis.

length. The solution potential profile can be found by substituting equation 3.48 into 3.19 [38]

$$\chi_s^{-1}\frac{d^2\phi_s}{dx^2}+\frac{azFDC\,(x)}{\delta}=0 \qquad 3.52$$

substituting 3.50 into 3.52

$$\frac{d^2\phi_s}{dx^2}=-\frac{azFDC_\circ\chi_s}{\delta}\exp\left(\frac{-x}{\lambda}\right) \qquad 3.53$$

integrating equation 3.53 twice and applying the boundary conditions 3.29 and 3.31 gives [38]

$$\phi_s = C_\circ zFU_{av}\,\chi_s\left[\lambda\left\{1-\exp\left(-\frac{x}{\lambda}\right)\right\}-x\right] \qquad 3.54$$

The metal phase potential profile can be found by substituting equation 3.48 into 3.18 gives

$$\chi_m^{-1}\frac{d^2\phi_s}{dx^2}-\frac{azFDC\,(x)}{\delta}=0$$

rearranging yields

$$\frac{d^2\phi_m}{dx^2}=\frac{azFDC_\circ\chi_m}{\delta}\exp\left(\frac{-x}{\lambda}\right)$$

by integrating this equation twice and applying 3.29 and 3.30 yields [38]

$$\phi_m = \phi_m^\circ - C_\circ zFU_{av}\,\chi_m\left[\lambda\left\{1-\exp\left(-\frac{x}{\lambda}\right)\right\}-x\,\exp\left(-\frac{L}{\lambda}\right)\right] \qquad 3.55$$

The current is found by substituting 3.48 into 3.49 [4]

$$I = C_\circ zFU_{av}\left[1-\exp(-L/\lambda)\right] \qquad 3.56$$

3.6.2 Modeling With Laplace Transformation (Present Work)

Alternative ways of finding the potential distributions are described below in a more convienent way than that mentioned before. Rearranging equation 3.34 to get

$$\frac{d\phi_s}{dx} = -i_s \chi_s \tag{3.57}$$

and equation 3.35 to get

$$\frac{d\phi_m}{dx} = -i_m \chi_m = -(I - i_m)\chi_m \tag{3.58}$$

subtract 3.57 from 3.58 to get

$$\frac{d\phi_m}{dx} - \frac{d\phi_s}{dx} = -(I - i_s)\chi_m + i_s \chi_s \tag{3.59}$$

differentiating equation 3.24 once with respect to x gives

$$\frac{d\eta}{dx} = \frac{d\phi_m}{dx} - \frac{d\phi_s}{dx} \tag{3.60}$$

substituting equation 3.60 into 3.59

$$\frac{d\eta}{dx} = -I\chi_m + i_s(\chi_s + \chi_m) \tag{3.61}$$

Substituting equation 3.34 into 3.61 leads to

$$\frac{d\eta}{dx} = -I\chi_m - (1 + \frac{\chi_m}{\chi_s})\frac{d\phi_s}{dx} \tag{3.62}$$

differentiate eqution 3.62 with respect to x

$$\frac{d^2\eta}{dx^2} = (\chi_s + \chi_m)\frac{di_s}{dx} \tag{3.63}$$

Scott [44] stated that the first derivative of the solution current with respect to x is equal to the local current density multiplied by the bed specific surface area per unit volume

$$\frac{di_s}{dx} = ai \qquad 3.64$$

substituting equation 3.64 into 3.63

$$\frac{d^2\eta}{dx^2} = (\chi_s + \chi_m)ai \qquad 3.65$$

Current density will be substituted in equation 3.65 for the three distinct cases of polarisation.

3.6.2.1 Linear Polarisation Region

At linear polarisation, the local current density is defined previously as

$$i = \frac{i_\circ zF\eta}{RT} \qquad 3.20$$

Substituting equation 3.20 into 3.65 gives the same as equation 3.26 which is

$$\frac{d^2\eta}{dx^2} = (\chi_s + \chi_m)a\frac{i_\circ zF\eta}{RT} \qquad 3.26$$

$$K' = (\chi_s + \chi_m)a\frac{i_\circ zF}{RT} \qquad 3.66$$

so, the equation can be reduced to

$$\frac{d^2\eta}{dx^2} = K'\eta \qquad 3.67$$

Taking Laplace transform [46] of equation 3.67 yields

$$\mathcal{L} \quad \eta(x)$$

$$s^2\eta(s) - s\,\eta(0) - \eta'(0) = K'\eta(s) \qquad 3.68$$

Overpotential $(\eta(x))$ at x=0 and the first derivative is found by applying the boundary condition of equations 3.29 into equation 3.37

so, $\eta(0) = \phi_m^\circ$ 3.69

by taking the first derivative, we get

$$\eta'(x) = -I\,\chi_m - (1+\frac{\chi_m}{\chi_s})\frac{d\phi_s}{dx}$$

$$\frac{d\phi_s}{dx} = 0 \quad \text{at x=0}$$

from equation 3.31

$$\eta'(0) = -I\,\chi_m \qquad 3.70$$

substituting equations 3.69 and 3.70 into equation 3.68 yields

$$s^2\eta(s) - s\phi_m^\circ + I\,\chi_m = K'\eta(s) \qquad 3.71$$

rearranging yields

$$\eta(s)(s^2 - K') = s\phi_m^\circ - I\,\chi_m$$

$$\eta(s) = \frac{s\phi_m^\circ}{(s^2 - K')} - \frac{I\,\chi_m}{(s^2 - K')}$$

taking inverse Laplace of former equation

$$\mathrm{L}^{-1}\ \eta(s)$$

$$\eta(x) = \phi_m^\circ \cosh\sqrt{K'}x - \frac{I\,\chi_m}{\sqrt{K}}\sinh\sqrt{K'}x \qquad 3.72$$

Equation 3.72 clearly satisfy boundary conditions previously defined, and could be further equilized with equation 3.37 to get the solution potential profile as:

$$\phi_s = \frac{1}{\left(1+\chi_m/\chi_s\right)}\left[\phi_m^\circ - I\,\chi_m x - \phi_m^\circ \cosh\sqrt{K'}x + \frac{I\,\chi_m}{\sqrt{K}}\sinh\sqrt{K'}x\right] \qquad 3.73$$

3.6.2.2 Tafel Polarisation Region

Considering equation 3.65 again, but substituing for the case of Tafel polarisation equation as following

$$\frac{d^2\eta}{dx^2} = (\chi_s + \chi_m)ai \qquad 3.65$$

and

$$i = f\,(\eta, C) = i_\circ \exp\left[\frac{\alpha zF\eta}{RT}\right] \qquad 3.40$$

substituting 3.40 into 3.65 gives

$$\frac{d^2\eta}{dx^2} = (\chi_s + \chi_m)ai_\circ \exp\left[\frac{\alpha zF\eta}{RT}\right] \qquad 3.74$$

Equation 3.74 can not be solved by Laplace transformation because the exponential term contains η, and the numerical solution of this equation gives results far from experimental. So, it will be integrated using analytical methode as in integrating equation 3.41 which gives the same as equation 3.45. Equation 3.45 can be rearranged in terms of solution potential as follows

let $$K_1 = 1 - \frac{I^2\chi_m^2}{\beta(\chi_m + \chi_s)} \exp -f\,\phi_m^\circ \qquad 3.75$$

and $$K_2 = \frac{1}{2} f\,\beta^{\frac{1}{2}}(\chi_m + \chi_s)^{\frac{1}{2}} \left\{1 - \frac{I^2\chi_m^2}{\beta(\chi_m + \chi_s)} \exp -f\,\phi_m^\circ\right\}^{\frac{1}{2}} \exp \frac{1}{2} f\,\phi_m^\circ \qquad 3.76$$

so, equation 3.45 can be written as

$$\cos^{-1}\{K_1\}^{\frac{1}{2}} + \cos^{-1}\left\{\frac{K_1}{\exp\left[-f\left(I\,\chi_m x + \left(\frac{\chi_m}{\chi_s} + 1\right)\phi_s\right)\right]}\right\}^{\frac{1}{2}} = K_2 x$$

by rearranging

$$\cos^{-1}\left\{\frac{K_1}{\exp\left[-f\left(I\,\chi_m x+\left(\frac{\chi_m}{\chi_s}+1\right)\phi_s\right)\right]}\right\}^{\frac{1}{2}} = K_2 x-\cos^{-1}\{K_1\}^{\frac{1}{2}}$$

taking cosine of both sides gives

$$\left\{\frac{K_1}{\exp\left[-f\left(I\,\chi_m x+\left(\frac{\chi_m}{\chi_s}+1\right)\phi_s\right)\right]}\right\}^{\frac{1}{2}} = \cos\left(K_2 x-\cos^{-1}\{K_1\}^{\frac{1}{2}}\right)$$

Squaring both sides of the equation

$$\frac{K_1}{\exp\left[-f\left(I\,\chi_m x+\left(\frac{\chi_m}{\chi_s}+1\right)\phi_s\right)\right]} = \cos^2\left(K_2 x-\cos^{-1}\{K_1\}^{\frac{1}{2}}\right)$$

$$\exp\left[-f\left(I\,\chi_m x+\left(\frac{\chi_m}{\chi_s}+1\right)\phi_s\right)\right] = \frac{K_1}{\cos^2\left(K_2 x-\cos^{-1}\{K_1\}^{\frac{1}{2}}\right)}$$

Taking natural logarithm of both sides

$$\left(I\,\chi_m x+\left(\frac{\chi_m}{\chi_s}+1\right)\phi_s\right) = \ln\left[\frac{\cos^2\left(K_2 x-\cos^{-1}\{K_1\}^{\frac{1}{2}}\right)}{K_1}\right]^{f}$$

$$\phi_s = -\frac{I\,\chi_m x}{\left(\frac{\chi_m}{\chi_s}+1\right)}+\frac{1}{\left(\frac{\chi_m}{\chi_s}+1\right)}\ln\left[\frac{\cos^2\left(K_2 x-\cos^{-1}\{K_1\}^{\frac{1}{2}}\right)}{K_1}\right]^{f}$$

$$\phi_s = -\frac{I\,\chi_m x}{\left(\frac{\chi_m}{\chi_s}+1\right)} + \frac{1}{\left(\frac{\chi_m}{\chi_s}+1\right)} \times$$

$$\ln\left[\frac{\cos^2\left(\frac{1}{2}fx\,\beta^{\frac{1}{2}}(\chi_m+\chi_s)^{\frac{1}{2}}\left\{1-\frac{I^2\chi_m^2}{\beta(\chi_m+\chi_s)}\exp-f\,\phi_m^\circ\right\}^{\frac{1}{2}}\exp\frac{1}{2}f\,\phi_m^\circ - \cos^{-1}\left\{1-\frac{I^2\chi_m^2}{\beta(\chi_m+\chi_s)}\exp-f\,\phi_m^\circ\right\}^{\frac{1}{2}}\right)}{1-\frac{I^2\chi_m^2}{\beta(\chi_m+\chi_s)}\exp-f\,\phi_m^\circ}\right]^f$$

……..3.77

3.6.2.2 Concentration Polarisation Region

For the concentration polarisation case. The local current density is found to be as

$$i = zFK_{av}C(x) = zFK_{av}C_\circ \exp\left(-\frac{x}{\lambda}\right) \qquad 3.78$$

substituting equation 3.78 into equation 3.65

$$\frac{d^2\eta}{dx^2} = (\chi_s+\chi_m)azFK_{av}C_\circ \exp\left(-\frac{x}{\lambda}\right) \qquad 3.79$$

let $K = (\chi_s+\chi_m)azFK_{av}C_\circ$ 3.80

$$\therefore \quad \frac{d^2\eta}{dx^2} = K\exp\left(-\frac{x}{\lambda}\right) \qquad 3.81$$

taking laplace of the equation 3.81 gives

$\mathcal{L}\quad \eta(x)$

$$s^2\eta(s) - s\eta(0) - \eta'(0) = \frac{K}{s+\frac{1}{\lambda}}$$

$$s^2\eta(s) = \frac{K}{s+\frac{1}{\lambda}} + s\phi_m^\circ - I\,\chi_m$$

$$\eta(s) = \frac{K}{s^2\left(s+\frac{1}{\lambda}\right)} + \frac{s\phi_m^\circ}{s^2} - \frac{I\,\chi_m}{s^2} \qquad 3.82$$

simplifying the second term

$$\frac{K}{s^2\left(s+\frac{1}{\lambda}\right)} = \frac{As+B}{s^2} + \frac{C}{s+\frac{1}{\lambda}}$$

$$K = As^2 + \frac{As}{\lambda} + Bs + \frac{B}{\lambda} + Cs^2$$

$$A = -C \quad : \qquad \frac{A}{\lambda} = -B$$

$$B = \lambda K$$

$$A = -\lambda^2 K$$

$$C = \lambda^2 K$$

substituting A, B, and C into gives

$$\eta(s) = \frac{-\lambda^2 Ks}{s^2} + \frac{\lambda K}{s^2} + \frac{\lambda^2 K}{s+\frac{1}{\lambda}} + \frac{s\phi_m^\circ}{s^2} - \frac{I\,\chi_m}{s^2} \qquad 3.83$$

taking laplace inverse of eqution 3.83 gives

$$\eta(x) = -\lambda^2 K - \lambda Kx + \lambda^2 K \exp\left(-\frac{x}{\lambda}\right) + \phi_m^\circ - I\,\chi_m x \qquad 3.84$$

equalizing equation 3.84 with equation 3.37

$$\phi_m^\circ - I\,\chi_m x - (1+\frac{\chi_m}{\chi_s})\phi_s = -\lambda^2 K - \lambda K x + \lambda^2 K \exp\left(-\frac{x}{\lambda}\right) + \phi_m^\circ - I\,\chi_m x$$

rearranging

$$\phi_s = \frac{1}{\left(1+\frac{\chi_m}{\chi_s}\right)}\left[\lambda^2 K + \lambda K x - \lambda^2 K \exp\left(-\frac{x}{\lambda}\right)\right] \qquad 3.85$$

substituting $K = (\chi_s + \chi_m) azFK_{av} C_\circ$ and rearranging yields

$$\phi_s = azFK_{av}\,\chi_s C_\circ \left[\lambda^2 + \lambda x - \lambda^2 \exp\left(-\frac{x}{\lambda}\right)\right] \qquad 3.86$$

or $$\phi_s = \frac{zFU_{av}\chi_s C_\circ}{\varepsilon}\left[\lambda + x - \lambda \exp\left(-\frac{x}{\lambda}\right)\right] \qquad 3.87$$

and the metal phase distribution is easily found for each case by substituting the values of solution metal in the over potential equation.

Chapter Four

Calculations and Interpretations

4.1 Hydrodynamic of fluidized bed

Considering spherical copper particles with different expansions and different particle sizes to find out how the superficial velocity of the fluid changes. The terminal settling velocity of particle is calculated from the following equations.

$$u_t = \frac{g(\rho_s - \rho)d^2}{18\mu} \qquad \text{for } Re_p<0.4 \qquad 3.6a$$

$$u_t = \left[\frac{4}{225}\frac{(\rho_m - \rho)^2 g^2}{\rho\mu}\right]^{1/3} d \qquad \text{for } 0.4<Re_p<500 \qquad 3.6b$$

$$u_t = \left[\frac{3.1g(\rho_m - \rho)d}{\rho}\right]^{1/2} \qquad \text{for } 500<Re_p<200{,}000 \qquad 3.6c$$

Noting that terminal settling velocity is independent of bed expansion.

The density of copper and solution are 8920, and1000 Kg/m^3 respectively and the solution viscosity is $10^{-3}Kg.m^{-1}.s^{-1}$. Data obtained from Perry's Chemical Engineers Handbook [42].

The sizes of particles are ranging normally from 200 to 2000 μm depending on number of references indicating that the particles practically used in electrochemical fluidized bed are within this range [13, 15, 29, and 31].

The average velocity is found by substituting terminal velocity and porosity into equation 3.5.

$$\varepsilon = \left(\frac{U_{av}}{u_t}\right)^{0.225\left(\frac{u_t d}{\upsilon}\right)^{0.1}} \qquad 3.5$$

Voidage (ε) is calculated from equation 3.4

$$\Gamma = \frac{\varepsilon - \varepsilon_\circ}{1 - \varepsilon} \qquad 3.4$$

$\varepsilon_\circ =$ volume of spaces between particles/ volume of bed

volume of spaces = volume of bed $-$ volume of particles

$\varepsilon_\circ = 1 -$ (volume of particles/ volume of bed)

$\varepsilon_\circ = 0.42$ for this system[4, 39]

This volume of spaces between particles at static condition is found experimentally by measurement of the volume of liquid displaced by a given volume of spheres.

By rearranging equation 3.4 we get

$$\varepsilon = \frac{\Gamma + \varepsilon_\circ}{\Gamma + 1} \qquad 4.1$$

Simple tables can be constructed for the variation of average velocity with expansion and particle diameter change. Average superficial velocity is calculated for 5, 10, and 20% expansion for copper particles ranging from 200 to 2000 μm in diameter.

For 5% expansion. The porosity is found from equation 4.1

$$\varepsilon = \frac{0.05 + 0.42}{0.05 + 1} = 0.448$$

$\varepsilon = 0.473$ at $\Gamma = 0.1$

$\varepsilon = 0.517$ at $\Gamma = 0.2$

Table 4.1 Average superficial and minimum fluidizing velocities change with copper particle diameter at 5% expansion .

Particle diameter in μm	Terminal velocity in m/s	Average velocity in m/s
200	0.0950	0.00666
300	0.1426	0.01229
400	0.1901	0.01879
500	0.2376	0.02598
600	0.2851	0.03375
700	0.3326	0.04201
800	0.3801	0.05070
900	0.4276	0.05978
1000	0.4752	0.06920
1200	0.5376	0.08296
1400	0.5807	0.09352
1600	0.6208	0.10367
1800	0.6584	0.11346
2000	0.6941	0.12294

Table 4.2 The variation of velocity with copper particle diameter for 10%, and 20% expansion.

Particle diameter in μm	Average velocity in m/s for 10% expansion	Average velocity in m/s for 20% expansion
200	0.007966	0.010694
300	0.014556	0.019096
400	0.021959	0.028376
500	0.030236	0.038636
600	0.038967	0.049359
700	0.048379	0.060841
800	0.05807	0.072591
900	0.068344	0.084989
1000	0.07879	0.097537
1200	0.100831	0.123871
1400	0.123988	0.151371
1600	0.148113	0.179876
1800	0.173094	0.209265
2000	0.19884	0.239442

The superficial average velocities in Tables 4.1 and 4.2 are plotted in the next figure.

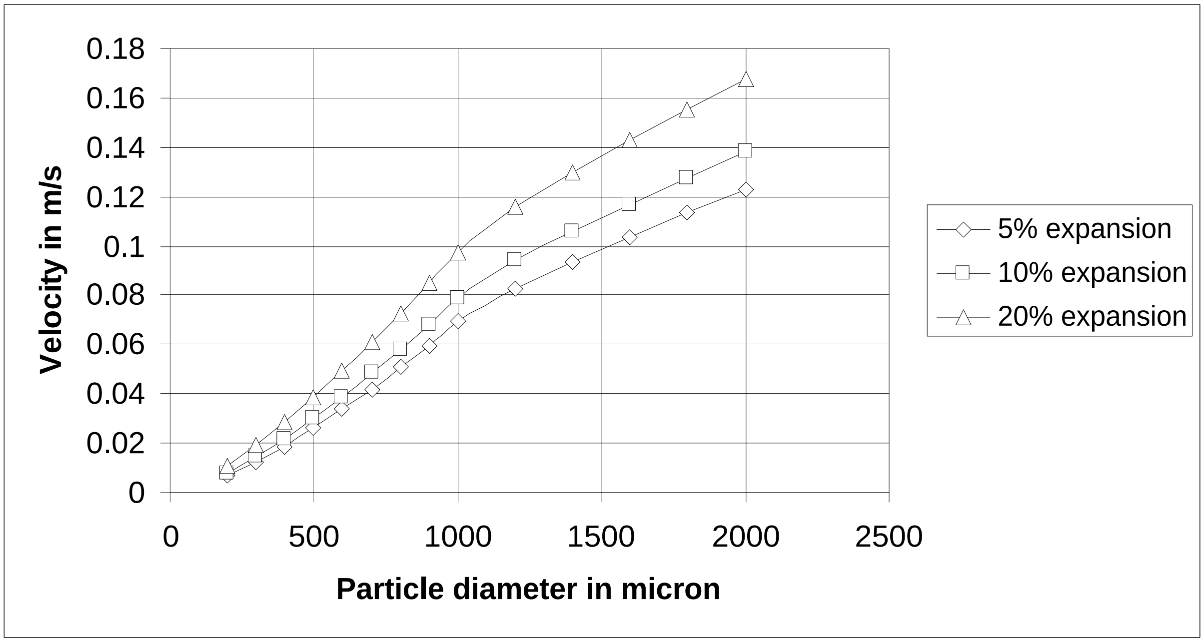

Fig. 4.1 Average velocity change with particle diameter at different fluidizing porosities.

From equation 3.11 , it is possible to calculate the pressure drop per unit length of the fluidized phase

$$\frac{\Delta p}{L} = (1-\varepsilon)(\rho_m - \rho)g \qquad 3.11$$

$$\frac{\Delta p}{L} = (1-\varepsilon)(8920-1000)9.81 = 77{,}695.2(1-\varepsilon)$$ Pa/m for copper particles bed.

By increasing porosity, the pressure drop decreases per unit length of the bed.

4.2 Solution and Metal Phase Resistivities

Fleischmann, Oldfield, and Tennakoon [19] worked on fluidized bed of 535 μm copper coated glass spheres. The density of copper coated glass spheres is 3000 Kg/m^3 and that of solution is 1000 Kg/m^3, Young's modulus is 10^{12} N/m^2, the viscosity is 10^{-3} Kg.m^{-1}.s^{-1}, the resistivity of solution is $0.02285\,\Omega.m$ and porosity at static condition is 0.42[19]. The terminal settling velocity is found from equation 3.6b

$$u_t = \left[\frac{4}{225}\times\frac{(3000-1000)^2\times 9.81^2}{1000\times 10^{-3}}\right]^{1/3}\times 535\times 10^{-6} = 0.1016 \text{ m/s}$$

$$Re_p = \frac{0.1016\times 535\times 10^{-6}}{10^{-6}} = 54.356 \text{ within the range of equation 3.6b}$$

porosity can be found from equation 4.1

$$\varepsilon = \frac{\Gamma+\varepsilon_\circ}{1+\Gamma} = \frac{\Gamma+0.42}{1+\Gamma}$$

and the average velocity is found from equation 3.5

$$\varepsilon = \left(\frac{U_{av}}{0.1016}\right)^{0.225\left(\frac{0.1016\times 535\times 10^{-6}}{10^{-6}}\right)^{0.1}}$$

Using equation 3.1, 2.47 and 3.3, a simple table can be constructed to find the solution and metal phase resistivities as a function of bed expansion. The interstitial velocity (v_p) equals U_{av}/ε

$$\chi_m = \frac{0.04179(1+\Gamma)^{\frac{2}{3}}((1+\Gamma)^{\frac{1}{3}}-1)E^{\frac{1}{3}}\chi_s}{(\rho_m-\rho\ )^{\frac{1}{3}}v_p^{\frac{2}{3}}} \qquad 3.1$$

Table 4.3 Solution and metal phase resistivities in $\Omega.m$ as function of percentage bed expansion for 535 μm copper coated glass spheres.

Bed expansion Γ %	Solution resistivity equation 3.3	Metal phase resistivity equation 3.1	Metal phase resistivity equation 2.47
0	0.0548	0.02085	0.139695
5	0.0514	0.1777	1.19059
10	0.0487	0.3182	2.13194
15	0.0464	0.4341	2.90847
20	0.0445	0.5332	3.57244
25	0.0429	0.6203	4.15601
30	0.0415	0.6988	4.68196

The metal phase resistivities of equation 3.1 and 2.47 and the solution phase resistivity from table 4.3 are plotted versus percentage expansion as shown.

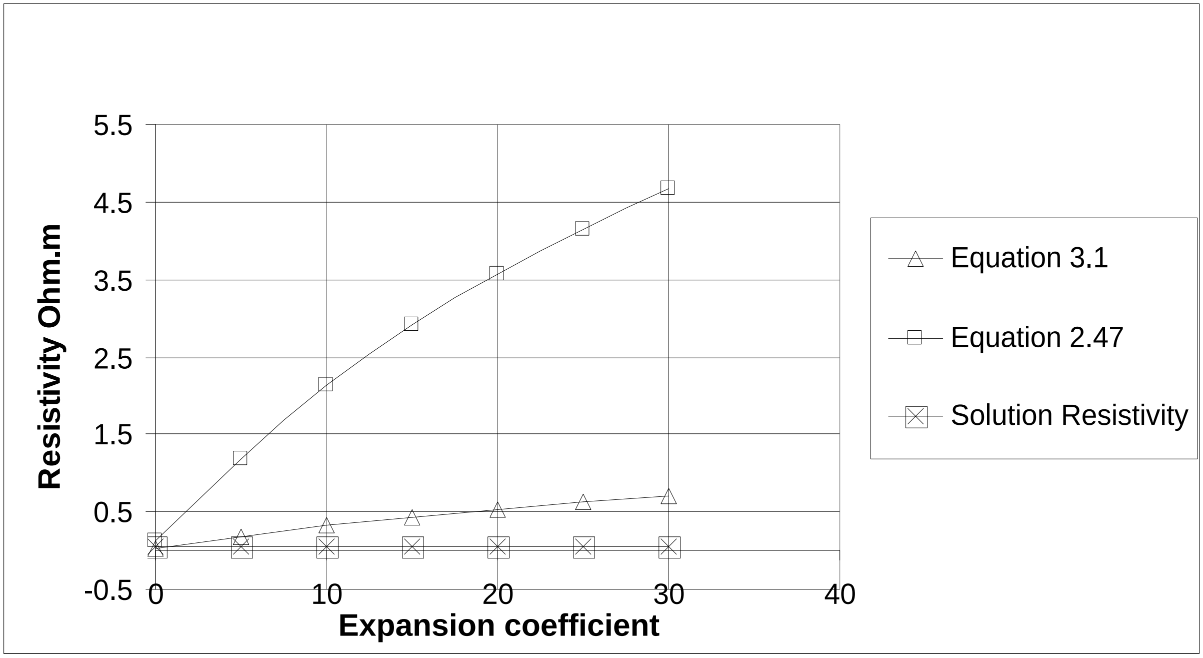

Fig. 4.2 Metal phase resistivities of equation 2.47 and 3.1 and solution phase resistivities with percent expansion.

Previous data of metal phase resistivities are calculated using matlab programming for many variables of electrolyte average velocity, porosity, particle diameter, or solution phase resistivity. The programs are in Appendix B-1,and B-2.

4.3 Potential Distribution Along an Electrochemical Fluidized Bed

In order to find a model, Fleischmann, Oldfield, and Tennakoon [19]worked on fluidized bed of 535 μm copper coated glass spheres. The density of copper coated glass spheres as mentioned before is 3000 Kg/m^3 and that of solution is 1000 Kg/m^3.The viscosity is 10^{-3} Kg.m^{-1}.s^{-1}, the diffusivity of copper ions is 4×10^{-10} m^2/s and porosity at static condition is 0.42 [19].

For 13.6 % expansion the porosity can be found by equation 4.1

$$\varepsilon = \frac{\Gamma + \varepsilon_\circ}{1+\Gamma} = \frac{0.136 + 0.42}{1+0.136} = 0.4894$$

The terminal settling velocity is found from equation 3.6b

$$u_t = \left[\frac{4}{225} \times \frac{(3000-1000)^2 \times 9.81^2}{1000 \times 10^{-3}} \right]^{1/3} \times 535 \times 10^{-6} = 0.1016 \text{ m/s}$$

and the average velocity is found from equation 3.5

$$\varepsilon = \left(\frac{U_{av}}{0.1016} \right)^{0.225 \left(\frac{0.1016 \times 535 \times 10^{-6}}{10^{-6}} \right)^{0.1}} \Rightarrow U_{av} = 0.012076 \text{ m/s}$$

$$\mathrm{Re}_d = \frac{U_{av}\, d}{\nu} = \frac{0.012076 \times 535 \times 10^{-6}}{10^{-6}} = 6.46075 \text{ within range of equation 3.6b.}$$

$L_\circ = 10.65$ mm [19]

From equation 3.4b it is found that $L = L_\circ \times (1+\Gamma)$

$\therefore L = 12.1$ mm

The surface area per unit volume is given as 5720 m^{-1}, and the inlet concentration of cupric sulphate is 10 mol/m^3. The reaction is activation controlled and far from equilibrium [10], so we can apply equation 3.77. To find the total current density, equation 3.44 has been solved by trial and error calculations as follows

$$\cos^{-1}\left\{1-\frac{I^2\chi_m^2}{\beta(\chi_m+\chi_s)}\exp-f\,\phi_m^\circ\right\}^{\frac{1}{2}}+\cos^{-1}\left\{\frac{1-\frac{I^2\chi_m^2}{\beta(\chi_m+\chi_s)}\exp-f\,\phi_m^\circ}{1-\frac{I^2(\chi_m^2-\chi_s^2)}{\beta(\chi_m+\chi_s)}\exp-f\,\phi_m^\circ}\right\}^{\frac{1}{2}}$$

$$=\frac{1}{2}Lf\,\beta^{\frac{1}{2}}(\chi_m+\chi_s)^{\frac{1}{2}}\left\{1-\frac{I^2\chi_m^2}{\beta(\chi_m+\chi_s)}\exp-f\,\phi_m^\circ\right\}^{\frac{1}{2}}\exp\frac{1}{2}f\,\phi_m^\circ \qquad 3.44$$

The reaction temperature is $25C^\circ$, the exchange coefficient (α) is 0.5, the reaction of deposition is

$$Cu^{+2}+2e^-\rightleftharpoons Cu \qquad 4.2$$

The number of electrons associated with the reaction (z) is 2, the exchange current density $(i_\circ)$ is 9.6 A/m^2. β and f are found from equation 3.46 and 3.47

$$\beta=\frac{2i_\circ aRT}{\alpha zF} \qquad 3.46$$

$$f=\frac{\alpha zF}{RT} \qquad 3.47$$

$$\beta=\frac{2\times 9.6\times 5720\times 8.314\times 298.15}{0.5\times 2\times 96500}=2{,}821.1AV\ /m$$

$$f=\frac{0.5\times 2\times 96500}{8.314\times 298.15}=38.929V^{-1}$$

The solution resistivity (χ_s°) is $0.02285\,\Omega.m$. So, by applying equation 3.3 we get

$$\chi_s=0.02285/0.4894=0.0467\ \Omega.m$$

and that of metal phase according to equation 3.1 is found to be

$$\chi_m = \frac{0.04179(1+0.136)^{\frac{2}{3}}((1+0.136)^{\frac{1}{3}}-1)(1.1\times10^{11})^{\frac{1}{3}}0.02285}{(3000-1000)^{\frac{1}{3}}\left(0.012076\big/ 0.4894\right)^{\frac{2}{3}}} = 0.414\Omega.m$$

and that according to equation 2.47

$$\chi_m = \frac{0.28(1+0.136)^{\frac{2}{3}}((1+0.136)^{\frac{1}{3}}-1)(1.1\times10^{11})^{\frac{1}{3}}0.02285}{(3000-1000)^{\frac{1}{3}}\left(0.012076\big/ 0.4894\right)^{\frac{2}{3}}} = 2.77\Omega.m$$

The value of total current density is found for different bed lengths, a program developed using Matlab Programming. The details of the program are in Appendix B-3

I=207 A/m^2 when L=12.1 mm and $\chi_m = 0.414\Omega.m$

I=82 A/m^2 when L=12.1 mm and $\chi_m = 2.77\Omega.m$

Noting that equation 2.47 gave much higher resistivity, but much lower current density, which is far from the experimental value I=210A/m^2. The current density is variable with L as in the following table, using resistivity of equation 3.1.

Table 4.4 Total current change with increasing length of bed at 13.6% expansion and $535\mu m$ diameter coppper particles.

Length of bed in mm	Total current density A/m^2
6	172
8	189
10	200
12	207
14	212
16	215
18	218
20	220
30	225
40	227
50	228

The data in Table 4.4 is plotted in Fig. 4.3

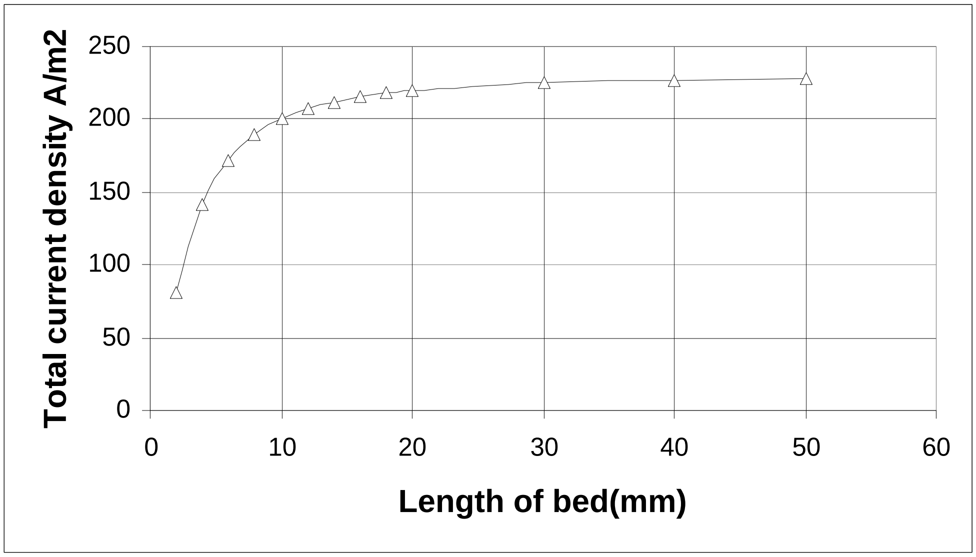

Fig.4.3 Total current requirement for different bed lengths.

The solution potential distribution from equation 3.77 is solved using Matlab program§ as follows and compared with experimental values [19] and using resistivity of equation 3.1 since equation 2.47 gives very low estimate of the current and much higher values of potential difference. An error exist because Fleischmann et al [37] suggested that metal phase resistivity is constant along the bed which is far from reality as will be explained later.

The error is taken as:

$$\text{error\%}=abs\left(\frac{theoretical-\exp erimental}{\exp erimental}\right)100\% \qquad 4.2$$

---

§ Details of program in Appendix B-4

Table 4.5 Theoretical and experimental potential distribution at 13.6%expansion.

Distance x in mm	Theoretical solution potential in V	Experimental solution potential in V	Error %
0	0	0	0
1	-0.0076	-0.002	280
2	-0.0155	-0.005	210
3	-0.0235	-0.011	113.6
4	-0.0317	-0.018	76.1
5	-0.0399	-0.024	66.25
6	-0.0483	-0.033	46.36
7	-0.0568	-0.042	35.24
8	-0.0653	-0.054	20.93
9	-0.0739	-0.065	13.69
10	-0.0826	-0.076	8.68
11	-0.0914	-0.086	6.28
12	-0.1002	-0.096	4.38

Figure 4.4 shows the theoretical and experimental solution potential profile.

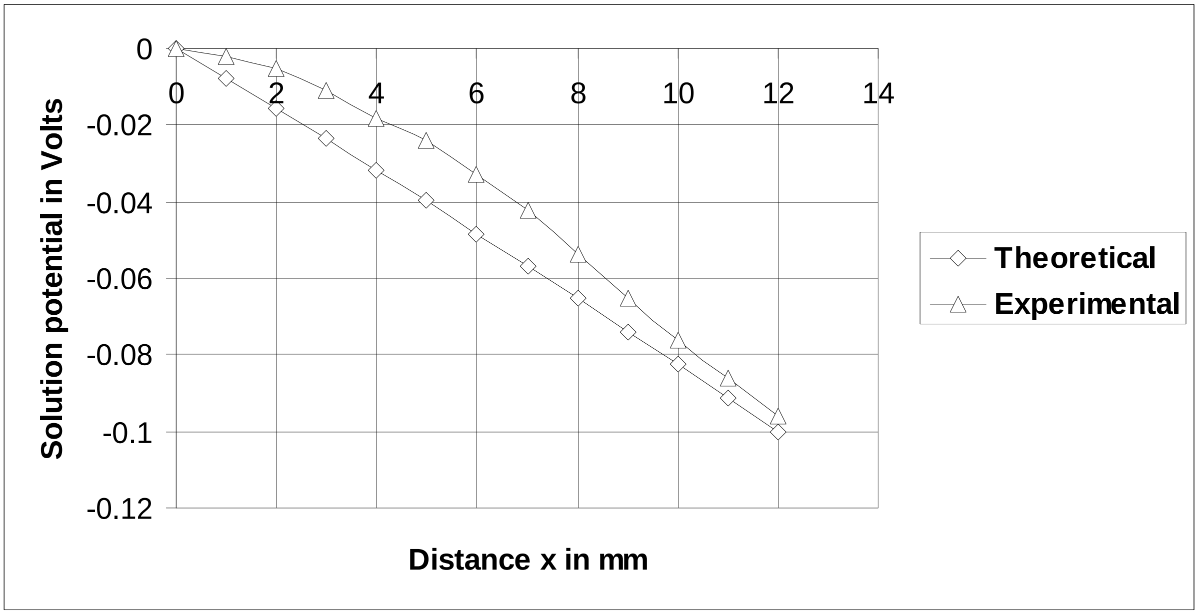

Fig. 4.4 Theoretical and experimental potential profiles at 13.6 % expansion.

For 18.2% expansion the same procedure has been repeated as follows

$\varepsilon = 0.5094 : u_t = 0.1509 m/s : U_{av} = 0.01359 m/s : v_p = 0.02668 m/s :$

$\chi_s = 0.04526 \Omega.m : \chi_m = 0.5159 \Omega.m : L = L_\circ \times (1+\Gamma) = 12.58 mm$

$$a = \frac{6}{d}(1-\varepsilon) = \frac{6}{535\times10^{-6}}(1-0.5094) = 5,500 \, m^2 \big/ m^3$$

$$\beta = \frac{2\times9.6\times5500\times8.314\times298.15}{0.5\times2\times96500} = 2,713.9 AV/m$$

$$f = \frac{0.5\times2\times96500}{8.314\times298.15} = 38.929 V^{-1}$$

The current is also found by trial and error calculation

$I = 188 \text{ A/m}^2$

So, the potential profile can be calculated and compared with experimental values, the following table can be constructed.

Table 4.6 Theoretical and experimental potential profiles at 18.2%expansion.

Distance x in mm	Theoretical solution potential in Volts	Experimental solution potential in Volts	Error%
0	0	0	0
1	-0.0069	-0.003	130
2	-0.014	-0.007	100
3	-0.0213	-0.013	63.84
4	-0.0287	-0.019	51.05
5	-0.0361	-0.025	44.4
6	-0.0437	-0.034	28.52
7	-0.0513	-0.041	25.12
8	-0.059	-0.047	25.53
9	-0.0667	-0.055	21.27
10	-0.0745	-0.064	16.40
11	-0.0823	-0.074	11.21
12	-0.0902	-0.083	8.67
13	-0.0982	-0.092	6.74

Data in Table 4.6 are plotted in Fig. 4.5 as shown

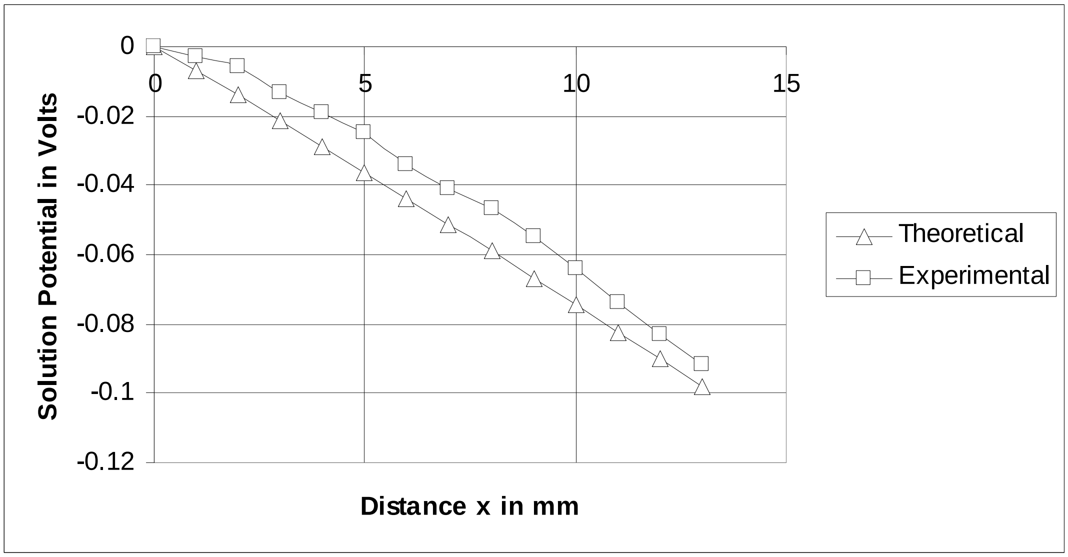

Fig. 4.5 Theoretical and experimental potential profiles at 18.2 % expansion.

At 27% expansion

$\varepsilon = 0.5433$: $u_t = 0.1509 m/s$: $U_{av} = 0.01647\ m/s$: $v_p = 0.0303\ m/s$:

$\chi_s = 0.04243 \Omega.m$: $\chi_m = 0.674 \Omega.m$

$$a = \frac{6}{d}(1-\varepsilon) = \frac{6}{535\times10^{-6}}(1-0.5435) = 5{,}120\, {m^2}\!\Big/{m^3}$$

$$\beta = \frac{2\times9.6\times5120\times8.314\times298.15}{0.5\times2\times96500} = 2{,}526.4 AV\ / m$$

$$f = \frac{0.5\times2\times96500}{8.314\times298.15} = 38.929 V^{-1}$$

$$L = L_\circ \times (1+\Gamma) = 13.52 mm$$

The current is equal to

I=161 A/m^2

So, the potential profile can be calculated and compared with experimental values, the following table can be constructed.

Table 4.7 Theoretical and experimental potential distributions at 27%expansion.

Distance x in mm	Theoretical solution potential in V	Experimental solution potential in V	Error%
0	0	0	0
1	-0.0057	-0.004	42.5
2	-0.0115	-0.008	43.75
3	-0.0175	-0.011	59.09
4	-0.0236	-0.017	38.82
5	-0.0297	-0.023	29.13
6	-0.0359	-0.028	28.21
7	-0.0421	-0.035	20.28
8	-0.0484	-0.041	18.05
9	-0.0547	-0.05	9.4
10	-0.0611	-0.057	7.19
11	-0.0675	-0.067	0.74
12	-0.0739	-0.077	4.03
13	-0.0804	-0.083	3.13
14	-0.0864	-0.091	5.05

Previous Data are plotted in the next figure.

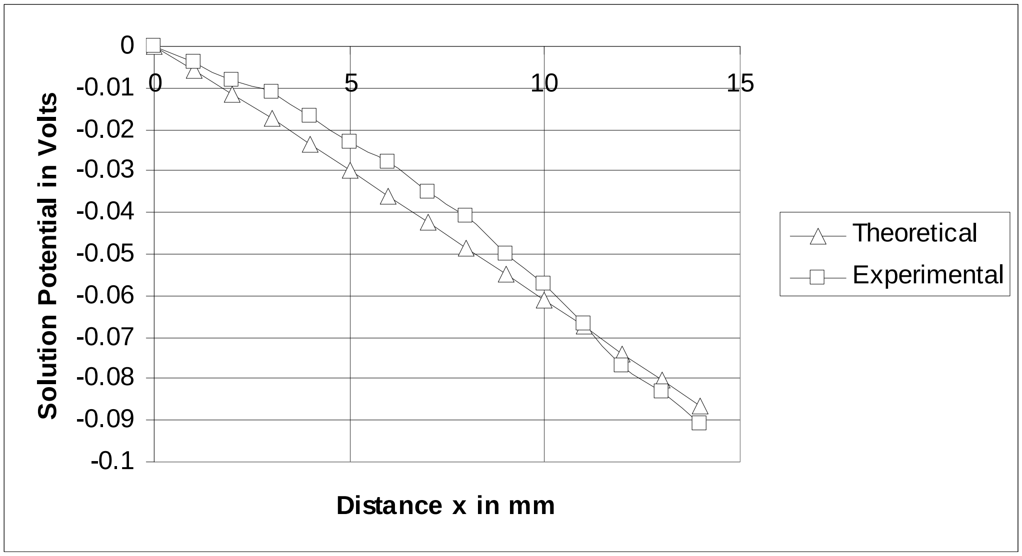

Fig. 4.6 Theoretical and experimental potential profiles at 27% expansion.

The maximum error is originated near the current feeder as shown in Fig. 4.4, 4.5, and 4.6. As we move toward the end of the reactor, the discrepancies become less evident. This is attributed to the assumptions that the metal phase resistivity is taken as a constant value along the bed, while in fact, the resistivity is variable along the bed since the particles are discrete at the bed entrance and closer at higher levels in the bed. It is also evident from Fig. 4.4, 4.5, and 4.6 that the difference between experimental and theoretical values of the potential become smaller with increasing bed expansion. This will be explained later. So, a factor will be introduced into the resistivity equation(equation 3.1) to replace the 6.7 suggested by Fleischmann, and Oldfield[37]

4.4 Local Metal Phase Resistivity or Local Dispersed Phase Resistivity

The value of metal phase resistivity at each point along the bed is found by using experimental values of solution potential in solving equation 3.77 by trial and error for χ_m values, as tabulated in Table 4.8.

$$\phi_s = -\frac{I\,\chi_m x}{\left(\dfrac{\chi_m}{\chi_s}+1\right)} + \frac{1}{\left(\dfrac{\chi_m}{\chi_s}+1\right)} \times$$

$$\ln\left[\frac{\cos^2\left(\dfrac{1}{2} f x\, \beta^{\frac{1}{2}} (\chi_m+\chi_s)^{\frac{1}{2}} \left\{1-\dfrac{I^2\chi_m^2}{\beta(\chi_m+\chi_s)} \exp{-f\,\phi_m^\circ}\right\}^{\frac{1}{2}} \exp\dfrac{1}{2} f\,\phi_m^\circ - \cos^{-1}\left\{1-\dfrac{I^2\chi_m^2}{\beta(\chi_m+\chi_s)}\exp{-f\,\phi_m^\circ}\right\}^{\frac{1}{2}}\right)}{1-\dfrac{I^2\chi_m^2}{\beta(\chi_m+\chi_s)}\exp{-f\,\phi_m^\circ}}\right]^f$$

……..3.77

Table 4.8 Local metal phase resistivity at 13.6, 18.2, and 27% expansion and 535 μm diameter.

Distance x in mm	Metal phase resistivity $\Omega.m$ at 13.6%expansion	Metal phase resistivity $\Omega.m$ at 18.2 % expansion	Metal phase resistivity $\Omega.m$ at 27% expansion
1	0.0125	0.027	0.0375
2	0.016	0.034	0.0495
3	0.028	0.0495	0.051
4	0.039	0.0575	0.0705
5	0.0415	0.0605	0.0715
6	0.0535	0.082	0.079
7	0.063	0.0835	0.092
8	0.0855	0.076	0.1005
9	0.1015	0.078	0.103
10	0.1125	0.0815	0.1095
11	0.1075	0.0855	0.1285
12	0.0925	0.078	0.1285
13	/	0.066	0.088
14	/	/	0.0675

The data before is plotted in Fig. 4.7

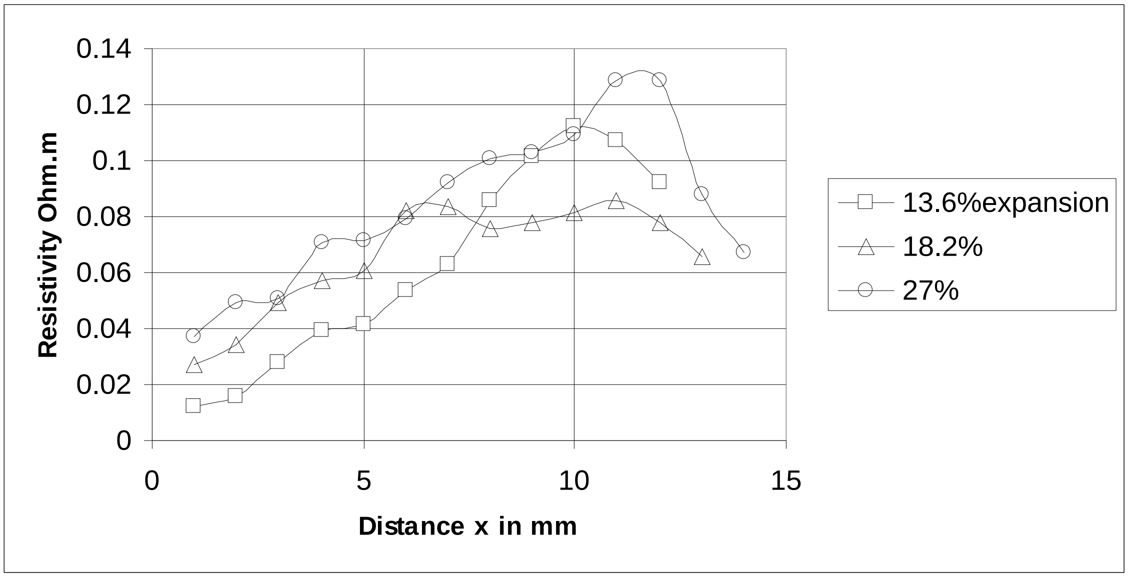

Fig. 4.7 Metal phase resistivity profiles at different expansions and 535 μm diameter copper particle.

Since there are too large differences in the values of metal phase resistivities between that calculated from equation 2.47 or even by inserting the factor 6.7 into it suggested by Fleischmann et.al. A correction factor is suggested to be introduced into equation 2.47. So, equation 2.47 could be written as:

$$\chi_m(x) = \Psi(x,\Gamma)\frac{0.28(1+\Gamma)^{\frac{2}{3}}((1+\Gamma)^{\frac{1}{3}}-1)E^{\frac{1}{3}}\chi_s}{(\rho_m-\rho)^{\frac{1}{3}}v_p^{\frac{2}{3}}} \qquad 4.3$$

where Ψ is suggested to be function of x and expansion coefficient (Γ). Dividing the local values of resistivity by that calculated from equation 2.47 will give local values for the correction factor (Ψ) as tabulated in Table 4.9.

Table 4.9 Correction factor distribution at 13.6, 18.2, and 27% expansion and 535 μm diameter.

Distance x in mm	Correction factor at 13.6%expansion	Correction factor at 18.2 % expansion	Correction factor at 27% expansion
1	0.004513	0.007895	0.008304
2	0.005776	0.009942	0.010961
3	0.010108	0.014474	0.011293
4	0.014079	0.016813	0.015611
5	0.014982	0.01769	0.015833
6	0.019314	0.023977	0.017493
7	0.022744	0.024415	0.020372
8	0.030866	0.022222	0.022254
9	0.036643	0.022807	0.022808
10	0.040614	0.02383	0.024247
11	0.038809	0.025	0.028454
12	0.033394	0.022807	0.028454
13	/	0.019298	0.019486
14	/	/	0.014947

The data in Table 4.9 is plotted in Fig.4.7

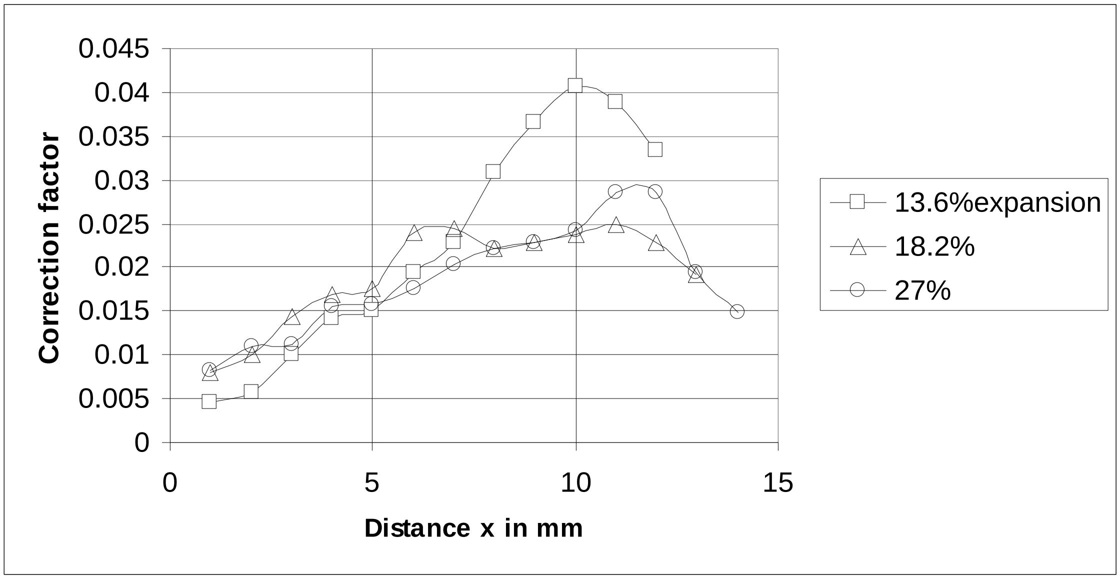

Fig. 4.8 Correction factor profiles at different expansions and535 μm particle diameter.

Now, by curve fitting, the following equations are concluded:

Fourth degree polynomial fit:

$$\Psi = a + bx + cx^2 + dx^3 + ex^4 \qquad 4.4$$

where x is in mm. The constants at different expansions are tabulated below:

Table 4.10 Coefficient of correction factor equation 4.4.

Coefficient	13.6% expansion	18.2% expansion	27% expansion
a	-0.003764	0.0035946	0.0031954
b	0.009995	0.0039096	0.0060247
c	-0.0029408	-0.00011876	-0.0013923
d	0.0004411	-6.4844×10^{-6}	0.00017467
e	-2.03335×10^{-5}	-4.19923×10^{-9}	-7.27829×10^{-6}

Converting this equation in terms of normalized length.

$$\Psi = a' + b'\frac{x}{L} + c'\frac{x^2}{L^2} + d'\frac{x^3}{L^3} + e'\frac{x^4}{L^4} \qquad 4.5$$

The constants related to dimensionless distance along the bed are as below

Table 4.11 Coefficient of correction factor equation 4.5.

Coefficient	13.6% expansion	18.2% expansion	27% expansion
a'	-0.003764	0.0035946	0.0031954
b'	0.1209395	0.049182768	0.081514191
c'	-0.430562528	-0.01879453	-0.254875691
d'	0.781435557	-0.012909568	0.432625097
e'	-0.435866631	-0.00010517	-0.24390491

Plotting the equations gives the following figure.

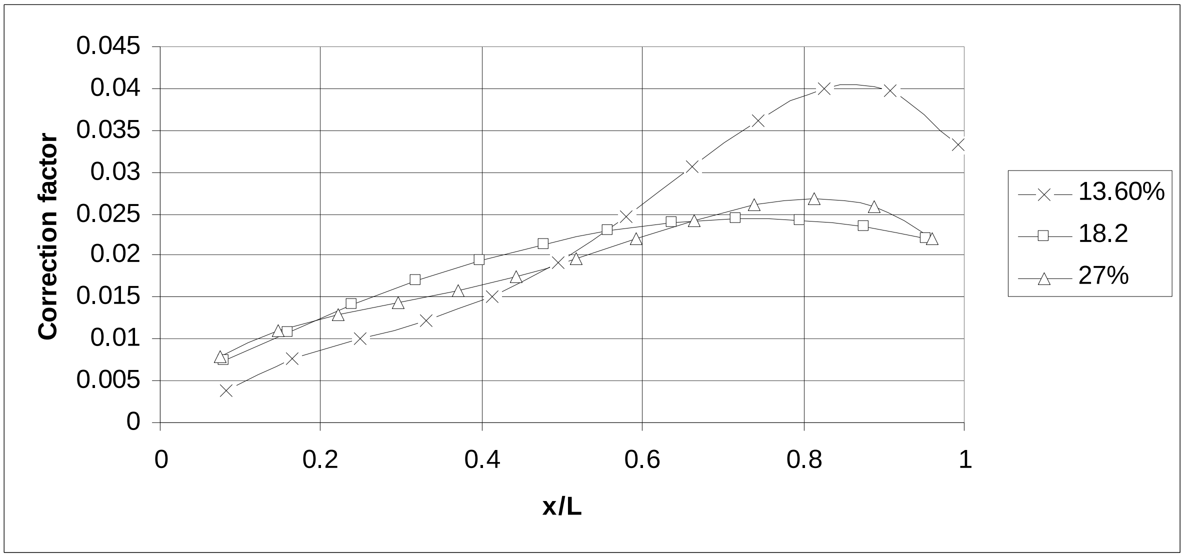

Fig. 4.9 Normalized correction factor profiles at different expansions and535 μm diameter copper particle.

By inserting the expansion coefficient as a variable. The general equation for expansions ranging between 5-30% becomes:

$a' =$ -0.010827+0.051935Γ

$b' =$ 0.1609532-0.294219Γ

$c' =$ -0.608872+1.3110958Γ

$d' =$ 1.1354521-2.603063Γ

$e' =$ -0.630693+1.4325502Γ

$$\Psi = a' + b'\frac{x}{L} + c'\frac{x^2}{L^2} + d\frac{x^3}{L^3} + e\frac{x^4}{L^4}$$

After this modification, the largest error in the values of metal phase resistivity is ranging between 7-30%. Now, the profiles of potential is calculated again using correction factor in the equations of resistivity and compared with Fleischmann assumption of constant resistivity.At 13.6% expansion, the potential profile is:

Table 4.12 Normalized theoretical potential profile at 13.6% expansion and 535 μm diameter after correction.

x/L	Theoretical solution potential in V
0	0
0.082645	-0.0017
0.165289	-0.0059
0.247934	-0.0109
0.330579	-0.0168
0.413223	-0.024
0.495868	-0.03492
0.578512	-0.043
0.661157	-0.0538
0.743802	-0.0648
0.826446	-0.0757
0.909091	-0.0863
0.991736	-0.0958

The data in Table 4.12 is plotted in Fig. 4.10. The two profiles after inserting this correction factor are not easily distinguished from each other.

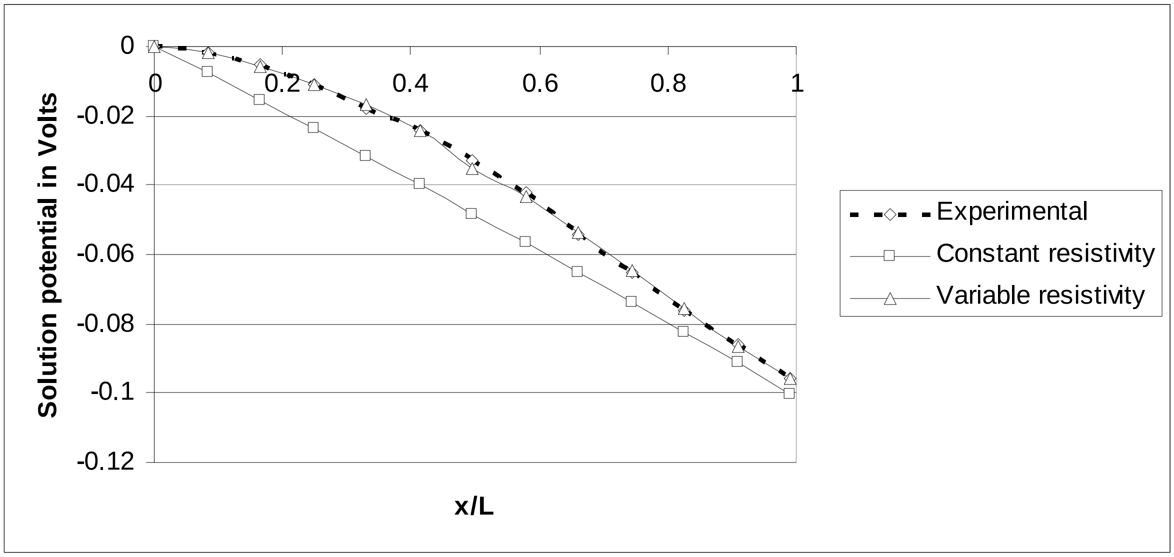

Fig. 4.10 Normalized experimental , constant, and variable resistivity solution potential profiles at 13.6% expansion and 535 μm diameter copper particles.

Table 4.13 Theoretical and experimental potential profile at 18.2% expansion and 535 μm diameter after correction.

Distance x in mm	Theoretical solution potential in V
0	0
1	-0.0023
2	-0.0066
3	-0.0115
4	-0.0171
5	-0.0237
6	-0.0314
7	-0.04
8	-0.0494
9	-0.0592
10	-0.069
11	-0.079
12	-0.089
12.58	-0.096

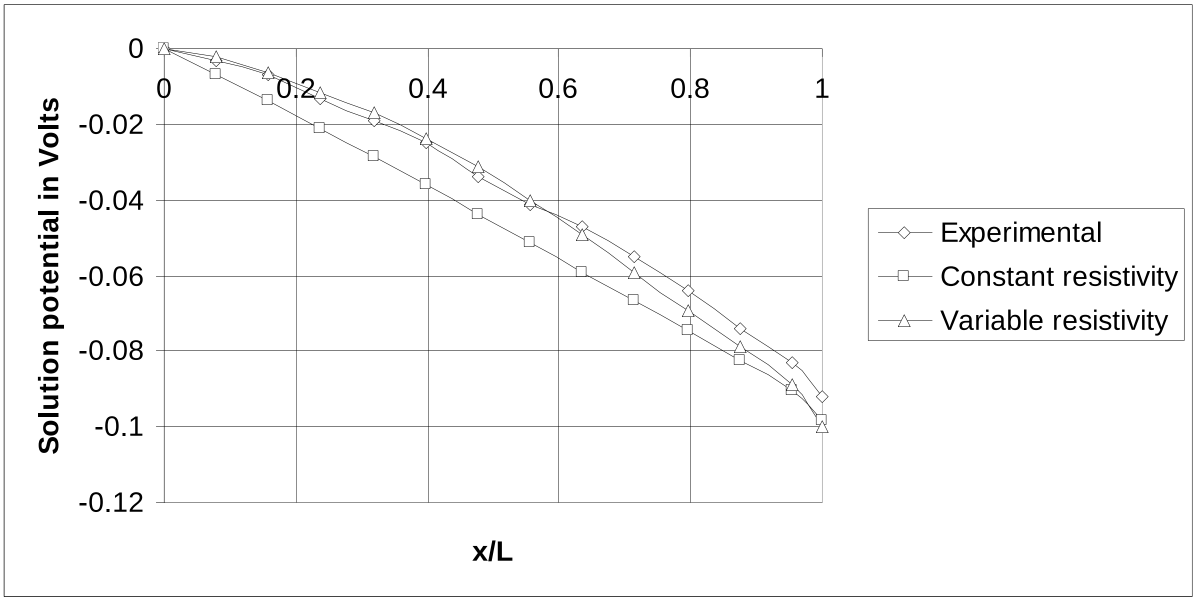

Fig. 4.11 Normalized experimental , constant, and variable resistivity solution potential profile at 18.2% expansion and 535 μm diameter copper particles.

Table 4.14 Normalized theoretical potential profile at 27% expansion and 535 μm diameter copper particles after correction.

Distance x in mm	Theoretical solution potential in V
0	0
1	-0.0029
2	-0.0069
3	-0.0115
4	-0.0165
5	-0.0219
6	-0.028
7	-0.0346
8	-0.0418
9	-0.0495
10	-0.057
11	-0.0664
12	-0.0757
13	-0.0852
14	-0.0888

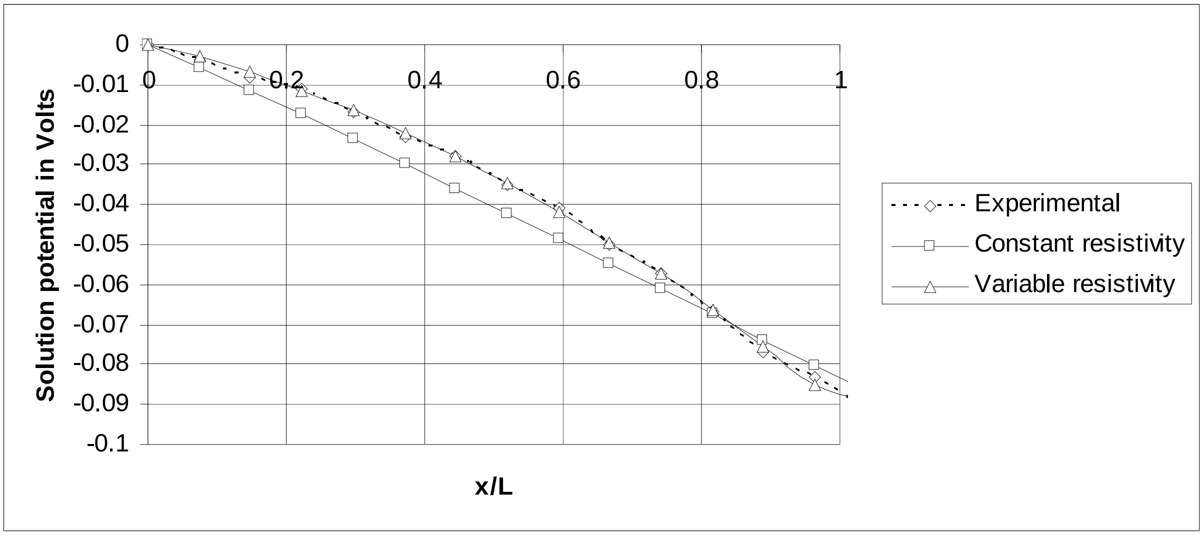

Fig. 4.12 Normalized experimental , constant, and variable resistivity solution potential profile at 27% expansion and 535 μm copper particles after correction.

Variable metal phase resistivity gives closer distribution to the experimental values than a single constant value as shown in the previous three figures. The metal phase potential profile at 27% can be found from equation [38]

$$\phi_m - \phi_s = \phi_m^\circ - I\,\chi_m x - (1 + \frac{\chi_m}{\chi_s})\phi_s \qquad 3.37$$

Local metal potential along the bed is obtained by adding ϕ_s for both sides of equation 3.37. So,

$$\phi_m = \phi_m^\circ - I\,\chi_m x - \frac{\chi_m}{\chi_s}\phi_s \qquad 4.6$$

Three sets of metal phase potential data will be obtained, the experimental data, that obtained from constant resistivity, and that from variable resistivity or local resistivity equation.

Table 4.15 Theoretical and experimental metal phase potential distributions at 27%expansion.

Distance x in mm	Metal phase potential for constant resistivity in V	Metal phase potential for variable resistivity in V	Experimental metal phase potential in V
0	0.0514	0.0514	0.0514
1	-0.01105	0.048049031	0.042
2	-0.05602	0.043501962	0.033
3	-0.09146	0.039068318	0.02
4	-0.12055	0.03486293	0.009
5	-0.14329	0.030757192	-0.002
6	-0.1549	0.027128981	-0.012
7	-0.15858	0.023769174	-0.019
8	-0.15272	0.021345913	-0.027
9	-0.13892	0.020419321	-0.036
10	-0.1283	0.019912171	-0.041
11	-0.08749	0.026345333	-0.046
12	-0.04827	0.03416645	-0.051
13	-0.00588	0.043026033	-0.049
14	-0.05721	0.04135139	-.083

The data in table 4.15 are plotted in Fig. 4.13 as shown

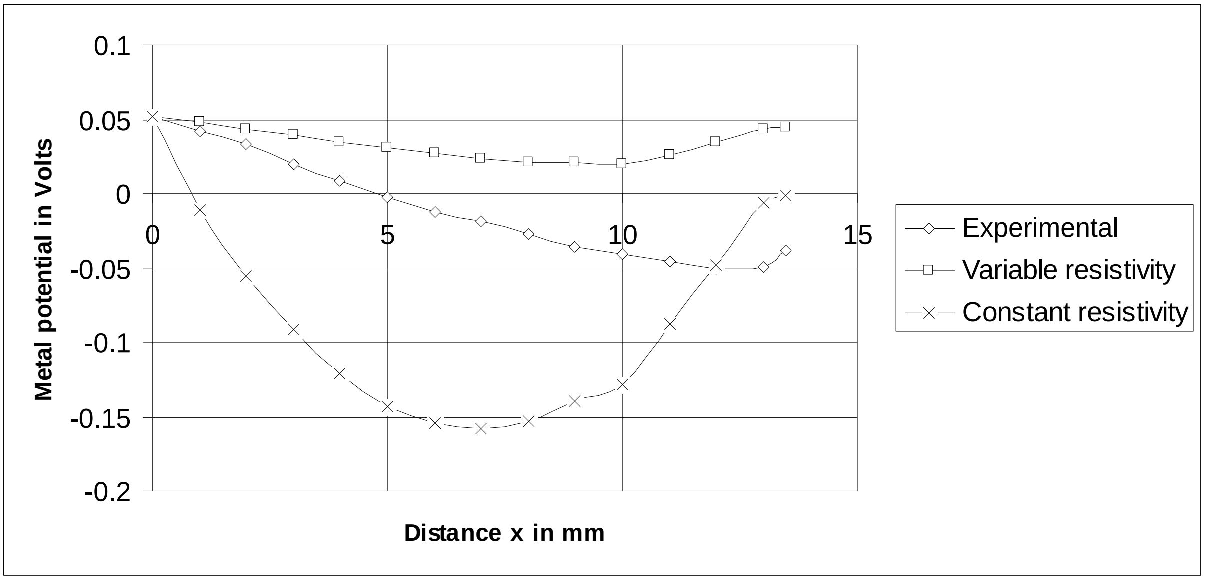

Fig. 4.13 Theoretical and experimental metal phase potential profiles at 27% expansion.

Table 4.15 and Fig. 4.13 show that neither the theoretical assumption of constant resistivity nor that of variable resistivity are precise. Using equation 3.24 and the experimental data to find the resistivity of metal phase and a new equation for the correction factor:

Table 4.16 Local metal phase resistivity and correction factor distributions at 27%expansion.

Distance x in mm along the bed	Metal phase resistivity in $\Omega.m$	Correction factor Ψ
1	0.101455	0.022467
2	0.115448	0.025565
3	0.148137	0.032804
4	0.166194	0.036803
5	0.184867	0.040938
6	0.207129	0.045868
7	0.225975	0.050041
8	0.258876	0.057327
9	0.30952	0.068542
10	0.346572	0.076747
11	0.472656	0.104667
12	0.69243	0.153335
13	1.251959	0.27724
14	0.672702	0.148966

$$\Psi = a + bx + cx^2 + dx^3 + ex^4 \qquad 4.4$$

The coefficient data for 27% expansion are

a =-0.0080944271

b =0.03629234

c =-0.0072445192

d = 0.000618544

e =-1.1335107×10^{-5}

or in dimensionless form

a' =-0.0080944

b' =0.48922

c'=-1.3164

d'=1.51508

e'=0.37427

$$\Psi = a' + b'\frac{x}{L} + c'\frac{x^2}{L^2} + d'\frac{x^3}{L^3} + e'\frac{x^4}{L^4} \qquad 4.7$$

The previous coefficient could be used to predict the metal potential profiles. It is noticeable that the equation 4.4 for calculating metal phase potential is extremely sensetive to any minor change in the solution potential or resistivity, which leads that equation 4.5 with the previous coefficients could be hardly generalized with precaution. Using constant resistivity for calculating potential profile will give very fragment and high numerical values of potential.

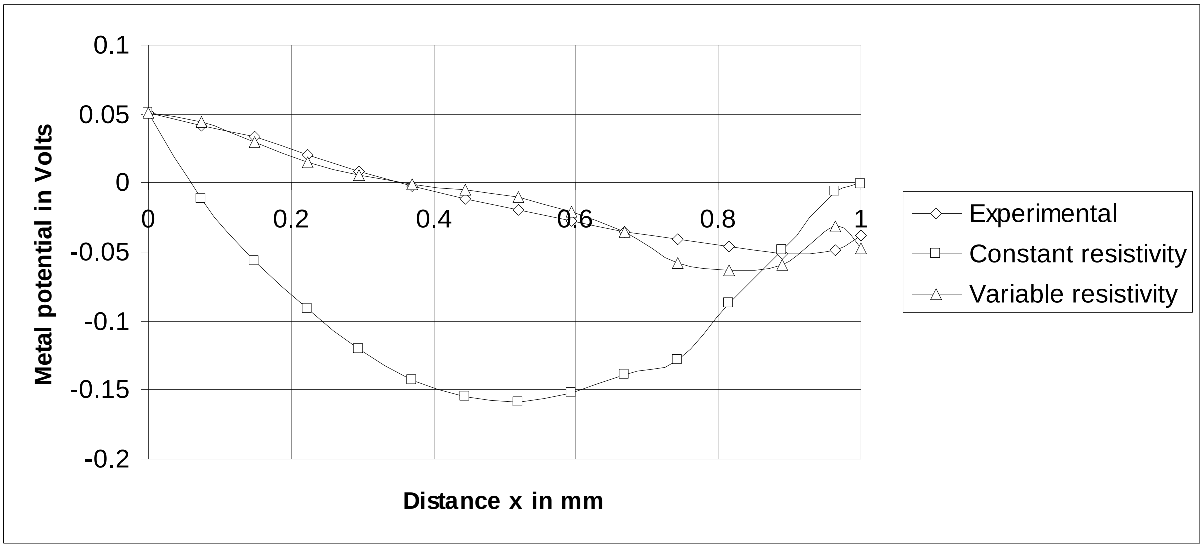

Fig.4.14 Normalized metal phase profiles at27% and 535 μm copper particles.

The overpotential is found by equation 3.13 as

$$\eta = \phi_m - \phi_s \qquad 3.24$$

Table 4.17 Theoretical and experimental overpotential profiles at 27%expansion.

Distance x in mm	Experimental overpotential in Volts	Theoretical overpotential at constant resistivity in V	Theoretical overpotential at variable resistivity in V
0	0.0514	0.0514	0.0514
1	0.046	-0.00535	0.047206
2	0.041	-0.04452	0.035929
3	0.031	-0.07396	0.026917
4	0.026	-0.09695	0.022367
5	0.021	-0.11359	0.021599
6	0.016	-0.119	0.023521
7	0.016	-0.11648	0.023935
8	0.014	-0.10432	0.021185
9	0.014	-0.08422	0.014534
10	0.016	-0.0672	-0.00085
11	0.021	-0.01999	0.003496
12	0.026	0.025626	0.016999
13	0.034	0.074519	0.053151
13.48	0.053	0.085618	0.042001

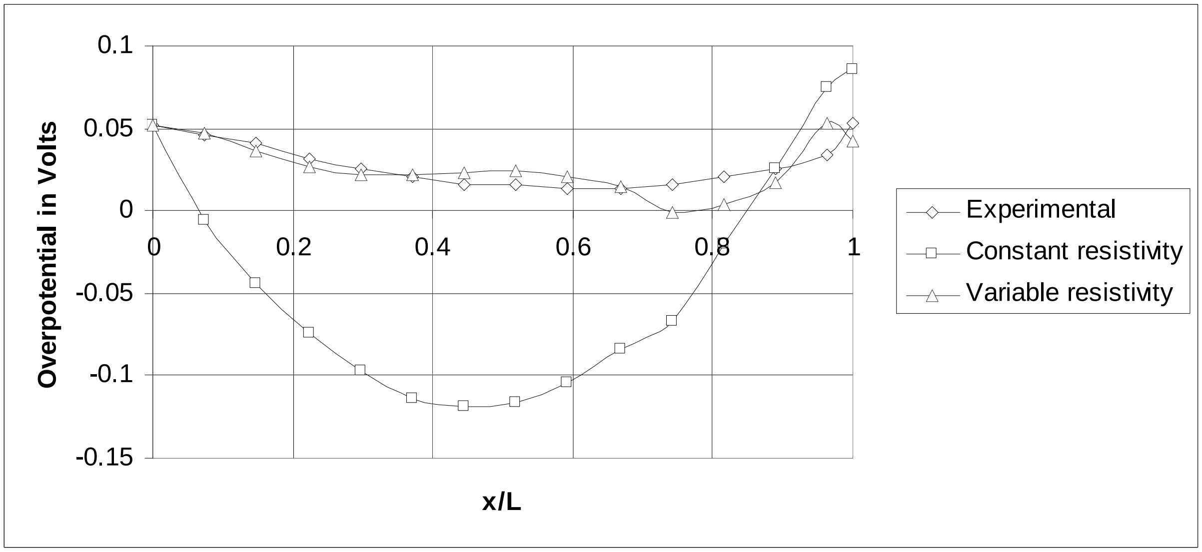

Fig. 4.15 Overpotentail distribution for 27% expansion and 535 μm copper particles.

4.5 Checking Correction Equation Suggested (Predicted Equation)

Germain and Goodridge [17] have published data of potential distribution for copper deposition in an electrochemical fluidized bed of 500 μm diameter copper particles. A bed height of 8.6mm is used, and 20% expansion. The total current density applied is 3010A/m^2, and the metal potential at standard conditions $\left(\phi_m^\circ\right)$ is -.045 Volt. The density of copper is 8920 Kg/m^3 and that for the solution is 1000Kg/m^3. The viscosity is 10^{-3} Kg.m^{-1}.s^{-1} . Checking the consistency of the assumption of local resistivity by the experimental data. So, the porosity from equation 3.4a is:

$$\varepsilon = \frac{\Gamma + \varepsilon_\circ}{\Gamma + 1} = 0.5167$$

The surface area per unit volume is calculated from equation 3.12 and 3.13

$$a_\circ = \frac{6}{d}(1-\varepsilon) = \frac{6}{500 \times 10^{-6}}(1-0.42) = 6980 \, {m^2}/{m^3}$$

$$a = a_\circ \frac{(1-\varepsilon)}{(1-\varepsilon_\circ)} = 6980 \times \frac{(1-0.5167)}{(1-.42)} = 5816 \, {m^2}/{m^3}$$

To calculate potential distribution, the constants β and f are found from equations 3.46 and 3.47

$$\beta = \frac{2 \times 9.6 \times 5816 \times 8.314 \times 298.15}{0.5 \times 2 \times 96500} = 2{,}867 AV \ / m$$

$$f = \frac{0.5 \times 2 \times 96500}{8.314 \times 298.15} = 38.929 V^{-1}$$

The terminal settling velocity is found from equation 3.6b

$$u_t = \left[\frac{4}{225} \frac{(\rho_m - \rho)^2 g^2}{\rho \mu} \right]^{1/3} d \qquad \text{for} \quad 0.4 < Re_p < 500 \qquad 3.6b$$

$$u_t = \left[\frac{4}{225} \frac{(8920-1000)^2 9.81^2}{1000 \times 10^{-3}} \right]^{1/3} \times 500 \times 10^{-6} = 0.2376 m/s$$

$$\mathrm{Re}_p = \frac{\upsilon_t d}{\nu} = \frac{0.2376 \times 500 \times 10^{-6}}{10^{-6}} = 118.8 \text{ within the range of equation 3.6b}$$

The average velocity is found from equation 3.5

$$\varepsilon = \left(\frac{U_{av}}{u_t} \right)^{0.225 \left(\frac{u_t d}{\upsilon} \right)^{0.1}} \qquad 3.5$$

$$0.5167 = \left(\frac{U_{av}}{0.2376} \right)^{0.225 \left(\frac{0.2376 \times 500 \times 10^{-6}}{10^{-6}} \right)^{0.1}} \Rightarrow U_{av} = 0.0364 m/s$$

The solution resistivity for the system is $0.044 \Omega.m$. The metal phase resistivity is found using equation 2.47 as:

$$\chi_m = \frac{0.28(1+\Gamma)^{\frac{2}{3}}((1+\Gamma)^{\frac{1}{3}}-1)E^{\frac{1}{3}}\chi_s}{(\rho_m - \rho\ )^{\frac{1}{3}} v_p^{\frac{2}{3}}} \qquad 2.47$$

where $v_p = \dfrac{U_{av}}{\varepsilon}$

$$\chi_m = \frac{0.28(1+0.2)^{\frac{2}{3}}((1+0.2)^{\frac{1}{3}}-1)\left(10^{12}\right)^{\frac{1}{3}} 0.044}{(8920-1000)^{\frac{1}{3}} \left(\frac{0.2364}{0.5167} \right)^{\frac{2}{3}}} = 0.7365 \Omega.m$$

The metal phase resistivity from equation 3.1 is

$$\chi_m = \frac{0.04179(1+0.2)^{\frac{2}{3}}((1+0.2)^{\frac{1}{3}}-1)\left(10^{12}\right)^{\frac{1}{3}} 0.044}{(8920-1000)^{\frac{1}{3}} \left(\frac{0.2364}{0.5167} \right)^{\frac{2}{3}}} = 0.1099 \Omega.m$$

Now, the local resistivity is calculated as:

$$\chi_m(x) = \Psi(x)\chi_m \qquad 4.4$$

$$\Psi(\frac{x}{L}) = a' + b'\frac{x}{L} + c'\frac{x^2}{L^2} + d'\frac{x^3}{L^3} + e'\frac{x^4}{L^4} \qquad 4.5$$

Using constants of equation 4.5 which are:

a' = -0.010827+0.051935Γ=-44$\times10^{-5}$

b' = 0.1609532-0.294219Γ=0.1021

c'= -0.608872+1.3110958Γ=-.3466

d'= 1.1354521-2.603063Γ=0.6148

e'= -0.630693+1.4325502Γ=-0.3442

Now using equation 4.5 to calculate the local resistivity at 20% expansion will give the following table:

Table 4.18 Normalized metal phase resistivity for 500 μm copper particles at 20% expansion.

$\frac{x}{L}$	Metal Phase potential in $\Omega.m$
0	0
0.116279	0.005634
0.232558	0.008311
0.348837	0.010311
0.465116	0.013124
0.581395	0.017129
0.697674	0.021592
0.813953	0.024667
0.930233	0.023395
1	0.018899

The data on previous table are drawn in the next figure.

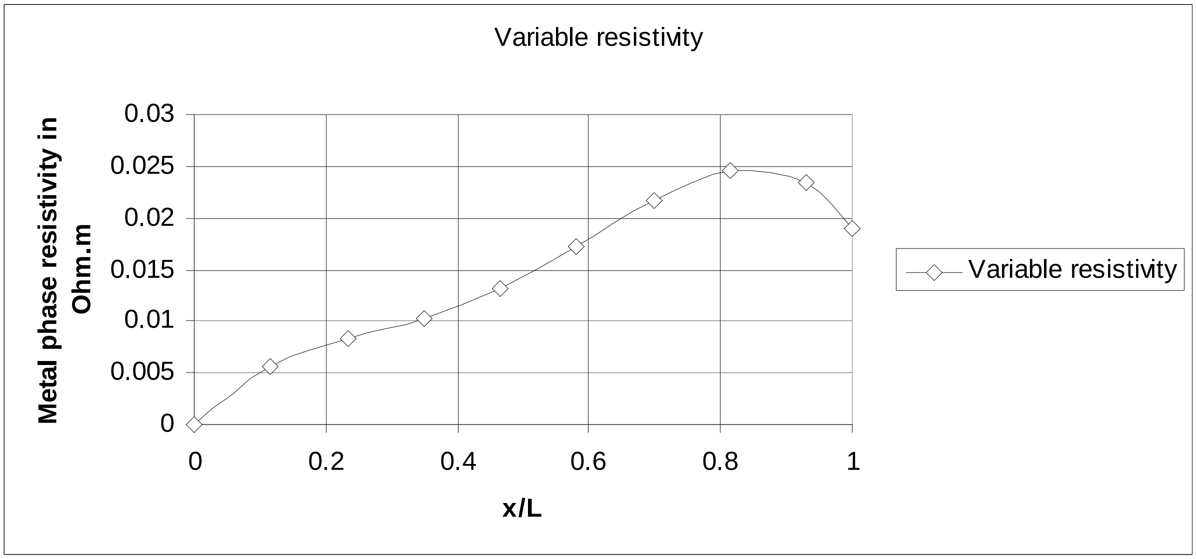

Fig.4.16 Normalized metal Phase resistivity for 500 μm copper particles at 20% expansion.

The local metal phase resistivity data are used to calculate the solution potential difference from equation 3.77. The following table can be constructed.

Table 4.19 Normalized experimental, variable resistivity, constant resistivity solution potential at 500 μm diameter copper particles at 20% expansion.

$\frac{x}{L}$	Solution potential at variable resistivity in Volts	Experimental solution potential in Volts	Solution potential at constant resistivity in Volts
0	0	0	0
0.116279	-0.0126	-0.005	-0.078
0.232558	-0.0356	-0.015	-0.156
0.348837	-0.0639	-0.03	-0.235
0.465116	-0.1031	-0.065	-0.313
0.581395	-0.1567	-0.12	-0.391
0.697674	-0.2201	-0.176	-0.47
0.813953	-0.2797	-0.235	-0.541
0.930233	-0.3095	-0.267	-0.628
1	-0.2899	-0.275	-0.673

the previous data are plotted in the next figure

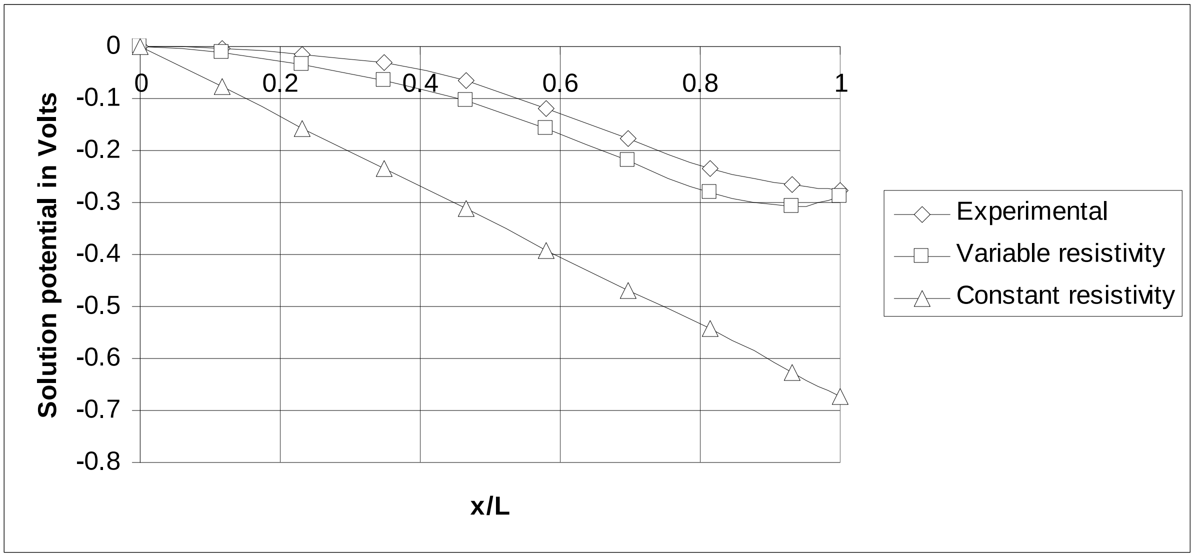

Fig.4.17 Normalized experimental, variable resistivity, constant resistivity solution potential at 500 μm diameter copper particles at 20% expansion.

Now, to calculate the metal phase resistivity to be used in equation 4.6

$$\phi_m = \phi_m^\circ - I\,\chi_m x - \frac{\chi_m}{\chi_s}\phi_s \qquad 4.6$$

The resistivity is found from equation 4.7 and the constants have been used earlier. So, the values of metal phase potential are found as:

Table 4.20 Normalized experimental, variable resistivity, constant resistivity metal phase potential at 500 μm diameter copper particles at 20% expansion.

$\frac{x}{L}$	Metal phase potential at variable resistivity in Volts	Experimental metal phase potential in Volts	Metal phase potential at constant resistivity in Volts
0	0.045	0.045	0.045
0.116279	0.029656	0.035	-0.09098
0.232558	0.001691	0.022	-0.22695
0.348837	-0.03314	0.013	-0.36043
0.465116	-0.08226	0.003	-0.49641
0.581395	-0.15179	-0.007	-0.63238
0.697674	-0.23694	-0.022	-0.76586
0.813953	-0.31793	-0.034	-0.91932
0.930233	-0.35379	-0.04	-1.03282
1	-0.31969	-0.042	-1.1189

The previous data is plotted in the next Figure

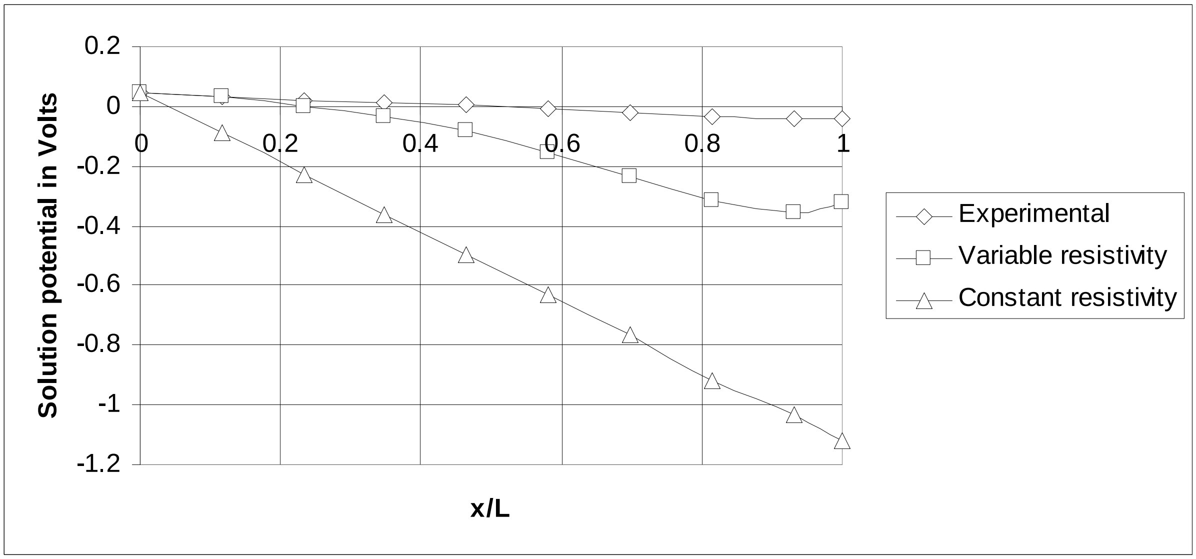

Fig. 4.18 Normalized experimental, variable resistivity, constant resistivity metal phase potential at 500 μm diameter copper particles at 20% expansion

4.6 Concentration Distribution

Concentration distribution along the bed could be obtained for the system in section 4.3 using mass transfer equations. A number of cases have been considered

4.6.1 Variable Expansion

$$C(x) = C_\circ \exp\left(\frac{-x}{\lambda}\right) \qquad 3.50$$

where

$$\lambda = \frac{U_{av}}{K_{av} a \varepsilon} \qquad 3.51$$

$$\frac{K_{av} d}{D} = \frac{(1-\varepsilon)^{1/2}}{\varepsilon} \mathrm{Re}_d^{1/2} Sc^{1/3} \qquad 3.14$$

at 13.6% expansion

$$K_{av} = 1.52 \frac{4\times10^{-10}}{535\times10^{-6}} \frac{(1-0.4894)^{0.5}}{0.4894} \left(\frac{0.012076 \ \times 535\times10^{-6}}{10^{-6}}\right)^{0.5} \left(\frac{10^{-6}}{4\times10^{-10}}\right)^{0.333}$$

$$K_{av} = 5.7228\times10^{-5}\,\mathrm{m/s} : \lambda = \frac{0.012076}{5.7228\times10^{-5}\times5720\times0.4894} = 0.0754m$$

at 18.2% expansion

$$K_{av} = 1.52 \frac{4\times10^{-10}}{535\times10^{-6}} \frac{(1-0.5094)^{0.5}}{0.5094} \left(\frac{0.01359\times535\times10^{-6}}{10^{-6}}\right)^{0.5} \left(\frac{10^{-6}}{4\times10^{-10}}\right)^{0.333}$$

$$K_{av} = 5.718\times10^{-5}\,\mathrm{m/s} : \lambda = \frac{0.01359}{3.765\times10^{-5}\times5500\times0.5094} = 0.0848m$$

at 27% expansion

$$K_{av} = 1.52 \frac{4\times10^{-10}}{535\times10^{-6}} \frac{(1-0.5433)^{0.5}}{0.5433} \left(\frac{0.01509\times535\times10^{-6}}{10^{-6}}\right)^{0.5} \left(\frac{10^{-6}}{4\times10^{-10}}\right)^{0.333}$$

$$K_{av} = 5.449 \times 10^{-5} \text{m/s} : \lambda = \frac{0.01647}{5.449 \times 10^{-5} \times 5120 \times 0.5433} = 0.1087m$$

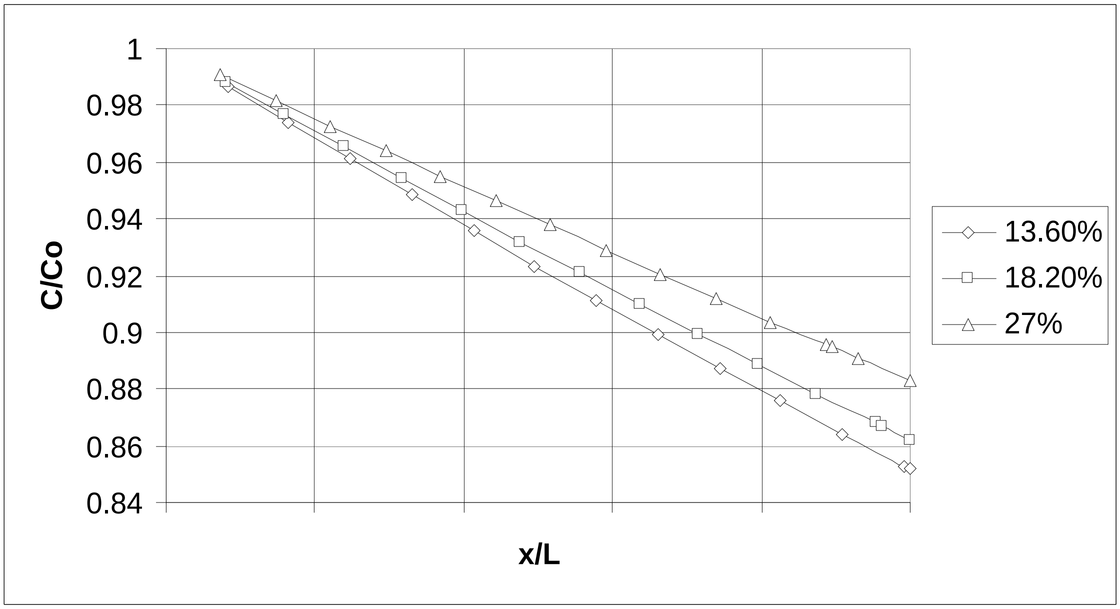

Fig. 4.19 Normalized concentration profile at 13.6, 18.2, and 27% expansion for 535 μm diameter copper particles.

4.6.2 Effect of particle Diameter

Considering number of copper particles at 27% expansion. $L_{\circ}$=10.6mm$\Rightarrow L$=13.48mm. Simple table can be constructed explaining concentration profile along the bed.

Table 4.21 Concentration Profile for a bed of 200, 500, 1000 μm copper particles at 27%.

$\frac{x}{L}$	$\frac{C}{C_\circ}$ at 200 μm	$\frac{C}{C_\circ}$ at 300 μm	$\frac{C}{C_\circ}$ at 500 μm	$\frac{C}{C_\circ}$ at 1000 μm
0.074184	0.953023	0.980427	0.993519	0.998543
0.148368	0.908253	0.961237	0.98708	0.997089
0.222552	0.865586	0.942423	0.980683	0.995637
0.296736	0.824923	0.923977	0.974327	0.994187
0.37092	0.786171	0.905892	0.968013	0.992739
0.445104	0.749239	0.88816	0.961739	0.991293
0.519288	0.714042	0.870776	0.955507	0.989849
0.593472	0.680498	0.853733	0.949314	0.988407
0.667656	0.648531	0.837023	0.943162	0.986967
0.74184	0.618064	0.820639	0.937049	0.98553
0.816024	0.58903	0.804577	0.930976	0.984094
0.890208	0.561359	0.788829	0.924943	0.982661
0.964392	0.534988	0.773389	0.918948	0.98123
1	0.522773	0.766086	0.916085	0.980543

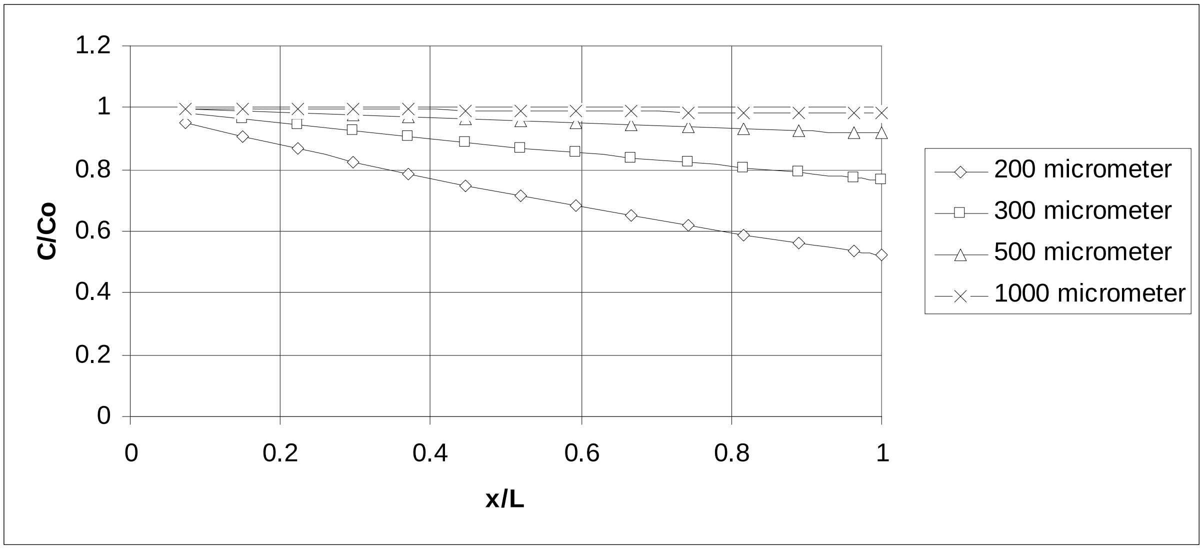

Fig. 4.20 Concentration Profile for a bed of 200, 500,1000 μm copper particles at 27%.

Chapter Five

Discussion

5.1 Hydrodynamics of Fluidized Bed

Studying hydrodynamics of fluidized bed showed a number of facts:

1) The terminal settling velocity of certain particle (e.g copper particles) is independent on flow conditions. It is function of the particle diameter and physical properties as shown in equations 3.6a, 3.6b, and 3.6c in a particular system and has no relation with bed expansion or flow velocity of that system.
2) By examining Fig. 5.1 for the deposition of copper coated glass spheres, it is found that increasing particles diameter due to deposition and keeping flow velocity unchanged will reduce the expansion of bed. To maintain the same expansion, an increase in the velocity of flow must take place. The spaces between larger particles are more, this leads that the fluid flows with ease in the spaces and reducing the upward force which overcome the gravitational force. The velocity change with particle diameter and expansion is plotted in Fig. 5.1.
3) The conditions of the system can be kept constant by feeding new particles to the system and venting out grown larger ones, due to deposition, from the bottom of the bed.
4) The pressure drop per unit length of fluidized bed drops as the porosity increases since the spaces between particles increases leading to a lower pressure drop.

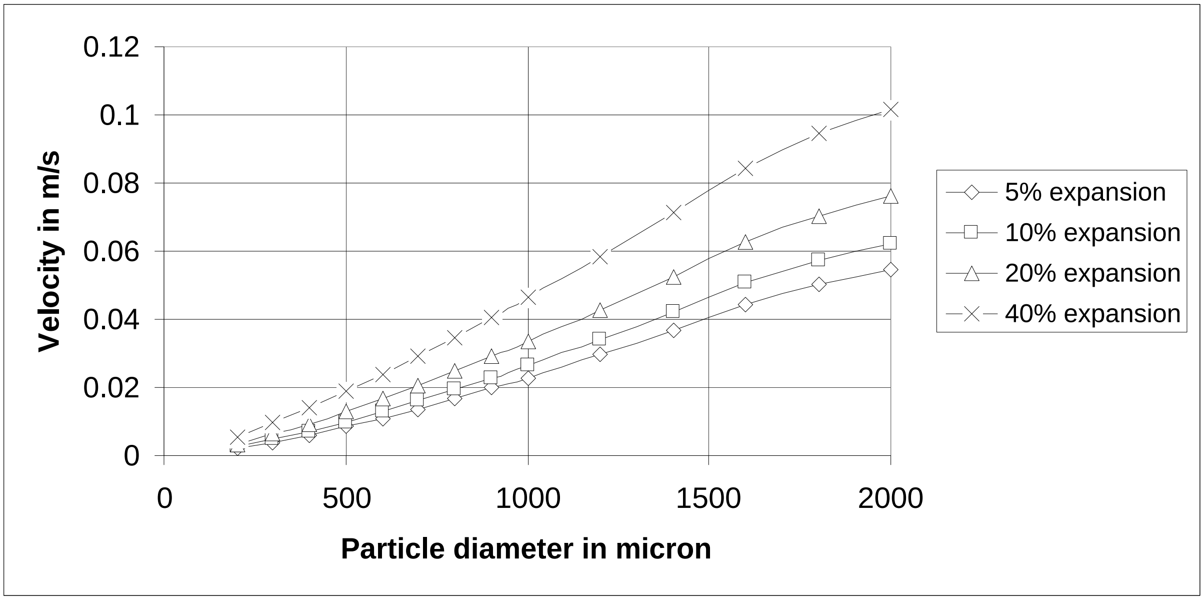

Fig. 5.1 Velocity change with expansion for different range of diameters.

5) In the context, the maximum particle size is 2mm or around, larger particles will give lower surface area for mass transfer as explained in equation 3.12 and leads that the electrical charge will pass through metallic phase because of the large particle diameter and small bed thickness(normally not more than 15mm).

5.2 Discussion of the Metal Phase Resistivity

Fleischmann et al [19] developed an expression for the metal phase resistivity based on elastic collision between particles. This expression has been tested by Fleischmann et al [37] and a correction factor of 6.7 was suggested to be used in the denominator of equation 2.47 [37] to become equation 3.1[19].

$$\chi_m = \frac{0.28(1+\Gamma)^{\frac{2}{3}}((1+\Gamma)^{\frac{1}{3}}-1)E^{\frac{1}{3}}\chi_s}{(\rho_m-\rho\ )^{\frac{1}{3}}\nu_p^{\frac{2}{3}}} \tag{2.47}$$

$$\chi_m = \frac{0.04179(1+\Gamma)^{\frac{2}{3}}((1+\Gamma)^{\frac{1}{3}}-1)E^{\frac{1}{3}}\chi_s}{(\rho_m-\rho\ )^{\frac{1}{3}}\nu_p^{\frac{2}{3}}} \qquad 3.1$$

Using equation 3.77 and 3.24 for calculating solution and metal phase potential profile

$$\phi_s = -\frac{I\,\chi_m x}{\left(\dfrac{\chi_m}{\chi_s}+1\right)} + \frac{1}{\left(\dfrac{\chi_m}{\chi_s}+1\right)} \times$$

$$\ln\left[\frac{\cos^2\left(\dfrac{1}{2}fx\,\beta^{\frac{1}{2}}(\chi_m+\chi_s)^{\frac{1}{2}}\left\{1-\dfrac{I^2\chi_m^2}{\beta(\chi_m+\chi_s)}\exp-f\,\phi_m^\circ\right\}^{\frac{1}{2}}\exp\dfrac{1}{2}f\,\phi_m^\circ-\cos^{-1}\left\{1-\dfrac{I^2\chi_m^2}{\beta(\chi_m+\chi_s)}\exp-f\,\phi_m^\circ\right\}^{\frac{1}{2}}\right)}{1-\dfrac{I^2\chi_m^2}{\beta(\chi_m+\chi_s)}\exp-f\,\phi_m^\circ}\right]^f$$

……..3.77

$$\phi_m = \phi_m^\circ - I\,\chi_m x - \frac{\chi_m}{\chi_s}\phi_s \qquad 4.6$$

It is found that the factor suggested to be used as a correction for the metal phase resistivity will not give an accurate solution potential profile and definitely high error metal phase potential profile. The assumption of constant metal phase resistivity is not valid since the electrical charges will have variable tracks each second and the concentraion of particles(number of particles per unit volume element) is changing continuously along the bed. Equation 3.1 will still give very high values of resistivity in spite of the factor 6.7 inserted in the denominator of equation 2.47. Therefore, it is necessary to find local values of the resistivity. Solving experimental data of solution potential for local values of metal phase resistivity as in section 4.4 give in general lower values of resistivity which means that the theory of elastic collision between particles is not precise and hence lower resistivities means higher conductance, it is suggested that the charge is transferred in different manner than that of elastic collision.

The assumption of local metal phase resistivity could be attributed to the fact that the particles concentration is low close to the entrance of the reactor and rising continously up to the end of the reactor. The following conclusions have been reached from the work in section 4.4:

1) Increasing the bed expansion will reduce the resistivity of the solution phase since the porosity increases leading that the particles will distribute on a larger volumes according to equation 3.3
2) Increasing the bed expansion will increase the resistivity of the discontinuous metal phase since the particles become more separated from each other as shown in Fig. 4.2 and table 4.3. It is worth saying that all the principle of metal phase resistivity is based on the collisions between particles, and larger spaces between particles leading to lower collisions and higher resistivity as given in equation 3.1.

The obtained equation of resistivity from this work will have the form

$$\chi_m(x) = \Psi(x,\Gamma)\frac{0.28(1+\Gamma)^{\frac{2}{3}}((1+\Gamma)^{\frac{1}{3}}-1)E^{\frac{1}{3}}\chi_s}{(\rho_m-\rho)^{\frac{1}{3}}v_p^{\frac{2}{3}}} \qquad 4.3$$

where $\Psi\left(\frac{x}{L},\Gamma\right)$ is the local correction factor inserted into equation 3.47. Using local resistivity equation is due to the following reasons:

1) The particles are discrete in the region close to the feeder because of the flow. The flow will displace most of the particles away from feeder, and leaving the rest of the particles which slipped from the upward force and the particles which are coming downward only.
2) Higher concentration of particles will reduce the resistivity of metal phase because of the increased collisions between particles.

The correction factor (Ψ) in this work is function of normalized local position and expansion and will have the following form:

$$\Psi = a' + b'\frac{x}{L} + c'\frac{x^2}{L^2} + d\frac{x^3}{L^3} + e\frac{x^4}{L^4} \qquad 4.5$$

where the constant are:

a' = -0.010827+0.051935Γ

b' = 0.1609532-0.294219Γ

c'= -0.608872+1.3110958Γ

d'= 1.1354521-2.603063Γ

e'= -0.630693+1.4325502Γ

For a 10 and 30% expansion, the following Figure is plotted

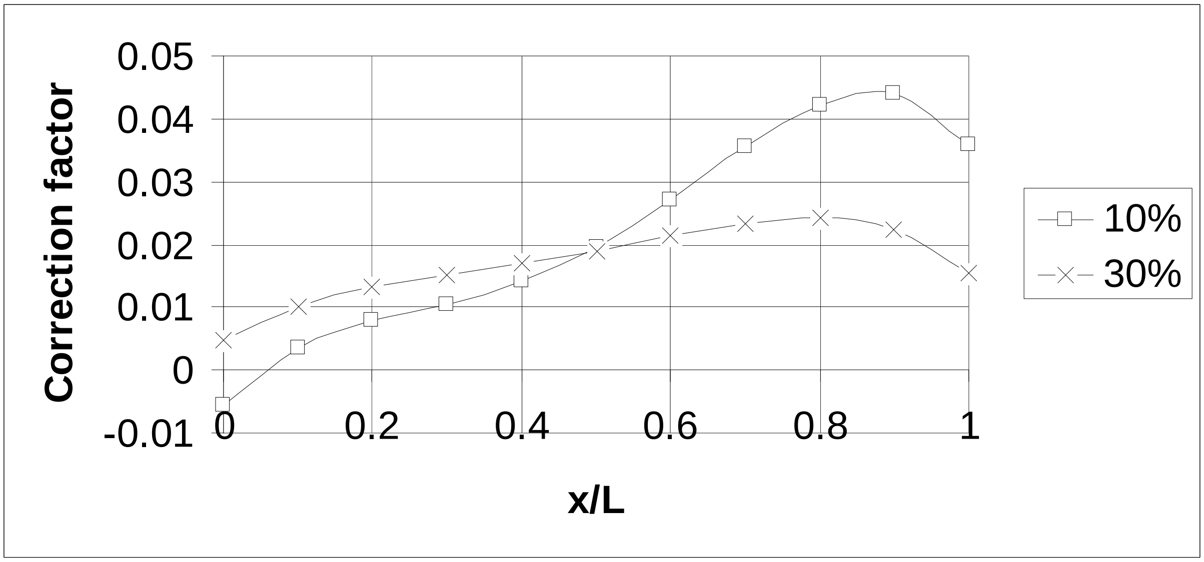

Fig. 5.2 Normalized correction factor with expansion change.

Noting from Fig.5.2 that the metal phase resistivity is rising up to 90% of the reactor and then falls. This is suggested to be due to the low concentration of the particles at the end of reactor due to low number of particles reaching the end. It could be due to fountain-like effect of particles distribution in the end of the reactor. Local phase resistivity equation will solve the problem started in the first place from integrating Ohm's law in the metal phase and assuming that the metal phase resistivity is constant with x.

5.3 Discussion of the Potential Profiles

The total current density for a certain system is function of bed length, increasing bed length at definite conditions will require an increment in the total current density applied to the bed as shown in Fig. 4.3.

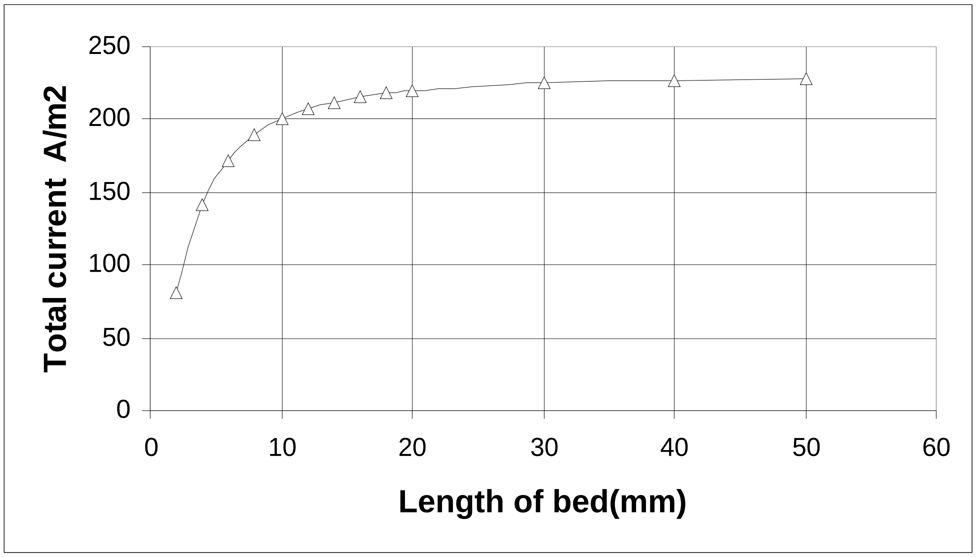

Fig.4.3 Total current requirement for different bed lengths.

However, the bed length could not be increased to very high values as shown in the same figure since the current becomes almost a constant value after 1.5 to 2.0 cm length normally for the case of activation polarisation. This means that increasing the bed length will not particularly increase the performance of the bed, since bipolar and inert regions will appear in the bed as shown in Fig. 3.4. Calculating the current using values of metal phase resistivity obtained from equation 2.47 will lead to false values of total current densities while equation 3.1 will give better estimate and closer to the experimental values. So, equation 3.1 will only be adopted for the calculation of total current density. In spite of the fact that the bed length can not exceed 15 to 20 mm as shown in Fig.4.3 and Fig.3.4. There will be no limitation for increasing bed in the other coordinates.

Solution potential profiles calculated using Fleischmann et al model [37] is not precise because of the concept that assumes constant metal phase resistivity along the bed. Calculating local values of resistivity gives more precise values.

This is evident by examining Fig. 4.10, 4.11, and 4.12. After correction factor equation is used, a more precise curves for solution potential profiles is obtained as shown in Fig. 4.12.

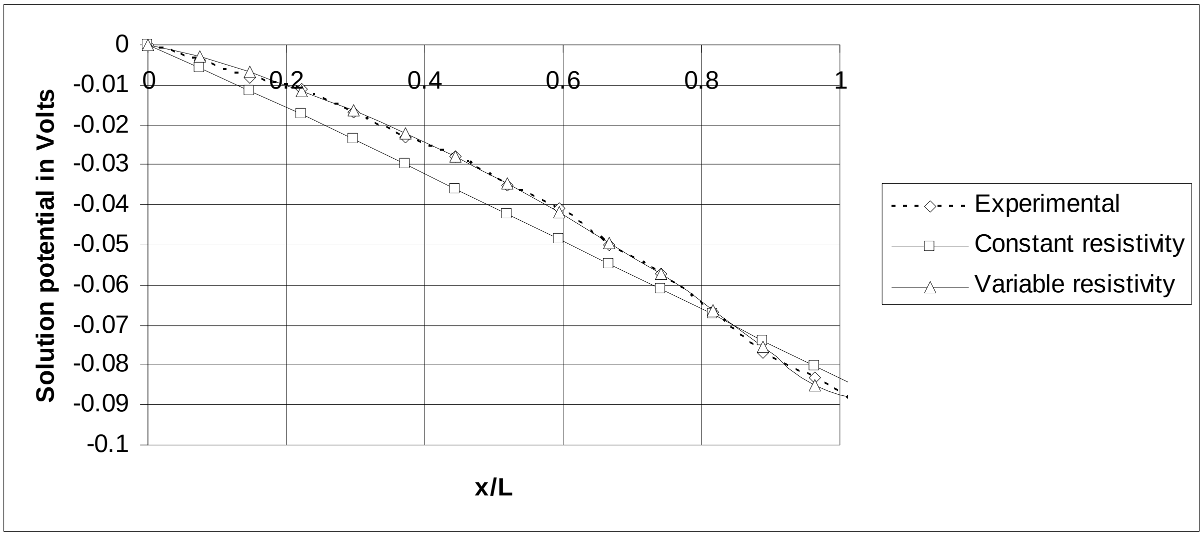

Fig. 4.12 Normalized experimental , constant, and variable resistivity solution potential profile at 27% expansion and 535 μm copper particles after correction.

The equation has been tested for a different system [17] of $500\mu m$ copper particles and a very good agreement is obtained. This is shown in Fig. 4.16

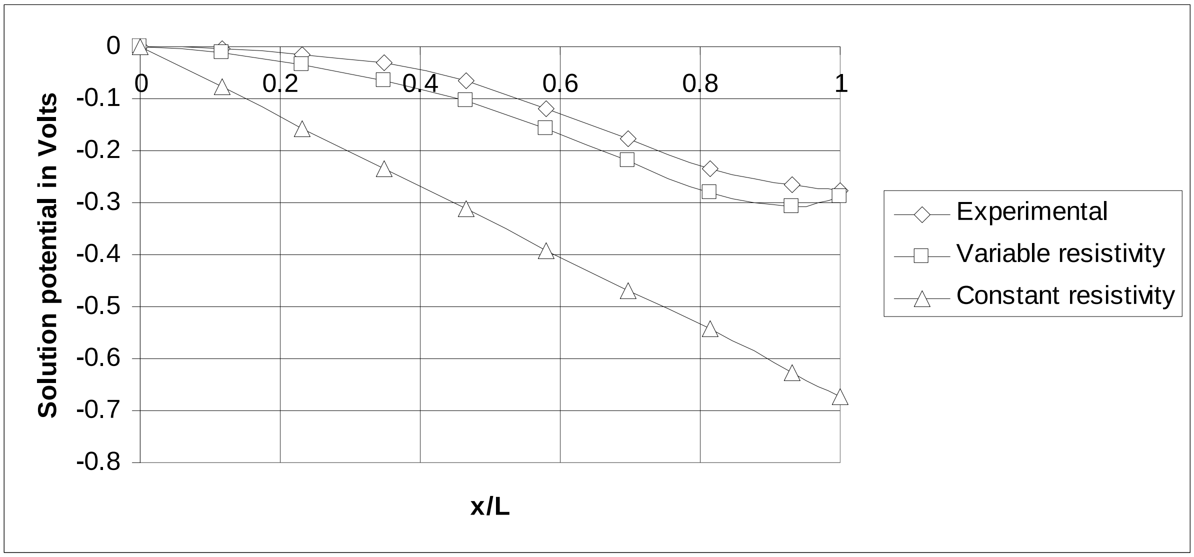

Fig.4.16 Normalized experimental, variable resistivity, constant resistivity solution potential at 500 μm diameter copper particles at 20% expansion.

From previous figure it is evident that the variable resistivity model will give better estimate and much closer values to the experimental work than Fleischmann constant resistivity assumption. The importance of using local metal phase resistiviy values is to find the potential difference along the bed which is the main problem in designing any electrochemical reactor. the second thing is that accurate solution and metal phase potential distribution will give us an idea when the bed is working effectively and to check if the bed is well cathodically protected(no anodic zones). For the case of metal phase potential the curve obtained from local resistivity model is much closer to the experimental work than the constant metal phase potential as shown in Fig. 4.16.

5.4 Concentration Profile

The concentration profile is studied for two cases as follows:

5.4.1 Effect of Expansion

From the work in section 4.6.1 it is found that increasing expansion will reduce the mass transfer rates in fluidized bed as shown in Fig. 4.19. the mass transfer coefficient is not greatly affected by increasing expansion as shown in table below. While expansion increases, the surface area per unit volume decreases. This leads that mass transfer rates decreases as shown in Fig. 4.19.

Table 5.1 Mass transfer coefficient for $535\mu m$ diameter copper particles.

Expansion %	K_{av} in m/s
13.6	5.7228×10^{-5}
18.2	5.718×10^{-5}
27	5.449×10^{-5}

5.4.2 Effect of Particle Diameter

Lower particle diameter leads to higher mass transfer rates as shown in Fig.4.20. As the diameter becomes smaller, higher transfer rates is accomplished. This is attributed to the surface area per unit volume which become greater for smaller particles. The conversion is relatively low due to thin bed thickness. The conversion could by greatly increased by recycling. The bed could be several millimeters in thickness but the other dimensions could be as large as wanted.

Chapter Six

Conclusions and Recommendations for Future Work

6.1 Conclusions

Fluidized bed represents one of the promising fields in electrochemical industries for a number of reasons. A number of conclusions have been reached from the previous work:

1) Variable metal phase resistivity will give very close estimate of the solution potential. So, this equation could be used in the range of 500 μm copper particles and will definitely give a closer estimate of solution potential. Larger particles or smaller ones could show little deviation from experiments.

2) Metal phase potential could be estimated with variable resistivity equation and will give much closer but not accurate values of the potential.

3) Fluidized bed could be used in continuous operation by adding new particles and venting out the larger ones resulted from particle growth by deposition. The self cleaning action due to the bipolarity of the particle and the continuous motion of particles will prohibit agglomeration in the reactor.

4) Conversion is relatively low and could be increased by series reactor or recycle streams.

5) The bed thickness could be up 2 cm in most cases. However, there is no limits to the other coordinates.

6.2 Recommendations for Future Work

Many issues could be studied for future work. The equation suggested as a correction could be developed by modifying it, changing numerical values for more accuracy, and inserting other variables such as particle diameter, temperature, and solution resistivity. Another issue is to study the case of two dimensional geometry where the current is perpendicular to the flow of electrolyte. Another point suggested by the examining committee is to use it in electromachining.

References

1) Goodridge F., and Kuhn A.T., Philosophical Transactions of the Royal Society of London, Volume A302, 275, (1981).
2) Epstein Norman, International Journal of Chemical Reactor Engineering, Volume 1, Review R1, (2003).
3) Hamann Carl H., Hamnett Andrew, and Vielstich Wolf, "Electro-chemistry", John Wiley and Sons, 1st edition, (2004).
4) Pickett D.J.," Electrochemical Reactor Design", Amsterdam Elsevier Scientific Publishing Co., 1st ed., (1977).
5) Newman John, and Aleya Karen E. Thomas, "Electrochemical Systems", John Wiley & Sons, 3rd edition, (2004).
6) Brett Christopher M.A., and Brett Ana Maria Oliveira, "Electrochemistry principles, Method, and Application", Oxford University Press, 1st edition, (1994).
7) Garrido Javier, Journal of Physical Chemistry, 108, 1, 18336, (2004).
8) Bagotsky V.S., "Fundamental of Electrochemistry", John Wiley and Sons INC., 1st edition, (2006).
9) Bard Allen J., and Faulkner Larry R., "Electrochemical Methods", John Wiley and Sons INC., 2nd edition, (2001).
10) Wang Joseph, "Analytical Electrochemistry", John Wiley and Sons, 2nd edition, (2001).
11) Levenspiel Octave, and Kunii Daizo, "Fluidization Engineering", Robert E. Krieger Publishing Company, 1st edition, (1969).
12) Goodridge F., Electrochimica Acta, 22, 11, 929, (1977).

13) Lee J.K., Shemilt L.W., and Chun H.S., Journal of Applied Electrochemistry, 19, 10, 877, (1989).

14) Goodridge F., King C.J.H., and Wright A.R., Electrochimica Acta, 22, 9, 1087, (1977).

15) Fleischman M, and Kersall G.H., Journal of Applied Electrochemistry, 14, 2, 269, (1984).

16) Coeuret F., Journal of Applied Electrochemistry, 10, 5, 687, (1980).

17) Germain S., and Goodridge F., Electrochimica Acta, 21, 3, 545, (1976).

18) Fleischmann M., and Kersall G.H., Journal of Applied Electrochemistry, 14, 2, 277, (1984).

19) Fleischmann M., Oldfield J.W., and Tennakoon L., Journal of Applied Electrochemistry, 1, 1, 103, (1971).

20) Kreysa G., Electrochimica Acta, 25, 6, 813, (1980).

21) LeRoy Rodney L., Electrochimica Acta, 23, 6, 815, (1978).

22) LeRoy Rodney L., Electrochimica Acta, 23, 6, 827, (1978).

23) Kreysa G., Juttner K., and Bisang J.M., Journal of Applied Electrochemistry, 23, 5, 707, (1993).

24) Dweik B.M., Liu C.C., and Savinell R.F., Journal of Applied Electrochemistry, 26, 7, 1093, (1996).

25) Hutin D., and Coeuret F., Journal of Applied Electrochemistry, 7, 5, 463, (1977).

26) Kreysa G., Electrochimica Acta, 23, 8, 1351, (1978).

27) Jiricny V., and Stanek V., Journal of Applied Electrochemistry, 24, 6, 930, (1994).

28) Walker A.T.S., and Wragg A.A., Electrochimica Acta, 25, 3, 323, (1980).

29) Shvab N.A., Stefanjak N.V., Kazdobin K.A., and Wragg A.A., Journal of Applied Electrochemistry, 30, 8, 1285, (2000).

30) Shvab N.A., Stefanjak N.V., Kazdobin K.A., and Wragg A.A., Journal of Applied Electrochemistry, 30, 8, 1293, (2000).

31) Roessler A., Crettenand D., Dossenbach O., and Rys P., Journal of Applied Electrochemistry, 33, 7, 901, (2003).

32) Scott K., Journal of Applied Electrochemistry, 18, 3, 504, (1988).

33) Huh T., Savaskan G., and Evans J.W., Journal of Applied Electrochemistry, 22, 6, 916, (1992).

34) Zhou Minghua, Wu Zucheng, Ma Xiangjuan, Cong Yanqing, Ye Qian, and Wang Dahui, Separation and Purification Technology, 34, 81, (2004).

35) Rozik R., Orinakova R, Markusova K., and Trnkova L., Journal of Solid State Electrochemistry, 10, 423, (2006).

36) Zhou M.H., and Lei L.C., Electrochimica Acta, 51, 12, 4489, (2006).

37) Fleischmann M., and Oldfield J.W., Journal of Electroanalytical Chemistry , 29, 231, (1971).

38) Fleischmann M., and Oldfield J.W., Journal of Electroanalytical Chemistry , 29, 211, (1971).

39) Brodkey Robert S., and Hershey Harry C., ”Transport Phenomena”, Mc-Graw Hill Book Company, 1st edition, (1988).

40) Pickett D.J., Journal of Applied Electrochemistry, 5, 1, 101, (1975).

41) Foust Alan S., Wenzel Leonard A., Clump Curtis W., and Andersen Bryce L., “Principles of Unit Operations”, John Wiley & Sons,(1980).

42) Perry Robert H., Green Donald W., and Don Green, “Perry's Chemical Engineers' Handbook on CD-ROM”, McGraw-Hill Professional, 7th edition, (1997).

43) Fleischmann M., and Oldfield J.W., Journal of Electroanalytical Chemistry , 29, 240, (1971).

44) Scott K., Electrochimica acta, 24, 3, 1109, (1979).

45) Grishkey Richard G., “Transport Phenomena and Unit Operations”, John Wiley and Sons, 1st edition, (2002).

46) Coughanowr Donald R., “Process System Analysis and Control”, Mc-Graw Hill Inc., 2nd edition, (1991).

47) King R.B., “Introduction to Practical Fluid Flow”, Elsevier Science, 1st edition, (2002).

48) Wrede Robert, and Spiegel Murray R., “Advanced Calculus”, Schaum’s Outline Series, 2nd edition, (2002).

49) Stubberud Allen R., and Williams Ivan J., “Feedback and Control Systems”, Schaum’s Outline Series, 2nd edition, (1990).

50) Chinneck, John W., “How to Organize Your Thesis”, http://www.sce.carleton .ca/faculty/chinneck/thesis.html, (1999).

Appendix A

A-1 Integration of Equation 3.26[48]

$$\frac{d^2\eta}{dx^2} - \frac{ai_\circ(\chi_m+\chi_s)zF\eta}{RT} = 0 \qquad 3.26$$

Let

$$K_1 = \frac{ai_\circ(\chi_m+\chi_s)zF}{RT}$$

So,

$$\frac{d^2\eta}{dx^2} - K_1\eta = 0$$

Let $p = \frac{d\eta}{dx} \Rightarrow \frac{dp}{dx} = \frac{dp}{d\eta}\frac{d\eta}{dx} = p\frac{dp}{d\eta} = \frac{d^2\eta}{dx^2}$

$\therefore$ $p\frac{dp}{d\eta} - K_1\eta = 0$

$$\int p\,dp = K_1\int \eta\,d\eta$$

$$\frac{p^2}{2} = K_1\frac{\eta^2}{2} + C_1 \Rightarrow p = \pm\left(K_1\eta^2 - Y_1\right)^{\frac{1}{2}} \text{ where } Y_1 = -\frac{C_1}{2}$$

$$\frac{d\eta}{dx} = \pm\left(K_1\eta^2 - Y_1\right)^{\frac{1}{2}} = \pm\left(\frac{ai_\circ(\chi_m+\chi_s)zF}{RT}\eta^2 - Y_1\right)^{\frac{1}{2}} \qquad 3.27$$

$$\frac{d\eta}{\left(K_1\eta^2 - Y_1\right)^{\frac{1}{2}}} = \pm dx$$

$$\int \frac{d\eta}{K_1^{\frac{1}{2}}\left(\eta^2 - \frac{Y_1}{K_1}\right)^{\frac{1}{2}}} = \pm\int dx$$

$$\cosh^{-1}\frac{\eta}{\left(Y_1/K_1\right)^{\frac{1}{2}}} = \pm K_1^{\frac{1}{2}}x + Y_2$$

Taking hyperbolic cosine for both sides

$$\frac{\eta}{\left(Y_1/K_1\right)^{\frac{1}{2}}} = \pm\cosh\left(K_1^{\frac{1}{2}}x + Y_2\right) \Rightarrow \eta = \pm\left(\frac{Y_1}{K_1}\right)^{\frac{1}{2}}\cosh\left(K_1^{\frac{1}{2}}x + Y_2\right)$$

$$\therefore \qquad \eta = \pm\left(\frac{RTY_1}{ai_\circ(\chi_m + \chi_s)zF}\right)^{\frac{1}{2}}\cosh\left(\left(\frac{ai_\circ(\chi_m + \chi_s)zF}{RT}\right)^{\frac{1}{2}}x + Y_2\right)$$

3.28

A-2 Integration of Equation 3.29[48]

$$\frac{d^2\eta}{dx^2} - ai_\circ(\chi_m + \chi_s)\exp\left(\alpha zF\eta/RT\right) = 0 \qquad 3.41$$

Let $K_2 = ai_\circ(\chi_m + \chi_s)$ and $K_3 = \frac{\alpha zF}{RT}$, so

$$\frac{d^2\eta}{dx^2} - K_2\exp\left(K_3\eta\right) = 0$$

Let $p = \frac{d\eta}{dx} \Rightarrow \frac{dp}{dx} = \frac{dp}{d\eta}\frac{d\eta}{dx} = p\frac{dp}{d\eta} = \frac{d^2\eta}{dx^2}$

$$p\frac{dp}{d\eta} - K_2\exp\left(K_3\eta\right) = 0$$

$$\int pdp = \int K_2\exp\left(K_3\eta\right)d\eta$$

$$\frac{p^2}{2} = \frac{K_2}{K_3}\exp\left(K_3\eta\right) + Y_3$$

$$p = \pm\left(\frac{2K_2}{K_3}\exp\left(K_3\eta\right)+Y_3\right)^{\frac{1}{2}}$$

$$\frac{d\eta}{dx} = \pm\left(\frac{2K_2}{K_3}\exp\left(K_3\eta\right)+Y_3\right)^{\frac{1}{2}} = \pm\left(\frac{2ai_{\circ}RT(\chi_m+\chi_s)}{\alpha zF}\exp\left(K_3\eta\right)+Y_3\right)^{\frac{1}{2}} \qquad 3.42$$

$$\frac{d\eta}{dx} = \pm\left(\frac{2K_2}{K_3}\exp\left(K_3\eta\right)+Y_3\right)^{\frac{1}{2}}$$

$$\frac{d\eta}{\left(\frac{2K_2}{K_3}\exp\left(K_3\eta\right)+Y_3\right)^{\frac{1}{2}}} = \pm dx$$

$$\frac{1}{Y_3^{\frac{1}{2}}}\cos^{-1}\left(\exp\left(K_3\eta\right)\right) = x+Y_4$$

$$\exp\left(K_3\eta\right) = \cos\left(\frac{K_3Y_3^{\frac{1}{2}}x}{2}+Y_4\right)$$

$$\eta = \pm\frac{1}{K_3}\left[\ln\left\{\cos\left(\frac{K_3Y_3^{\frac{1}{2}}x}{2}\right)\right\}-\ln\left\{\frac{K_3Y_3^{\frac{1}{2}}}{2K_2}\right\}\right]$$

$$\eta = \pm\frac{RT}{\alpha zF}\left[\ln\left\{\cos\left(\frac{\alpha zFY_3^{\frac{1}{2}}x}{2RT}\right)\right\}-\ln\left\{\frac{\alpha zFY_3^{\frac{1}{2}}}{2ai_{\circ}RT(\chi_m+\chi_s)}\right\}\right] \qquad 3.43$$

Appendix B

Matlab Programs

B-1 Matlab Program for Calculating Metal Phase Resistivity Using Equation 3.1

```
YO=input('Young Modulus=')
RSO=input('Resistivity of solution=')
D=input('Density of solution=')
DS=input('Density of solid=')
EO=input('Initial porosity=')
V=input('Viscosity=')
d=input('Particle diameter=')
EX=input('Expansion=')
E=(EX+EO)/(EX+1);
VT=(4*(DS-D)^2*9.81^2/(225*D*V))^0.3333*d;
C=0.225*(VT*d*D/V)^0.1;
U=E^(1/C)*VT;
VP=U/E;
RS=RSO/E;
RM=0.04179*(1+EX)^0.6667*((1+EX)^0.3333-1)*YO^0.3333*RS/((DS-D)^0.3333*VP^0.6667)
```

B-2 Matlab Program for Calculating Metal Phase Resistivity Using Equation 2.50

```
YO=input('Young Modulus=')
```

```
RSO=input('Resistivity of solution=')
D=input('Density of solution=')
DS=input('Density of solid=')
EO=input('Initial porosity=')
V=input('Viscosity=')
d=input('Particle diameter=')
EX=input('Expansion=')
E=(EX+EO)/(EX+1);
VT=(4*(DS-D)^2*9.81^2/(225*D*V))^0.3333*d;
C=0.225*(VT*d*D/V)^0.1;
U=E^(1/C)*VT;
VP=U/E;
RS=RSO/E;
RM=0.28*(1+EX)^0.6667*((1+EX)^0.3333-1)*YO^0.3333*RS/((DS-D)^0.3333*VP^0.6667)
```

B-3 Matlab Program for Calculating The Total Current Density for a Number of Different Conditions

```
B=input('Beta Value=')
f=input('f value=')
L=input('Length=')
XS=input('Solution resistivity=')
XM=input('Metal phase resistivity=')
PMO=input('Standard metal potential=')
```

```
for I=1:10000
K1=1-(I^2)*(XM^2)*exp(f*PMO)/(B*(XM+XS));
K2=0.5*L*f*B^0.5*(XM+XS)^0.5*(K1)^0.5*exp(0.5*f*PMO);
K3=1-(I^2*(XM^2-XS^2)*exp(f*PMO)/(B*(XS+XM)));
fn=acos(K1^0.5)+acos((K1/K3)^0.5)-K2;
if abs(fn)<=0.1
break
end
end
```

B-4 Matlab Program for Calculating The Solution Potential Distribution Profile at Different Bed Conditions

```
B=input('Beta Value=')
f=input('f value=')
I=input('Total current density=')
XS=input('Solution resistivity=')
XM=input('Metal phase resistivity=')
PMO=input('Standard metal potential=')
L=input('Bed length approximated for the nearest millimeter=')
K1=1-(I^2)*(XM^2)*exp(f*PMO)/(B*(XM+XS));
for x=.001:0.001:L
K2=0.5*x*f*B^0.5*(XM+XS)^0.5*(K1)^0.5*exp(0.5*f*PMO);
PS=(-I*XM*x-log(K1/(cos(K2-acos(K1^0.5)))^2)/f)*(1+XM/XS)^-1
end
```

B-5 Program For Calculating Local Metal Phase Resistivity

```
B=input('Beta Value=')
f=input('f value=')
I=input('Total current density=')
XS=input('Solution resistivity=')
PMO=input('Standard metal potential=')
L=input('Length of bed for nearest millimeter=')
for x=0.001:0.001:L
PS=input('Solution potential=')
for XM=.001:0.001:10
K1=1-(I^2)*(XM^2)*exp(f*PMO)/(B*(XM+XS));
K2=0.5*x*f*B^0.5*(XM+XS)^0.5*(K1)^0.5*exp(0.5*f*PMO);
D=PS-(-I*XM*x-log(K1/(cos(K2-acos(K1^0.5)))^2)/f)*(1+XM/XS)^-1;
if abs(D)<0.0001
x
XM
break
end
end
end
```

B-6 Matlab Program for Calculating The Solution Potential Distribution Profile Using Local Values of Resistivity

```
B=input('Beta Value=')
```

```
f=input('f value=')
I=input('Total current density=')
XS=input('Solution resistivity=')
PMO=input('Standard metal potential=')
L=input('Bed length approximated for the nearest millimeter=')
for x=.000:0.001:L
XM=input('Metal phase resistivity=')
K1=1-(I^2)*(XM^2)*exp(f*PMO)/(B*(XM+XS));
K2=0.5*x*f*B^0.5*(XM+XS)^0.5*(K1)^0.5*exp(0.5*f*PMO);
PS=(-I*XM*x-log(K1/(cos(K2-acos(K1^0.5)))^2)/f)*(1+XM/XS)^-1
end
```

الخلاصة

تم في هذه الرسالة محاولة إيجاد نموذج يصف التغير في فرق الجهد و التيار و التركيز بالإضافة إلى الصفات الهيدروديناميكية في مفاعل كهروكيمياوي حشوي مسيل. يتكون المفاعل من حشوة من الكرات التي تتحرك و تزداد المسافة فيما بينها نتيجة جريان محلول موصل باتجاه الأعلى. وبتسليط فرق في الجهد بين الطرفين العلوي و السفلي من المفاعل يؤدي إلى حدوث التفاعل الكهروكيمياوي على سطح الكرات. ان هذا المفاعل يمثل واحد من اكثر التطبيقات فائدة في الهندسة الكهروكيمياوية ومن أهم استخداماته هي: الاستخلاص الكهروكيمياوي و منع التلوث والتنقية.

ثلاث حالات تمت دراستها هي: الاستقطاب الخطي, الاستقطاب Tafel, الاستقطاب بالتركيز. تم اختبار الاستقطاب Tafel و وجد أن معادلة المقاومة التي تم اقتراحها من قبل Fleischmann et.al. في سنة ١٩٧١غير صحيحة بسبب ان المعادلة المقترحة تفترض قيمة ثابتة لمقاومة الطور المعدني على طول المفاعل بينما في الواقع هي ليست كذلك كون الكرات متباعدة في أسفل المفاعل وتصبح أكثر تقاربا باتجاه نهاية المفاعل. لذلك تم تطوير صيغة لوصف مقاومة الطور المعدني اعتمادا على الموقع و عامل التمدد.معامل تصحيح تم استعماله وإدخاله للمعادلة المقترحة من قبل Fleischmann وهي تغطي مدى واسع من أقطار الكرات. تم تقليل الخطأ بنسبة كبيرة وذلك بواسطة هذه المعادلة لكل من فرق الجهد في المعدن والمحلول. تم أيضا دراسة تغير التركيز في هذا العمل بالإضافة إلى تغير السرعة وتغير الضغط مع معامل التمدد للمفاعل.

شكر و تقدير

أتوجه بالشكر والتقدير إلى المشرف و رئيس قسم الهندسة الكيمياوية في جامعة النهرين الأستاذ الدكتور قاسم جبار السليمـان لإرشاداته وتوجيهاته القيمة التي ساعدت في أتمام هذا الرسالة والى الأساتذة الأعزاء في القسم. والى كادر قسم الهندسة الكيمياوية وعمادة كلية الهندسة و زملائي في الدراسة. وأتقدم بالشكر الجزيل إلى كادر المكتبة المركزية والى أقسام الدوريات في مكتبة كلية الهندسة في جامعة بغداد والجامعة التكنولوجية والى كادر المكتبة ألافتراضية العراقية على الإنترنت والى جميع من ساهم في إتمام وانجاز هذه الرسالـة............

المحاكاة الرياضية
لمفاعل كهروكيمياوي حشوي مسيل

رسالة
مقدمة الى كلية الهندسة في جامعة النهرين
وهي جزء من متطلبات نيل درجة ماجستير علوم
في الهندسة الكيمياوية

من قبل
مهند جواد كاظم
بكلوريوس علوم في الهندسة الكيمياوية ٢٠٠٤

ذي القعدة ١٤٢٨
تشرين الأول ٢٠٠٧